Master Energy Science

A Technoeconomic Analysis of a Low Temperature Geothermal District Heat Pump Network in Residential Zwijndrecht

Date: 24th September 2021

Andrew Rhodes
Student number: 6975852
Email: a.p.rhodes@students.uu.nl

Master programme: Energy Science
Course: Master Thesis (GEO4-2510)

Utrecht University

Supervisor UU: Dr. Wen Liu
Supervisor TNO: Dr. Marianne van Unen
2nd reader UU: Wina Crijns-Graus

(EC 30)

Contents

Acknowledgements

I would first like to thank TNO as a whole for the opportunity, for welcoming me into the many avenues of information and for acquainting me to a professional working environment. It was a privilege to be surrounded by such an abundance of knowledgeable experts, especially for such a multi-disciplinary research topic. A special thanks to Marianne van Unen and Wen Liu for their thoughtful guidance, supervision and big picture perspectives of how to effectively conduct the research process. To Lies Peters and Jan-Diederik van Wees, for their patient guidance and for providing the geotechnical explanations and data required. I found that the monthly presentations were always fruitful, with each meeting leaving me with a new thought-provoking perspective on how to modify the model. To Ryvo Octaviano and Can Tümer, for their patience guidance of the CHESS tool operation and kind and prompt resolutions to CHESS bottlenecks. Finally, a thanks to the WarmingUP project and HVC for providing me with heat network data which facilitated a reliable economic model. Thank you all for a pleasureful experience and I wish you all the best going forward into the future.

Abstract

Inefficient buildings are expected to produce higher relative shares of built environment heat emissions due to sustainable barriers. New thermal production systems are required. Large modes of thermal production often have improved economic and environmental performance compared to individual thermal systems. Stakeholders are increasingly engaged with district heating networks, which facilitate technologies otherwise unavailable to small individual users. Many high temperature geothermal district heating networks are currently in operation globally, however shallow low temperature systems are relatively unexplored. Despite large synchronicities between subsurface potential and urban heat demands, inefficient buildings cannot utilise shallow low temperatures directly and require thermal upgrades such as from heat pumps. Centralised heat pumps within district heating networks often utilise medium temperature thermal resources or supply low-medium temperatures from a low temperature resource. No documented heat network example exists which supplies a residential district with a heat pump temperature difference higher than 50°C. Despite technical viability in many areas, low temperature geothermal heat pump systems for inefficient buildings do not attract commercial investment. Theoretical system efficiencies are low and investment magnitude and risk is high. However, commercial interest has arisen for such a system in the residential district of Zuid-Zwijndrecht in The Netherlands. A techno-economic analysis was conducted for a low temperature geothermal system (31°C) connected a collective heat pump, which supplies 80°C to 2000 homes. Geotechnical data derived from a contextualised aquifer characterisation has been translated into P90 and P50 maximum flowrate constraints for use within the dynamic heat network modelling tool CHESS. This range of geotechnical uncertainty has facilitated a robust indication of economic and emission performance amongst flowrate and revenue uncertainty. Compared to individual natural gas boilers, the P90 and P50 heat network scenarios have estimated $CO2_{-eq}$ emissions reductions of 67.7% and 72.9% and estimated levelized cost of heat (LCOH) reductions of 5.48% and 6.6%, respectively. The P50 and P90 scenarios are then assessed amongst low, medium and high revenue uncertainty scenarios. The NPV ranges from €-4.7m to €11.7m. All subsidy scenarios brackets with a €2500 connection fee (BAK) have a positive NPV irrespective of heat price. If low flowrates are produced and no subsidies are awarded, the connection fee required to break even is €3522 and €1622 for the 2021 and 2030 heat prices respectively. Recommended CHESS model improvements are provided in the context of different thermal production systems.

1.0 Introduction

The provisional agreement of the European Green Deal has set objectives to reduce greenhouse gas emissions (GHGs) by at least 55% by 2030 compared to 1990 levels, and a climate-neutral EU economy is the target for 2050 [1]. Thus, integrating carbon neutral sustainable energy systems is required amongst all sectors. One solution is geothermal energy, which is feasible in many areas globally. Geothermal heat can be used directly, or in combination with a turbine to convert steam to electricity. Geothermal can replace conventional baseload systems such as coal-fired heat and power. Compared to solar and wind energy, geothermal has the benefit of low temporal variability and intermittence [2][3]

In 2020, onshore geothermal power plants operated in 29 countries with a total installed power generation capacity of 15.4 GW and could double in the next 15 years [4]. However, ~135°C is required for conventional electricity generation (steam) and ~80°C is feasible if using a secondary fluid with a low boiling point (Organic Rankine Cycle) [5]. Near tectonic plate boundaries, high subsurface temperatures occur at relatively shallow depths [6]. This does not represent the common global subsurface condition and ultra-deep drilling is often required to achieve temperatures high enough for electricity generation. However, permeability often decreases exponentially before reaching such temperatures, meaning open loop systems (which use groundwater) for electricity generation is rare [7].

Direct application of low temperature geothermal (LTG) is for space heating, balneotherapy, horticulture (greenhouses), aquaculture (fish farming) and industrial processes (drying) [5]. The installed geothermal capacity in The Netherlands is mostly amongst horticultural. From 2018-2019, 12 geothermal projects became 24 [8][9]. Many Dutch buildings which use conventional radiators are too inefficient to utilise direct geothermal for space heating. Without low temperature emitter systems, such as underfloor heating, thermal upgrades are required. Upgrades such as from heat pumps (HPs), are common amongst small individual systems. In recent years, interest has shifted towards large collective systems within district heating networks (DHNs) [10]

In 2020, 6.2 PJ of heat was produced in The Netherlands [11], and by 2030, between 100 and 300 PJ of total geothermal capacity could be developed [12]. If interest into DHNs continues, 100 PJ of networks in 2050 (3.3 million homes), could supply 40% of the total Dutch built environment heat demand [13]. Under current Dutch policy, the 363,000 DHN connected dwellings in 2013 will become 549,000 in 2030 (≈17% new constructions). However, the 13 large DHN systems predominantly used production from gas and coal-fired boilers. Collective heat pumps were just 1% of the small DHN (>5000 consumers) capacity [14][15].

The WarmingUP project [16] is reviewing production sources for a new DHN in the residential district of Zuid-Zwijndrecht in The Netherlands. This study considers the cost and emission performance of a low temperature geothermal (LTG) system connected a collective heat pump (LTG-HP). The DHN satisfies all the necessary spatial and technical criteria for the residential area of Zuid-Zwijndrecht. Seismic surveys have already been interpreted, and the viable aquifer is within the Brussels Sand Member [16]. LTG data is used within CHESS, a DHN modelling tool which facilitates an accurate techno-economic analysis of an LTG-HP system combined with auxiliary technologies.

2.0 Background and Societal Relevance

2.1 The Built Environment

World population is projected to increase from 7.8 billion in 2020 to 9.7 billion in 2050 [17]. Economic development is a greater long-term causal factor to increased energy demand. The United Nations predicted that around 6 billion people will live in cities in 2050, many of which are highly vulnerable to environmental change [18]. In 2007, the built environment consumed 40% of all global energy, which is responsible for 30% of the global greenhouse gas (GHG) emissions. Operational emissions from heating, cooling, and lighting were 80% of lifecycle building emissions, roughly 24% of the global total [19]. A decade later in 2017, the global GHG emissions of the building sector became 39%. This translates to 28% from operational emissions and 11% from materials, construction, and deconstruction [20]. As building demand increases, decarbonisation is required to significantly reduce global GHG emissions.

Large reductions can only occur from committed investment and policy. The biggest investors of global renewable capacities from 2010-2019, were China (31%), Europe (28%) and the U.S (14%) [21]. This implies that 73% of global renewable capacity investments are from 32% of the global population [17]. Likely areas of infrastructural investment are regions with projected emission reductions, as seen in Fig. 1. [22] Gross Domestic Product (GDP) and average national temperature are negatively correlated [23], whilst GDP and renewable energy consumption are positively correlated [24]. Although such trends have anomalies, colder regions are likely to attract more sustainable investment per person. Thus, researching ways to reduce operational built environment heat emissions is particularly pragmatic. This can be from efficiency measures and new modes of thermal production.

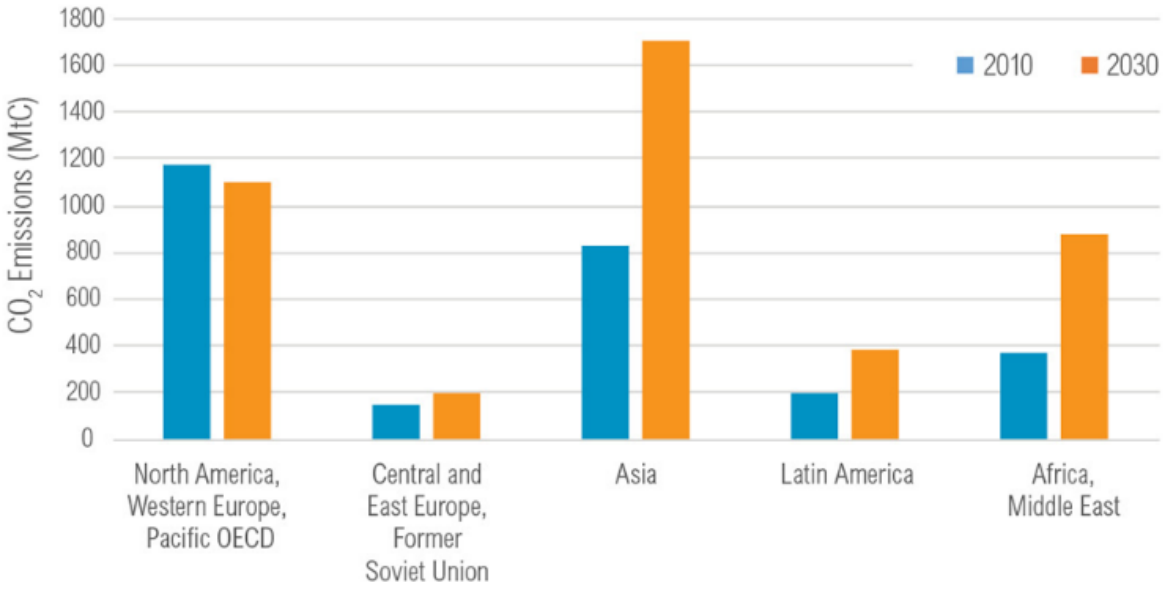

Fig. 1: The projected change in total building emissions (construction and operation) from 2010-2030 by region

2.2 Thermal Efficiency

In a 2010 sample of moderate-cold climate buildings, the average space and water heating consumption was 60% of the total operational energy use [22]. In 2018, the global built environment heating consumption was 45% from natural gas and 37% from oil [25]. High building emissions are intensified when old buildings in cold urban environments have poor insulation. Fig. 2 shows that the building sector has the largest unrealised potential of cost-effective efficiency savings of energy and emissions globally. Residential and commercial buildings represent 34% of the total opportunity to improve productivity by sector, namely the energy consumption per unit of GDP [22]. The theoretical potential to lower global GHG emissions via efficiency measures, was noted to be 83% less than the business-as-usual scenario relative to 2050 projections [26]. However, techno-economic constraints often prevent such potential, with sub-optimal efficiency improvements from low renovations often being 'locked in' [27].

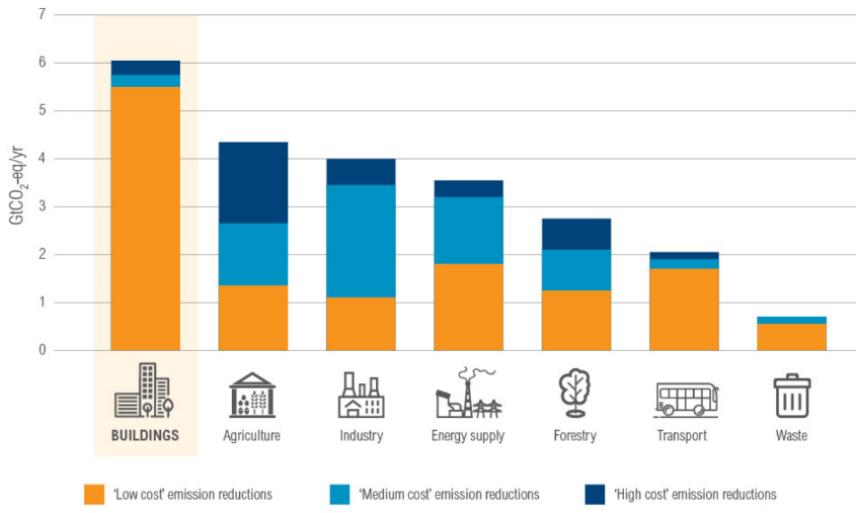

Fig. 2: Demonstration of different sectors and their cost and emission reductions, showing buildings to have the largest unrealised potential of cost-effective efficiency savings globally

The theoretical potential of 83% is optimistic, as deep renovations are unlikely at the global scale. Superinsulation measures, such as those seen from 'passive houses' are currently unrealistic without significant market changes and policy [28]. In 2016, only 60,000 passive homes existed, mostly in Europe, U.S., Canada, and Japan [29]. Therefore, whilst proof of concept exists, achieving high thermal efficiency is rare and is mostly present amongst new buildings. Replacing an existing building envelope with thick, super-insulated material, is evidently an unpragmatic, impractical or technically impossible endeavour.

Multiple cold-climate studies showed that cost-effective insulation measures could only reduce 20–50% of demand [30]-[32]. A positive business case also depends on low temperatures and discount rates, and high fuel costs, technological learning rates and subsidies [33]. As the economic viability of insulation measures is a barrier, large uncertainty regarding the extent of emission reduction potential in moderate to cold climates is added. The global correlation between increased GDP and increased energy consumption is very strong. However, the policy to reduce energy demand is limited and contested [34].

This relationship is further corroborated by Fig. 3, which highlights projected residential built environment data towards 2050. As population and economic development increase, so does total and relative (per person) building requirements. As shown, the predicted energy demand is higher than the 7% efficiency savings (energy per area) which offsets demand [30]. As the theoretical maximum efficiency savings are likely to be less than the additional energy demanded, new sustainable modes of building heat production is required.

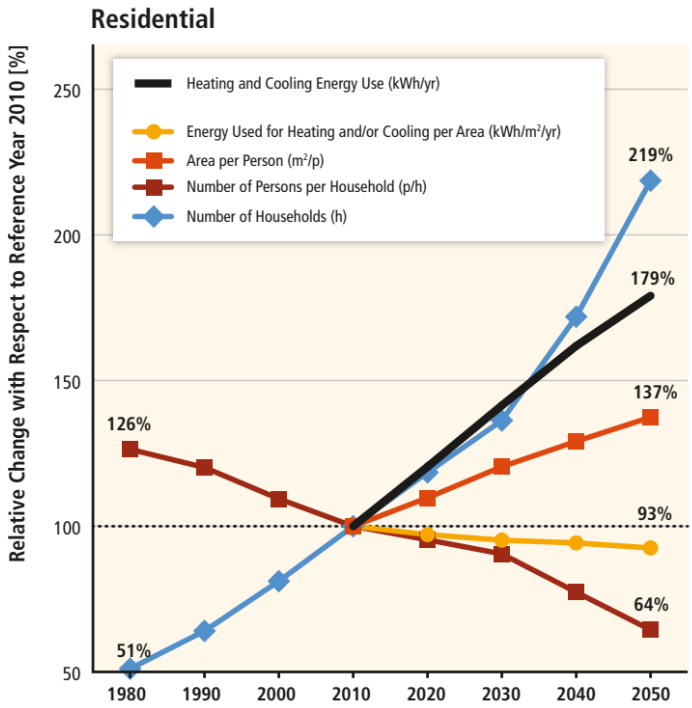

Fig. 3: Projected residential built environment data towards 2050

In Europe, improving building efficiency is particularly hard due to the prevalence of the landlord-tenant dilemma. Therefore, there is little incentive for landlords to invest in efficiency improvements of rental properties [35]. The Netherlands has low insulation renovations rates (3 label steps). This is partly explained by the large numbers of rental properties [36] and cost-ineffectiveness of insulation investment [37]. If energy prices remain stable, energy label B renovations are mostly cost-ineffective. When simulating high energy prices and low insulation investment, only 25% of buildings have cost-effective renovations [38]. Without changes to current market mechanisms, techno-economic and social barriers will continue to determine low insulation renovation rates amongst existing buildings.

Whilst minimum efficiency restrictions are emerging for new constructions, existing buildings will have higher relative heat demands per area. If sustainable production systems are not implemented in existing buildings, this results in higher relative shares of future built environment heat emissions. This spatial trend will increase in developed nations, as existing stocks are large, whilst new buildings are built relatively slowly [30] and become more constrained to efficiency standards. Conversely, in developing countries, building life spans are shorter (25-35 years), and the rate of new building stock is rapid [27].

To summarise, emission reduction potential is large from efficiency measures, but in practice the extent of efficiency investment is constrained for the existing building stock. Developed, often cold regions, have low building construction rates, whilst the existing building stock has low renovation rates. As resolving building efficiency barriers is uncertain, so is large GHG reductions from thermal efficiency alone. Especially as domestic heated water (DHW) demand is largely unaffected when the building envelope is changed (only space heating) [39]. Thus, new sustainable thermal production systems are required to resolve these apparent barriers facing existing buildings, particularly in moderate-cold climates.

2.3 Thermal Production

New modes of sustainable thermal production can reduce the emissions associated with an increasing space heating and DHW demand. However, this extent differs amongst built environments globally. The EU-28 (28 EU member states) is used as reference frame due to the abundance of sustainable thermal production literature, political interest, and prior investment trend predictions. In 2015, many large and cold countries have some of the highest CO_2 intensity amongst the EU-28 (Fig. 4). The EU-28 residential heat consumption fuel mix is shown in Fig. 5. Natural gas comprised the majority (53%) of emissions, followed by oil and coal at 23% each. Note that, biomass is assumed carbon neutral [40], however biomass has substantially higher particulate matter (PM) emissions compared to natural gas [41]. If unmitigated, PM is a contributing variable to increased mortality. In 2016, $PM_{2.5}$ was associated with 4.1 million deaths globally (95% confidence interval) [42]. Thus, importing rurally generated electricity to facilitate new modes of thermal production can vastly improve urban air quality and health from an operational perspective.

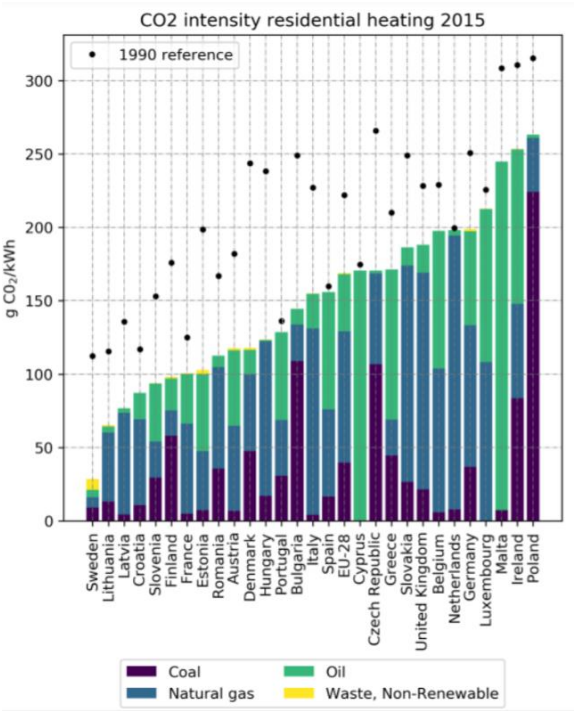

Fig. 4: CO_2 intensity of EU residential heating in 2015

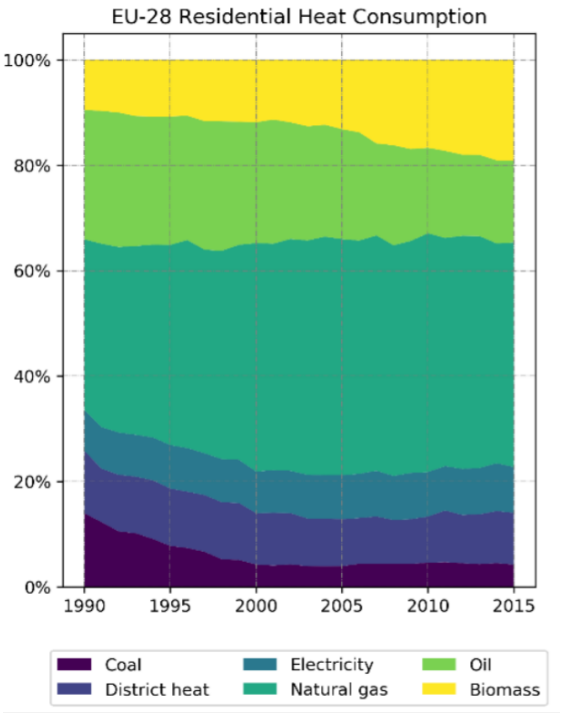

Fig 5: The share and development of final energy consumption of residential heating in the EU-28 from 1990-2015

2.3.1 Air Source Heat Pumps

As renewable power generation costs continue to fall [43], heat electrification is becoming an increasingly more economically attractive option. Power to heat (P2H) technologies such as electrically driven heat pumps (HPs), if powered by a high renewable share, can reduce built environment heat emissions [44]. The electricity production mix is an important consideration in determining the emission reduction potential. In 2021, individual HPs were considered highly sustainable in Latvia and Lithuania. Conversely, the Estonian electricity mix has a high emission factor, meaning natural gas boilers have lower operational CO_2 emissions [45]. However, relative to fossil-fuel combustion, individual all-electric Air-source heat pumps (ASHPs) reduce air pollutants, namely SO_2 (sulphur dioxide), NO_x (nitrogen oxides) and particulate matter (PM) [45]. In Latvia, ASHPs had the highest sustainability index, from 19 indicators. Notably, from significantly less PM relative to wood and oil boilers [41].

As well as the electricity mix, the effectiveness of emission reduction via HPs depends on the timing of the peak electricity and heat demand, which varies amongst different climates. In Western Europe, the residential heat demand coincides with the peak non-heating electricity demand [46]. Peak electricity demands are typically generated from natural gas-fired turbines, of which offer high operational flexibility (fast ramping), at the expense of high operational costs [47]. ASHPs are relatively inefficient, but have the lowest investment, and are commonly deployed to individual buildings [48]. Thus, the aggregation of numerous distributed inefficient ASHPs, can result in peak demands with high associated emissions and end-user electricity costs. ASHPs are also less cost-effective over the lifetime than high investment and efficiency ground-source heat pump (GSHP) [48]. Thus, the aggregation of many decentralised ASHP capacities is both environmentally and economically sub-optimal from a macro-perspective.

If buildings are poorly insulated, techno-economic restrictions may also apply to individual all electric ASHPs. For Dutch buildings, all-electric ASHPs are unsuitable for buildings less efficient than label C, and label B is required for comfort in pre-war constructions. Technical unsuitability relates to inefficiency, creating a peak demand larger than the voltage constraint. Economic unsuitability relates to peak electricity prices coinciding with peak heat demand [49]-[51]. Furthermore, both technical and economic unsuitability relates to the higher supply temperatures required for comfort. Fig. 6 shows that higher supply temperatures will result in an exponentially lower Coefficient of Performance (COP), namely the efficiency. Note, that the COP range represents the variance from different HP refrigerants [52].

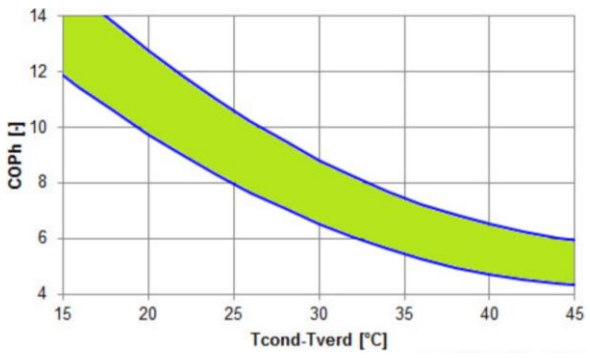

Fig 6: Exponential increase in COP as the temperature difference between the HP source and supply decreases

2.3.2 Ground Source Heat Pumps

As individual all-electric HPs are particularly unsuitable for buildings less efficient than label C, larger and more efficient systems are required to supply buildings constrained to higher supply temperatures. A ground source heat pump (GSHP) is widely regarded as a shallow, low enthalpy geothermal system. A fluid is circulated through soil, bedrock, and a borehole heat exchanger, typically 50-200m deep [53]. GSHPs are often closed loop systems in urban environments with strict water safety regulations. The fluid is typically water, or for more efficient thermal transfer, the less corrosive but toxic, glycol is used. However, this is not recommended due to the risk of drinking water contamination [53]. In moderate-cold climates, GSHPs are economically and environmentally preferred over ASHPs, due to the utilisation of seasonally consistent subsurface temperatures [48].

GSHPs were deemed the most cost-effective way to reduce primary energy consumption amongst two apartment case studies in Finland (constructed in 1960-1970), relative to insulation measures and other sustainable production [54][55]. However, in The Netherlands, an emission reduction objective within an office building model indicated sub-optimal GSHP operation. Fig. 7 shows the emission reductions to be very low past 70% HP capacity, whilst the annualised costs (investment and operation) rise enormously [56]. A hybrid system, namely, electricity and natural gas is thus required. From Fig. 7, at least 30% of the peak load should be covered by natural gas for a cost-effective heating system. Note that, the 2018 Dutch emission factor and electricity cost is used, thus conditions will change in the future.

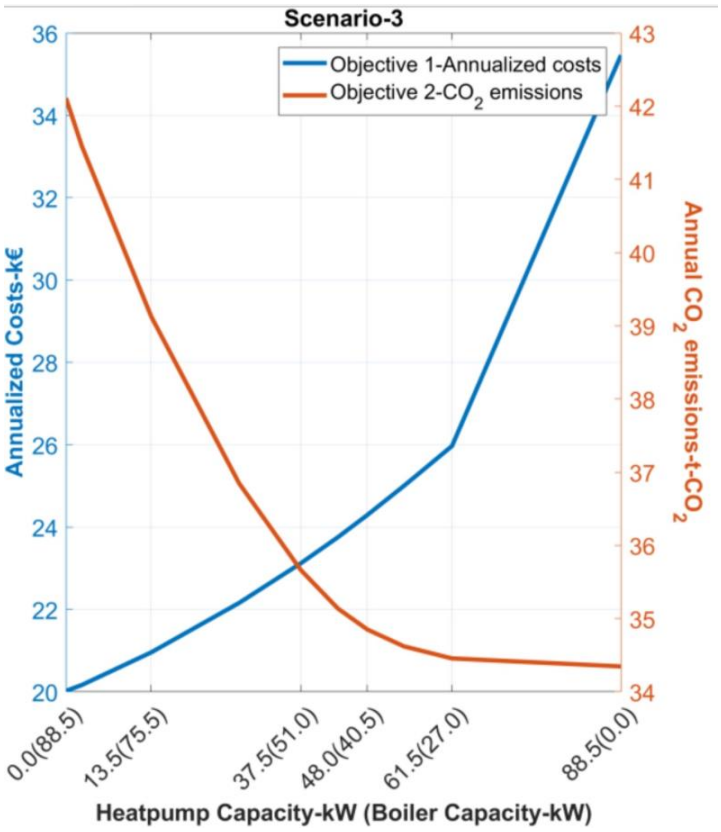

Fig 7: Computational simulation results from an emission optimisation objective of a Dutch office building

2.3.3 Groundwater Heat Pumps

For equal flowrate and generalised pressure correlation assumptions, a higher thermal baseload and efficiency occurs at depth [49]. Thus, a higher thermal baseload from deeper subsurface drilling will generally reduce relative operational emissions. Note that, this is a general trend as technical anomalies exist, and aquifer-specific characteristics differ geographically. Drilling deeper for a higher source temperature is required for buildings in cold regions such as The Netherlands, which require a supply of around 70-90°C [49]. Unfeasible permeability often prevents viable extraction deeper than 2-3 km. Thus, for a geothermal gradient of 31.3°C/km [57], thermal upgrades such as from HPs are required to supply residential temperatures. The prior all-electric GSHP study [56] suggests that cost-effective emission reductions, require a cheaper auxiliary heat source (natural gas), for a Dutch peak demand. This is due to natural gas being cheaper than electricity [58], while the electricity grid emission factor is shown to be relatively high in The Netherlands. The emission factor is expected to reduce in the EU, with Fig. 8 showing the average reductions towards 2030 [59].

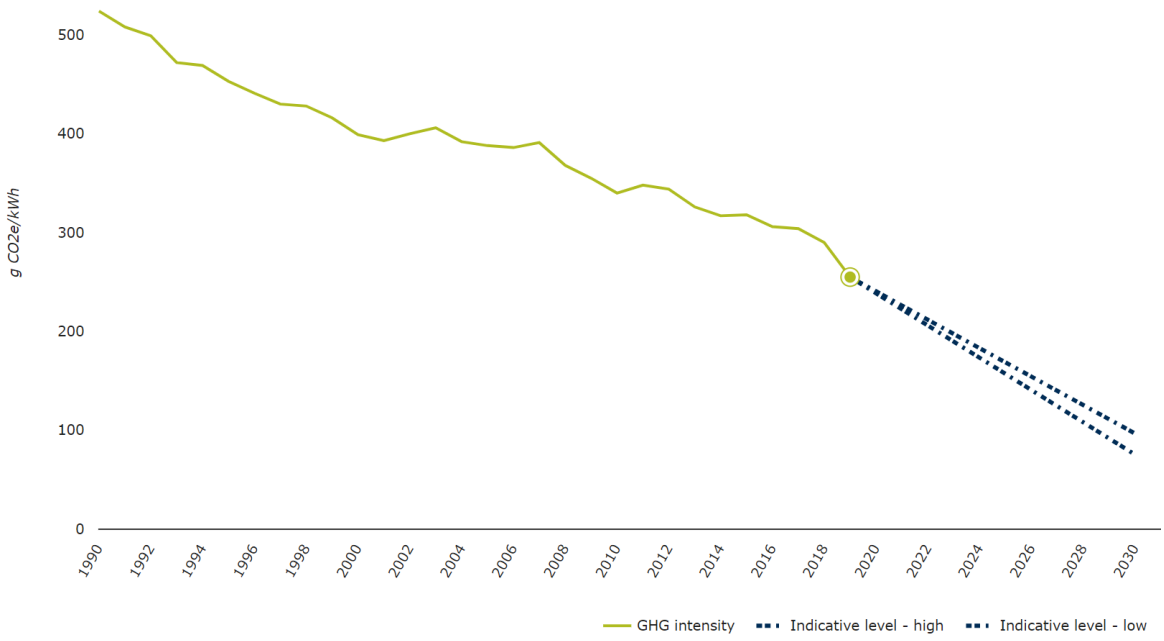

Fig 8: GHG emission intensity (g CO_2/kWh) from public electricity production in the EU

In many dense urban contexts, GSHPs are often spatially unfeasible for application to single buildings [60]. The aggregation of many GSHPs is evidently less space-efficient than the equivalent capacity concentrated in a larger central location. The heat distribution grid is often spatially feasible, as excavation is typically 0.8m underground [61]. Thus, up to a point, deeper systems are a spatial-legislatively and techno-economically pragmatic solution. Groundwater heat pumps (GWHPs) are less common than GSHPs and circulate groundwater between two or more wells in an open system [62]. GSHPs are more commonly acknowledged as shallow and closed-loop systems, whilst GWHPs are deeper and open-loop [62].

GWHPs in a Danish case study were indicated as more cost-effective over the system lifetime than decentralised ASHPs and GSHPs [63]. Thus, the benefits of higher efficiencies, cheaper fuels and lower relative investment was higher than the additional thermal losses and costs of the distribution network. Although emission reductions were not compared [63], operational emissions per unit of heat produced are likely to reduce with depth (larger thermal baseload). Thus, considering favourable aquifer conditions apply, deeper (than GSHP) GWHPs are particularly pragmatic for countries transitioning away from high electricity grid emission factors. The following HP-related substantiations are now made to favour a high capacity centralised GWHP system and not multiple small capacity GSHP systems:

- Large central consumers can attain power regulating market benefits, lower distribution tariff per MWh and cheaper power prices as a large consumer [13].
- High-capacity HPs have a lower investment per energy. Table 1 shows GWHPs have particularly large relative capacity costs reductions towards 4-10MW, nearly the same investment as the equivalent capacity of an inefficient ASHP [64].
- For the same distributed demand, a central HP capacity is lower than individual HP systems, as peak demands do not occur simultaneously [65].
- Electricity grid losses are proportional to the square of the power transmitted, noted as significant for peak demands in France. Smaller units on the low voltage network are also less efficient [66]. Efficient HP systems connected to higher voltages induce lower relative electricity grid reinforcement costs [50].

Table 1: Specific total investment costs for different HP projects depending on the heat source and capacity [64]

Specific costs, million €/MW	Flue gas	Sewage water	Excess heat	Groundwater	Air
0.5 MW ≤ $HP_{Capacity}$ < 1 MW	0.63 to 0.53	1.91 to 1.23	1.30 to 0.97	1.72 to 1.18	1.12 to 0.90
1 MW ≤ $HP_{Capacity}$ < 4 MW	0.53 to 0.46	1.23 to 0.72	0.97 to 0.72	1.18 to 0.77	0.90 to 0.73
4 MW ≤ $HP_{Capacity}$ ≤ 10 MW	0.46 to 0.44	0.72 to 0.62	0.72 to 0.67	0.77 to 0.69	0.73 to 0.70

2.3.4. Low Temperature Geothermal Heat Pump

The GWHP system is preferred but the depth has not yet been delineated. For geothermal applications, the source temperature increases linearly with depth. For equal flowrates, this results in geothermal power increasing with depth. However, flowrates are geologically restricted, as shown in Fig. 9, by the decreasing geothermal power and levelized cost of energy (LCOE) amongst aquifers deeper than 1.82km. Namely, the contribution to geothermal power from linear temperature additions is less than the negated flowrate from exponentially reductions in permeability and thus transmissivity (product of permeability and net thickness) [7]. Furthermore, the decrease in LCOE deeper than 1.82km is more pronounced than the geothermal power reduction. This results from an exponential increase in operational power requirements for the hydraulic production pump to overcome resistance amongst more pressurised formations. This is highlighted in Fig. 10, in which a linear increase in pump pressure difference for a linear addition in flowrate (and thus geothermal power), will cause exponential reductions in geothermal COP [67].

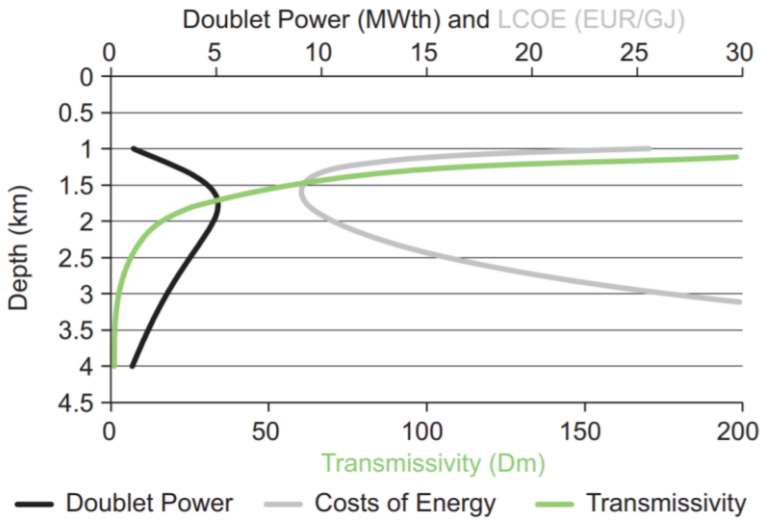

Figure 9: Doublet power and LCOE depth relationship from a DoubletCalc model of the Rotliegend Group

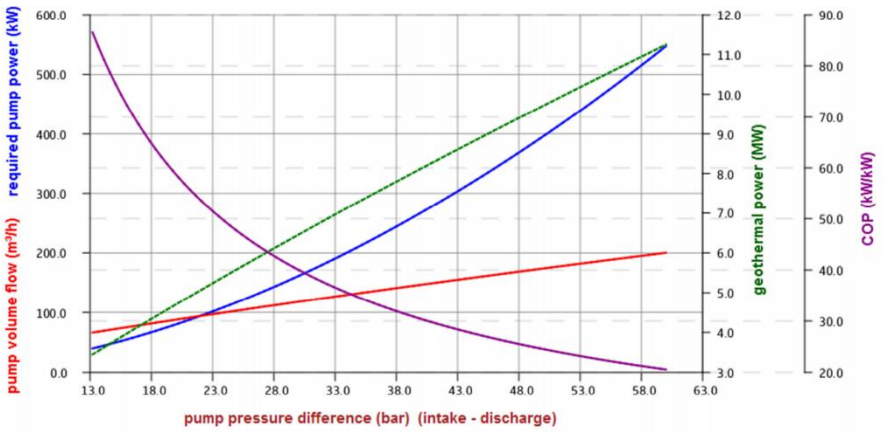

Figure 10: Fingerprint plot showing pump pressure sensitivity to input and output parameters

Although up to around 1.82km depth is generally cost-effective, a shallower geothermal system is a more pragmatic research avenue within dense urban environments. Compared to deep systems, shallower geothermal systems are likely to have:

- Lower relative drill price per m (depth is an exponential in the CAPEX equation) [68]
- Less space requirements [49], thus a viable geological formation is more likely to be synchronised to a spatial-legislatively viable urban space. Having production close to demand will reduce pipe length and thus distribution costs and thermal losses
- Lower investment and techno-economic risk during the drill and early operation phase, a benefit for attracting commercial interest [49]
- A deep geothermal project in Groningen was halted due to induced seismicity [69]. Shallower systems have a lower temperature difference and sediments are often less consolidated. These conditions both result in less stress and seismicity [70][71]

Shallow geothermal systems are preferred and hereafter discussed as the techno-economically pragmatic research solution for residential heat demand. The subsurface is often divided by depth for supervision and subsidy allocations. Shallow geothermal resources are often noted as 400-500m-bgl (below ground level) in several countries [72][73]. However, for research purposes, temperature is a far better and transferable technical delineation. Therefore, low temperature geothermal (LTG) is used, which is broadly standardised as being 20 to 55°C. This represents a common subsurface condition between 250 and 1250m-bgl [49]. Temperatures can be higher within these depths, but anomalously high geothermal gradients synchronised to urban environments are comparatively rare. Many outliers exist globally, such as cities with hot springs, which is a feature which may have once attracted the initial development.

For equal supply temperature and flowrate, the geothermal temperature increases linearly with depth. As previously shown in Fig. 6, the HP-only efficiency exponentially increases as the difference between source and supply temperature decreases. However, for the combined LTG-HP system efficiency, it is more complicated. As previously shown in Fig. 10, a higher-pressure difference (seen within deeper formations), will have a reduced hydraulic pump efficiency. Thus, exponentially less pump power is required to overcome hydraulic resistance at shallow depths which contain a lower pressure difference. Fig. 11 combines these two opposing forces of temperature difference (HP-only) and pressure (LTG), to determine the combined LTG-HP system efficiency amongst different LTG source temperatures. This is denoted as the seasonal performance factor (SPF), namely, the annual average COP. A fixed 70°C supply was used, as well as generalised pressure interpolations and equal flowrates for transferability [49].

Fig. 11 shows the SPF for the combined LTG-HP is relatively high for 15°C. However, many buildings require 80-90°C for comfort (not 70°C) [49]. Thus, a higher supply temperature will reduce the HP-only efficiency for a fixed 15°C source. A deeper LTG source can reduce absolute emissions if flowrates facilitate higher geothermal power, and if natural gas bycatch and electricity emission factors are low. However, as seen in Fig. 11, the 20°C source is modelled as having sub-optimal LTG-HP efficiencies. Above 30°C, higher relative LTG-HP efficiencies are noted, thus the relative and absolute emissions per thermal production is lower. The profitability depends on the additional heat benefits for higher drilling and pumping costs.

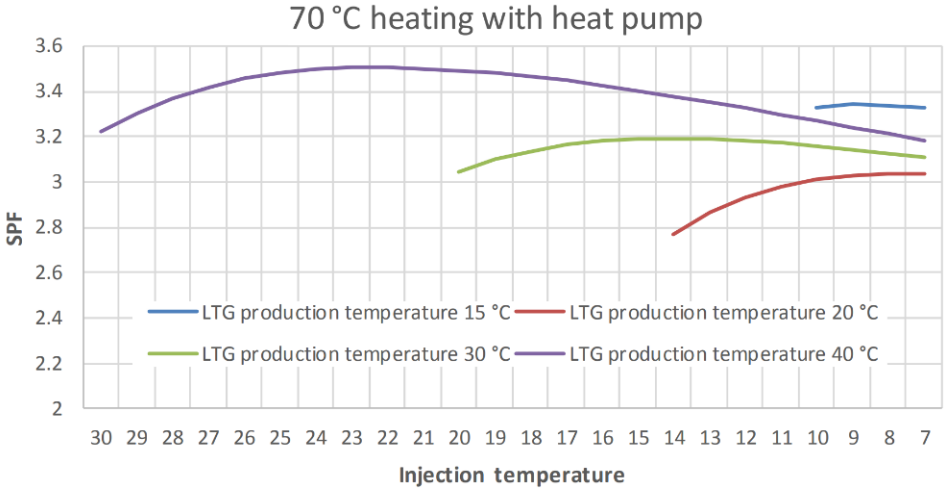

Figure 11: LTG-HP system efficiency trend amongst different source temperatures for a fixed 70°C supply [49]

2.4 District Heating Networks

Large heat demand revenues are required to warrant investments for drilling deeper. Thus, for residential application, often district heating networks (DHNs) are required to supply many individual end-users. DHNs distribute centrally generated heat via insulated water pipes and heat exchangers for space heating and sometimes domestic hot water (DHW) [74]. DHNs can facilitate technological inputs which are otherwise, spatially and/or economically unfeasible for decentralised consumers, such as GWHPs and waste heat from industry [13]. DHNs also allow more flexibility than individual system design, in the type and extent of auxiliary production and thermal storage. Also, numerous thermal technologies provide more nodes for the realisation of optimal cost and emission operational objectives. Therefore, flexible design and operation can accommodate economic and environmental stakeholder preferences [74].

4th generation district heating (4GDH) signifies the condition in which smart IT and lower network supply temperatures (30-70°C) can be applied [75]. These supply temperatures are possible amongst efficient buildings with low temperature heat emitter systems (floor, wall, and roof heating). Superinsulation facilitates very low space heating supply temperatures, however, DHW requires 55°C to avoid legionella bacteria. Higher temperatures are required if home storage is used, or large volumes exist between the heat exchanger and tap [76]. Many newly built low energy buildings regimes operate on a 55°C supply and 25°C return [77]. However, older buildings which have not been renovated require higher space heating supply temperatures, as the heating requirement per m^2 is higher [38].

Denmark, Lithuania, Sweden and Germany are in the transition from 3GDH to 4GDH. In 2016, the range of characteristic DHN supply and return temperatures were 80-86°C and 40-47°C respectively [78]. These annual average temperature regimes are characteristic to pre-1980 constructions in South Sweden [79]. A GSHP system in Germany for 127 buildings within a DHN (40°C space heating and 60°C DHW) had an estimated 64% less CO_2 emissions and 5% less annualised costs than the natural gas reference scenario [80]. As seen in Fig. 12, a newly established DHN (65/30°C) in Denmark which uses an all-electric collective GWHP is more cost-effective than 1800 individual home systems [63]. Therefore, the high GWHP efficiency and low relative investment capacity and electricity price resulted in cost reductions higher than the DHN investment and heat loss costs. Note that, different costs, benefits, taxes and subsidises apply elsewhere [63]. However, a large GWHP within newly built DHNs is indicated to be economically feasible for a 65/30°C regime in Denmark.

LTG-HPs within DHNs can be collective or individual. Collective is when a central HP system upgrades LTG before distribution. Individual is when LTG is distributed to multiple individual HPs within buildings or neighbourhoods [38]. No relevant documentation is available to determine the preferred system. The collective HP is favoured from the following deductive reasoning. The theoretical techno-economic benefits (Section 2.3.3) are shown to provide an optimal model for a collective LTG-HP within a Danish DHN. As the techno-economic performance of neighbourhood HPs within DHNs, lies between individual and collective HPs, the collective HP system is more likely to be economically (as well as spatially) pragmatic. Compared to low temperature distribution of the same supply magnitude, higher temperatures require lower DHN pipe volumes [81]. Fig. 13 shows that the lowest DHN costs occur when pipe diameters minimised, up to a limit, as cost increases exponentially for very low diameters (pump power costs rise exponentially). Thus, a large central HP system which supplies medium-high temperatures (80°C) to many existing buildings will have cheaper total DHN costs than the equivalent low temperature DHN [81].

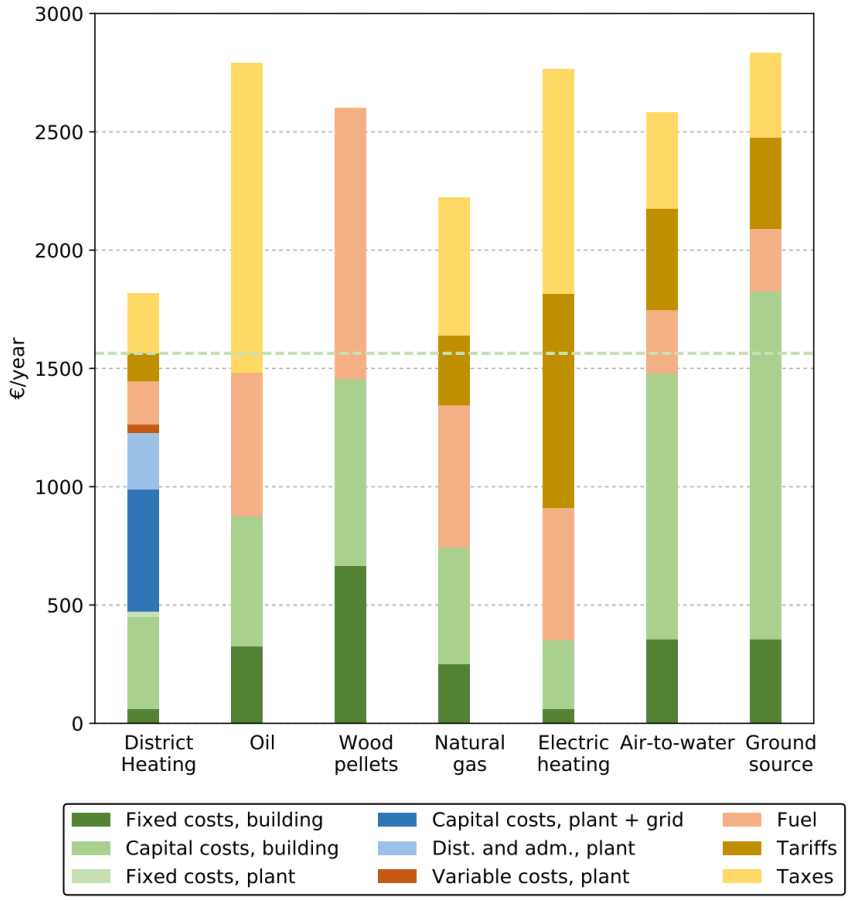

Figure 12: Danish heat price comparison between an all-electric HP within a newly established DHN and various individual systems

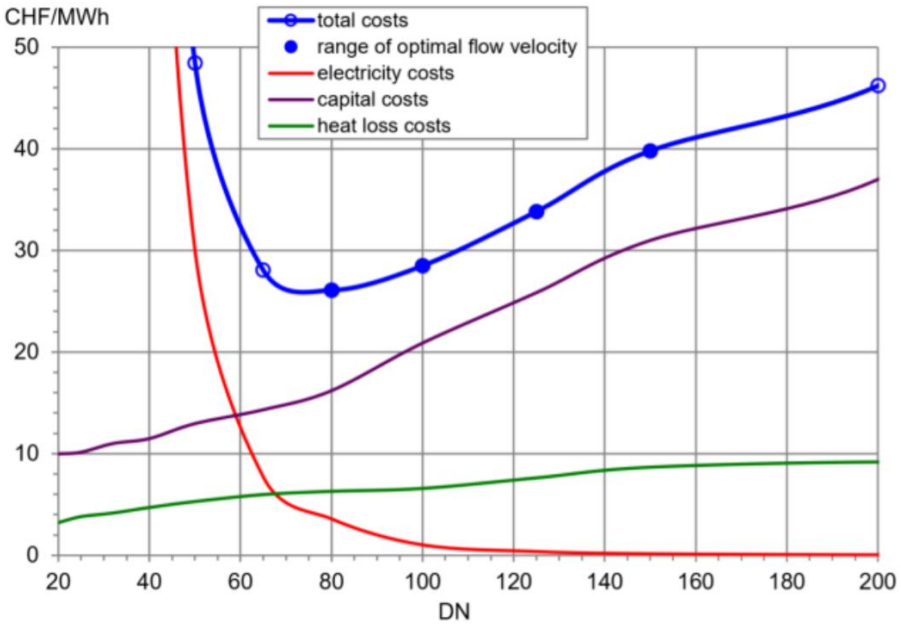

Figure 13: DHN (80°C) total costs as a function of the nominal diameter and divided into capital, heat loss and electricity costs

3.0 Scientific Relevance

Heat electrification has large theoretical emission reduction potential for fossil-fired buildings in countries with low or reducing electricity grid emission factors. It was deduced in section 2 that cold climates are more pragmatic avenues of investment. No universally optimal system exists as contextualisation is required to neighbourhood-specific production, storage and building conditions and barriers. The compatibility of individual ASHPs depends on the supply temperature and thus, the thermal efficiency of the building envelope. Also, compared to subsurface sources, ASHP systems are cost-ineffective, whilst larger GWHP systems within DHNs have theoretical and proof of concept techno-economic benefits. General subsurface indications of efficiency and cost-effectiveness suggest deeper than 700m is preferred [7][49]. This is corroborated by a Danish rule of thumb, which states that between 800-3000m-bgl is profitable [82]. This range matches the LTG in Albertslund, in which a 35-40°C source supplies space heating to 2200 high efficiency buildings via a DHN [83].

Deep and large systems in urban environments are more likely to have geological barriers and spatial-legislative restrictions, thus LTG is a technically and spatially pragmatic solution in urban environments. However, the subsurface between 250m and 1500m-bgl is relatively unexplored [49]. LTG is operational within residential DHNs in Thisted (Denmark), which has some of the lowest residential heat prices in Denmark. An LTG source of 48°C (1200m) and 44°C (1250m) is used in combination with biomass-fired absorption HPs, boilers and waste incineration heat [82][84]. Geothermal district heating is well established in France, with supply temperatures ranging from 56-85°C (1600-1800m) [85]. Despite viability in many areas, LTG-HP systems are inefficient for high supply temperatures. When large economic risk is considered, LTG attracts low commercial interest for old and inefficient buildings. Thus, LTG-HP research may be an economically viable option for such buildings, thus providing stakeholder another option to consider in the sustainable heat transition.

The documented operational or modelled centralised HP systems [49][63][80][82][84] within DHNs, utilise either medium-high temperature thermal resources, or supply residents with low-medium temperatures via a low-medium temperature geothermal resource. There is no available documented DHN which supplies a residential district with an LTG-HP temperature difference higher than 50°C. The only relevant and available detailed techno-economic analyses of LTG-HPs within medium-high temperature residential DHNs are in Denmark and The Netherlands [13][49]. However, difference prices and taxes apply and so the economic viability is mixed. Both studies used generalised parameters, thus the model robustness is low. The missing scientific gaps are hereafter discussed.

Denmark

The only available literature which economically compares residential LTG-HP systems within DHNs to individual systems is in Denmark. The study [13] indicated that an all-electric GWHP system has a better economic performance compared to individual systems. Low emissions are expected but the extent was unquantified. Although the economic methodology was detailed, the technical methodology was generalised, thus lacking overall accuracy. Table 2 describes this along with that an ideal, but unrepresentative system condition was examined. Resolutions to guide the system conditions and methodology is explained.

Table 2: The scientific gaps in the Danish case study [13] and respective resolutions to guide the research

Problem Description	Resolution
No Subsurface Context: As many systems were compared, LTG-HP is very generalised. The HP supplied 65°C from a DHN return temperature of 30°C, whilst the LTG source temperature is unsubstantiated. No depth is indicated, and as the LTG flowrate is unknown, the temperature cannot be solved from power. Using Fig. 11 (70°C supply) as a rough guideline, the COP of 4 used in the study suggests an LTG temperature of 40°C (1000m-bgl)	Using reliable subsurface parameters will facilitate accurate costs and HP efficiency. Thus, geological expertise is required to characterise a viable aquifer. The flowrate and temperatures can then be applied within a dynamic DHN model. This results in an hourly HP-only COP which can then be combined with the LTG production pump for an accurate LTG-HP system COP
Topology: The GWHP had both a static COP of 4 and pipe thermal losses of 8.5%. Capacity was generalised from a simultaneity factor and demand was determined via heat output per m^2 (using an outside temperature function). Furthermore, the ratio between LTG-HP (€0.7m/MW_{th}) and peak electric boiler capacity (€0.08m/MW_{th}) is unknown	Use a high resolution and representative thermal demand profile within a DHN thermal solver. This can facilitate accurate estimates of the HP-only COP, heat losses and topology capacity ratios. Such ratios can be rationalised from the thermal balance and tailored to the peak heat demand
Building Condition: 130m^2 buildings demanding up to 13800 kWh/year (49.68 GJ/year), and the minimum air temperature (-14°C) is an uncommon building condition. Thus, the model uses very high revenues per connection, especially for a supply temperature of 65°C. As shown, in section 1.2, the building efficiency barriers result in temperature regimes higher than 65/30°C. Thus, the COP will also be lower, adding further uncertainty to the economic viability for an average building	As the revenue per connection and COP (low supply temperature), is a higher than usual, a representative North European urban building condition is required. This is noted as being an average area of 71 m^2 [86], a demand of 36 GJ/year [87] and a minimum air temperature of 0°C [88]. The North European average DHN temperature regime is around 80/40°C (supply-return) [78] and an energy label D home [89]

The Netherlands

A static model concluded an LTG-HP system in The Netherlands can reduce primary energy consumption and CO_2 emissions relative to gas-fired heating systems (Table 3). Emission reductions expected to increase towards 2030 [49], as renewable capacities in the Dutch electricity mix increase. However, a positive LTG-HP business case (600m at 27°C for 1770 existing homes), is only possible if a connection fee of €2000-4000 per dwelling is applied. This is an additional fee on top of the SDE+ subsidy for an LTG-HP system. Although, economic data is detailed, accuracy is lost from technical data derived from static factors and annual averages. This was highlighted as a limitation and thus, an area of recommended further research. Contextual LTG data and a dynamic heat demand within a DHN model will facilitate accuracy. Namely, DHN pipe size and thermal losses and the GWHP electricity requirement, thermal output, and capacity. Auxiliary systems facilitate a thermal balance, and technical data provides a robust foundation for an economic and emission model.

Table 3: Modelled CO_2 emission reductions towards 2030 of a Dutch LTG system, with and without a centralised HP, relative to individual natural gas boilers [49]

Jaar	70°C with heat pump	50°C with heat pump	40°C direct
2017	35-38%	49-52%	71-80%
2020	47-50%	58-61%	76-84%
2030	61-63%	69-72%	83-88%

A contextual approach is required using hourly heat demand profiles. A thermal solver can then facilitate an accurate sizing of system capacities and the expected operational output amongst production, distribution, and storage. Different outcomes to [49] may be seen when accurately quantifying economic and emission topological performance. This can be achieved using the dynamic thermal solver CHESS (Controlled Hybrid Energy Systems Simulator), a proprietary software tool developed by TNO. Production and storage can be assigned an activation priority and the solver will attempt a thermal balance based on the desired temperature regime [90]. Therefore, CHESS serves as the technical foundation for the economic and emission analysis.

As the Dutch study [49] focused on providing transferable depth relationships, not a contextual approach, the technical subsurface and thus, topology parameters were generalised. The LTG in the approximate business assumed a max flowrate of 300 m^3/hr of 27°C geothermal fluid with an unknown Cp (specific heat capacity). The injection temperature was fixed at 8°C and operated at 2800 full load hours a year. However, injection temperatures should fluctuate with heat demand, and the flowrate methodology was unsubstantiated. Thus, 3D geotechnical data derived from a contextualised aquifer characterisation can facilitate a reliable indication of the maximum LTG flowrate. Then, CHESS simulates output profiles of flowrate and injection temperature (production temperature is fixed) for a robust estimate of LTG full load hours.

The extent of economic uncertainty (+/-30%) relates to unsubstantiated and approximate cost indices [49]. A rationalised economic and geotechnical uncertainty range is more reliable. A different study noted that the heat price was the most sensitive variable to the NPV (net present value) for a deep geothermal doublet [91]. The technical uncertainty for a geothermal project mostly relates to geological variables which influence the flowrate, as a fixed depth provides a relatively fixed temperature. Thus, geotechnical data derived from an aquifer characterisation can facilitate a rationalised estimated uncertainty range of flowrates. Although the residential heat demand uncertainty is also large, thermal renovations are difficult to predict and quantify with accuracy. Thus, the future development of the heat price is likely to be the most sensitive parameter, whilst also being a more justifiable range to embed within revenue scenarios.

To conclude, a positive economic conclusion from the Danish study is an unrepresentative and economically favourable building condition. However, the negative economic conclusion from the Dutch study is based on generalised technical inputs of the subsurface and DHN system. The only relevant and available literature on an LTG-HP system within a DHN has conflicting economic indications. However, both use generalised inputs and different cost and revenue structures. A more contextual approach for existing moderate-cold climate buildings is required. An aquifer characterisation is required for contextual accuracy, whilst also facilitating rationalised geological uncertainty ranges. When combining this data into the dynamic solver-based model CHESS, the cost and emission performance of the combined LTG-HP, thermal storage, and auxiliary production within a DHN, can be indicated. This facilitates the required accuracy for policymakers and project developers to accurately assess the viability.

A lack of existing residential LTG-HP systems and documented feasibility studies result in a lack of investment. Especially as preliminary indications of economic viability from tools such as ThermoGIS, indicate low probability of profit [92]. This is shown in Fig. 14, which shows an LTG-HP that utilises the Brussels Sand aquifer in The Netherlands (≈ 600m-bgl). The prevalence of 'indication' areas imply that many systems will have a 10% chance of breaking even (P10). Very few locations have a 'moderate' indication (P30) and even less areas have a 'good' indication (P50) [92]. While LTG-HPs are spatially pragmatic and technically feasible in many locations, investment is likely deterred from a P10 or P30 indication.

Most commercial investors require a business case based on P90 economic certainty [49]. Thus, at least P50 is required to persuade most stakeholders to fund a detailed feasibility study. The ThermoGIS regional indications characterise aquifers based on available borehole data in the 1x1km grid [68]. Thus, if data availability is low, interpolation will induce a high uncertainty. The average aquifer characteristics simply cannot represent the site-specific detail of fine-scale 3D models. Therefore, to facilitate a robust techno-economic model, the use of contextualised geotechnical data from well logs in combination with seismic interpretation is required.

ThermoGIS also assumes a vertical drill orientation, without flowrate stimulation measures. Additionally, an economic lifetime of 15 years is assumed, namely that investments must be returned within the duration of the SDE+ subsidy [68]. Although geothermal system lifetimes are often double or triple this [93], from an economic perspective, 30 years is a pragmatic time [94]. Note that, residential payback period requirements are cited to be around 7 years for a GSHP system [95]. As Fig. 14 shows, the LTG-HP system in the Brussels Sand Member within The Netherlands is unlikely to attract commercial interest in most areas. Despite this, a heat company who have experience with DHNs are interested in an LTG-HP system in the Brussels Sand aquifer in Zuid-Zwijndrecht, an area which has a projected P10 economic indication.

Figure 14: ThermoGIS regional economic potential within the Brussels Sand Member in The Netherlands

ThermoGIS omits the DHN costs, meaning heat is sold at wholesale heat prices to an external system operator. Yet, the wholesale price is only attainable and relevant for an economically viable system for both parties. Thus, for a realistic economic analysis, the responsibility of producer, distribution system operator and supplier, must be assumed. Before environmental performance estimates can apply, the economic viability of LTG-HP must first be guaranteed through comparison to individual systems. In the EU-28, heating systems are mostly fired by natural gas (Fig. 4) and the LTG-HP system must be cheaper to persuade end-users. This is also embedded in Dutch law, namely the "not more than otherwise principle' in which the Netherlands Authority for Consumers & Markets (ACM) determines the heat price at the end of each year [96]. As 95% of Dutch buildings are natural gas-fired, mostly boilers [12], a positive business case only applies when the sold heat is less than or equal to the projected equivalent annualised costs for individual natural gas boilers throughout the economic lifetime.

To conclude, new sustainable thermal production systems are required as built environment emission reductions are techno-economically constrained. Namely, the increased demand is projected to be higher than the energy saved from improved efficiency measures. Geothermal DHNs are a solution which, at greater depths, generally have an increase in techno-economic performance (costs and efficiency). Therefore, many deep systems within residential DHNs are in operation. However, shallower systems are likely to have less induced seismicity and spatial-legislative barriers within urban environments. Thus, LTG (20-55°C) combined with a large, centralised HP, is a pragmatic solution for many urban buildings. However, no operational LTG-HP within a residential medium-high temperature DHN is known to exist.

As the Dutch approximate business case [49] used generalised metrics, there is a need for more precise LTG and DHN data. For geotechnical ranges of maximum flowrate, the dynamic DHN thermal solver CHESS can estimate the LTG full load hours and injection temperatures from a specific heat demand profile. The output and capacity of all production, storage, and pipes, as well as thermal losses, aids in sizing the individual systems. Thus, CHESS facilitates a robust estimate of the required operational parameters of a single year, which is then used as an input for determining the techno-economic performance of the system lifetime. As the CHESS tool is in the development phase, the process of designing and modelling the network can facilitate user-orientated insights and recommendations to advance the tools development into the future.

4.0 Research Question

A generalised Dutch case study (28°C) [49] and a P10 ThermoGIS indication shown in Fig. 14 (31°C) suggests a low probability of economic viability. The Netherlands is an interesting research area for a contextual insight into seemingly negative yet generalised, LTG-HP economic indications. WarmingUP [16] are investigating various modes of DHN production in the town of Zwijndrecht. This is the research area due to confirmed geotechnical and spatial feasibility. Experts within HVC, a company with extended knowledge on collective production systems within DHNs, can provide reliable techno-economic data. Therefore, combined with a contextualised aquifer characterisation for reliable geotechnical data, and a dynamic DHN model CHESS for topological output and sizing, the techno-economic model will be robust.

This paper quantifies the economic and environmental performance of an LTG-HP system within a residential DHN in Zuid-Zwijndrecht. Performance is compared to individual natural gas boilers as per the not more than otherwise principle economic constraint. Therefore, an individual natural gas boiler becomes the reference scenario, noted as the business-as-usual (BAU) scenario. This scenario is compared to the collective LTG-HP system, via the levelized cost of heat (LCOH) and CO_2-eq (equivalent) emissions. For assessing the economic viability of the collective system, the net present value (NPV) is used. As heat prices were noted as the most sensitive parameter to a particular geothermal NPV [91], the economic performance considers current and projected heat prices, subsidy allocation brackets and connection fees.

This leads to the following research question:

What is the estimated economic and emission performance of a collective LTG-HP system within a Dutch residential district heating network when considering geological and economic uncertainty?

This is expanded into the following sub-questions:

1. What are the technoeconomic inputs, performance indicators, constraints, assumptions and factors required to develop an LTG-HP system within a residential DHN?
2. How can CHESS modelling facilitate estimates of annual operational output, capacity and efficiency amongst DHN components?
3. What is the estimated LCOH and operational CO_2-eq emission ranges over the 30-year system lifetime for the BAU and collective system?
4. What is the NPV of the collective system when considering geotechnical (flowrate) and revenue uncertainty?
5. What limitations and recommended required future research can be deduced from the modelling?

5.0 Scope: The Netherlands (Zwijndrecht)

In 2019, total operational emissions for the built environment reached a historical peak [97], accounting for 12.3% of total GHG emissions by sector, of which 70% were residential [98]. Following the Paris climate agreement, the Dutch government set targets for a 49% greenhouse gas (GHG) emission reduction by 2030 and 95% by 2050, compared to the 1990 level [98]. The Netherlands relied on natural gas more than any other country in the EU in 2019 and ≈95% of buildings were natural gas heated [12]. If new measures do not double annual $CO_{2\text{-eq}}$ reduction rates, the 2030 Dutch target is predicted to fail based on 2019 policy [98]. Centrally generated electricity emissions are projected to reduce 81.3% in 2030 relative to 2019 levels [98][59]. Therefore, electrification infrastructure designed and implemented today can reduce Dutch built environment heat emissions.

Groningen is Europe's largest onshore natural gas field. Production has consistently dropped since 2012 from environmental and seismic concerns, leading to The Netherlands becoming a net gas importer in 2018 [99]. Production will end in 2022, eight years earlier than planned [12], thus more gas imports can be expected without self-sufficient technological transition. Positive geopolitical foreign relations between gas producing and consuming countries, as well as pipeline countries in between is required. Germany provides most of the gas flows to The Netherlands of which extraction and transit depends on Norway, Russia and Denmark [100]. More secure and self-sufficient heat is required to reduce vulnerability of societal risk.

Groningen planned to become the first city to incorporate deep geothermal heat to a large urban area [101]. However, plans were halted due to induced seismicity [102]. No residential DHNs exist for the Dutch built environment which utilise LTG heat for upgrades via large collective HPs. Only an LTG-HP exists (31→60°C) in Zevenbergen for greenhouses. The Netherlands is a moderate climate with pragmatic potential from established technical, financial, and political infrastructure and support (subsidies). Also, the Dutch indications highlighted in Section 3 make provide a basis of comparison to the contextual study.

Investigations are ongoing for a collective LTG-HP within a DHN in the populated town of Zwijndrecht Spatial-legislative feasibility is known, and expert-interpreted well log and seismic surveys have confirmed the geological feasibility within the Brussels Sand Member. Zwijndrecht is annotated on Fig. 15, which shows the aggregated LTG potential overlain with a demand fraction map. Note that, the low synchronicity between thermal capacity and demand in Zwijndrecht, is not only the Brussels Sand, but an aggregation of all LTG layers. Fig. 16 shows the buildings in the system boundary were mostly constructed between 1950-1960 [103]. Fig. 17 shows the buildings are mostly between energy labels C and G [104. The space heating demand is derived from a DHN load recording in Alkmaar. When adding the DHW demand, the annual heat demand per home is 37.6 GJ/year (see section 6.6).

In nearby Dordrecht, HVC have applied waste incineration heat in DHNs and are considering an LTG-HP utilising an ≈ 650m-bgl aquifer in the Brussels Sand in Zuid-Zwijndrecht. The specific connection years and demand cluster magnitudes are withheld for privacy reasons and 2000 residential connections are assumed. Final connections are expected in 2028, with temporary natural gas boilers to be used until LTG-HP is operational. Geothermal drilling typically takes 2 years [68] and an economic doublet lifetime of 30 years is practical [94]. Thus, year 0 of the system lifetime occurs in 2028-29 (transitionary phase) and the full economic system lifetime when the LTG-HP is operational occurs from 2030-2060.

Figure 15: Zwijndrecht research area annotated on a demand fraction map overlain with LTG potential (all layers) in The Netherlands [49]

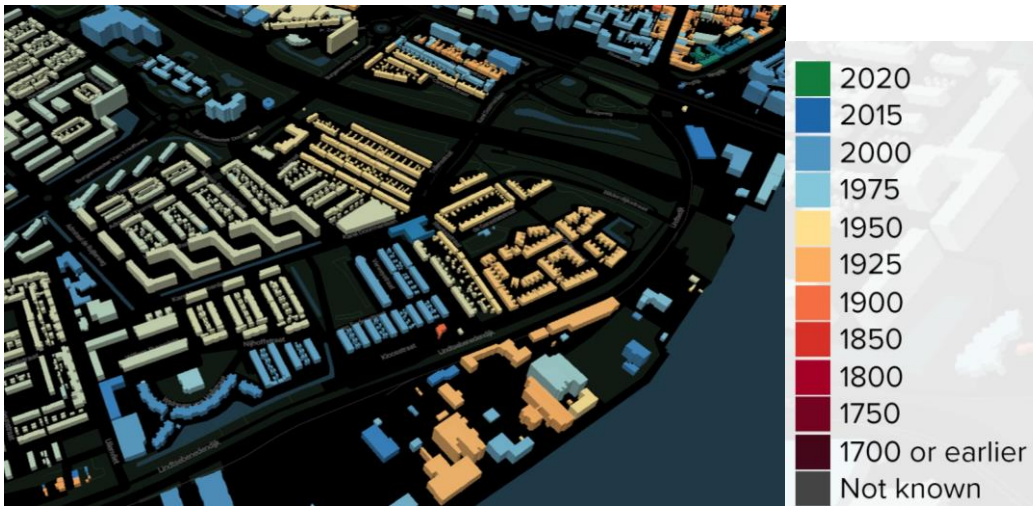

Figure 16: Construction year of buildings within the Zwijndrecht research area [103]

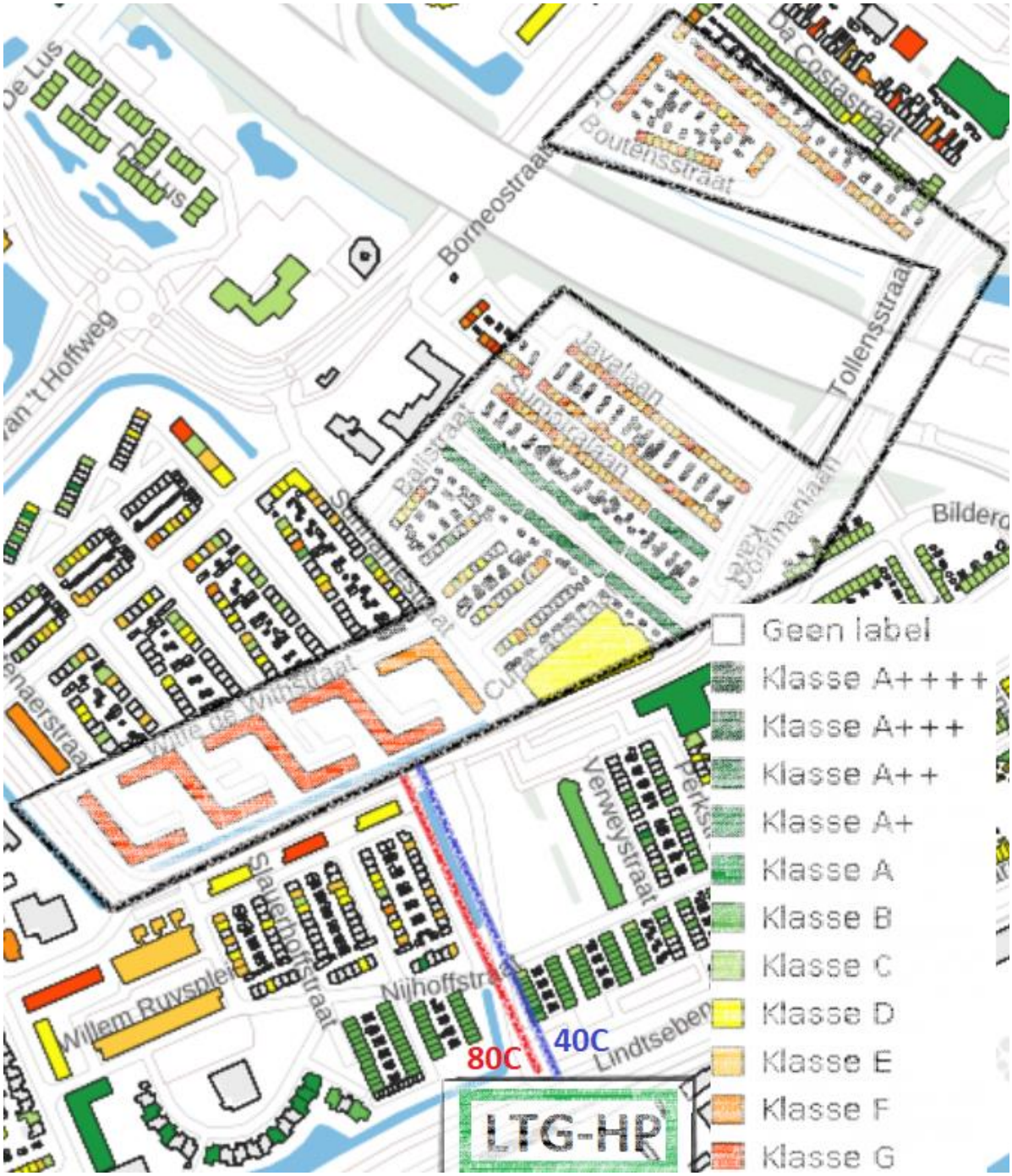

Figure 17: The research area in Zuid-Zwijndrecht annotated on the National Energy Atlas map, showing a mix in the distribution of energy labels [104]

6.0 Technical Methodology

To answer the sub-questions, the following phases in Fig. 18 guide the research process. Note that, national and regional feasibility indicators have been covered in section 5. The aquifer characterisation provided by WarmingUP is first described for LTG constraints, assumptions, and geotechnical data. The respective data is applied to the DoubletCalc1D tool, which derives the maximum flowrate and associated maximum production pump power requirement. The maximum flowrate then becomes an LTG constraint in the CHESS tool, for the primary side of the GWHP source. CHESS attempts to bring the topology into steady state (thermal balance) by solving for the user-defined heat demand profiles. The DHN component performance then provides techno-economic outputs for post-processing to derive annual operation and capacity parameters amongst production, distribution and storage. Note that, the methodological process is not so chronologically distinct in practice. As shown later, much overlap between the tools is required to refine the model for technical accuracy and to embed assumptions for the other.

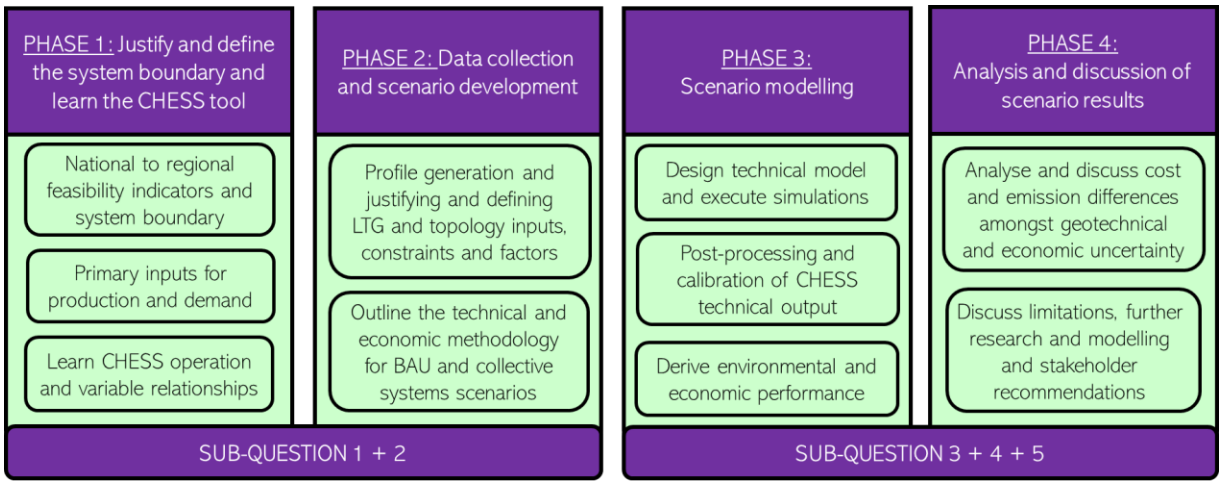

Figure 18: Phases and sub-questions of the research process

6.1 The Brussels Sand (Characterisation)

WarmingUP have characterised the reservoir properties of the Brussels Sand, namely porosity, permeability and geomechanical properties. A model covering 44x33km provides reliable reservoir properties estimations from 37 well logs, with a localised interpolation closer to Zwijndrecht from six wells [16]. The defining feature of a good quality aquifer for geothermal application is a thick layer of low hydraulic conductivity, adjacent to the aquifer. These are known as aquitards and reduce thermal dissipation which provide longevity to the thermal resource [105][106]. Also, thicker layers create higher aquifer pressures, which lead to more natural artesian flow [107] thus, reducing production pump power requirements.

Well logs provide mineral data which defines the type of equipment needed to detect the specific signal. Gamma ray logs detect radioactive clay minerals [108]. Glauconite (mica) was used by WarmingUP as a marker to defines the aquitard-aquifer transitionary boundaries in the Brussels Sand [16]. Fig. 19 and Fig. 20 show this in Zuid-Zwijndrecht and Appendix A

shows a 3D image of the porosity and permeability measurements within the Brussels Sand. No faults were detected and the aquifer temperature of 31°C is estimated by WarmingUP. The aquitard-aquifer transition from low permeable shaly-sand to clean sands is well defined, as well as the vertical and lateral extent of the reservoir. This facilitates an accurate estimate of drill length and transmissivity data for flowrate. The characterisation concludes a top depth of 550m, gross thickness of 200m and a net reservoir of 80m, mainly in the upper 100m (unit S3). Then transitionary shaly-sand (S2) occurs up to the transition towards the shale at 744m. The reservoir model concluded that 90% of the flow can be achieved at 700m and 95% at 733m. Thus, drilling deeper into layer S1 (740m) provides constant thermal benefit, but cost-ineffective flow rate benefits as permeability and porosity reduces. WarmingUP interpreted sonic logs to detect intermittent low permeable streaks (LPS) of carbonates. Although thin, the lateral extent is relatively large, thus the vertical permeability uncertainty is high. The transmissivity, estimated in Dm (Darcy metres), is a function of aquifer thickness, area, pressure, viscosity and permeability [109]. WarmingUP estimate 35-40 Dm in the region of Zwijndrecht. A low estimate of 30 Dm provides conservative leeway to account for LPS.

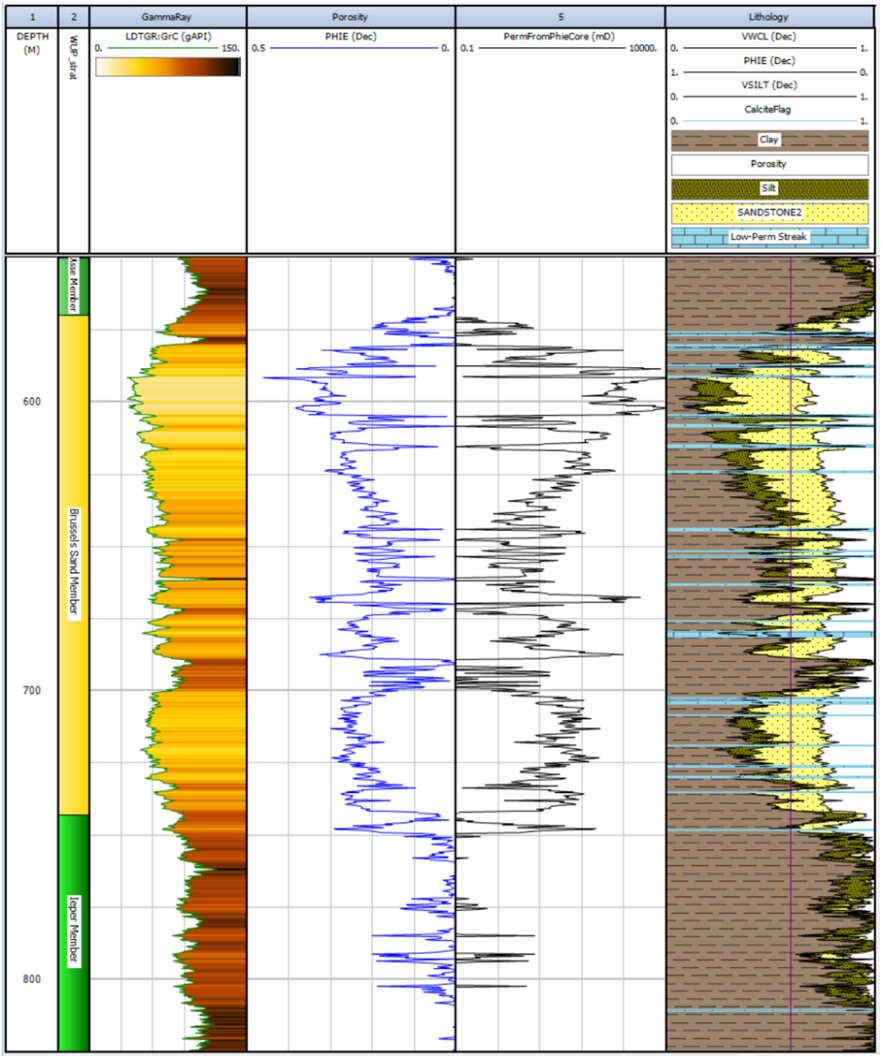

Figure 19: The reservoir properties of the Brussels Sand near Zuid-Zwijndrecht showing: Effective porosity (PHIE), permeability (PhieCore) and lithological compositions

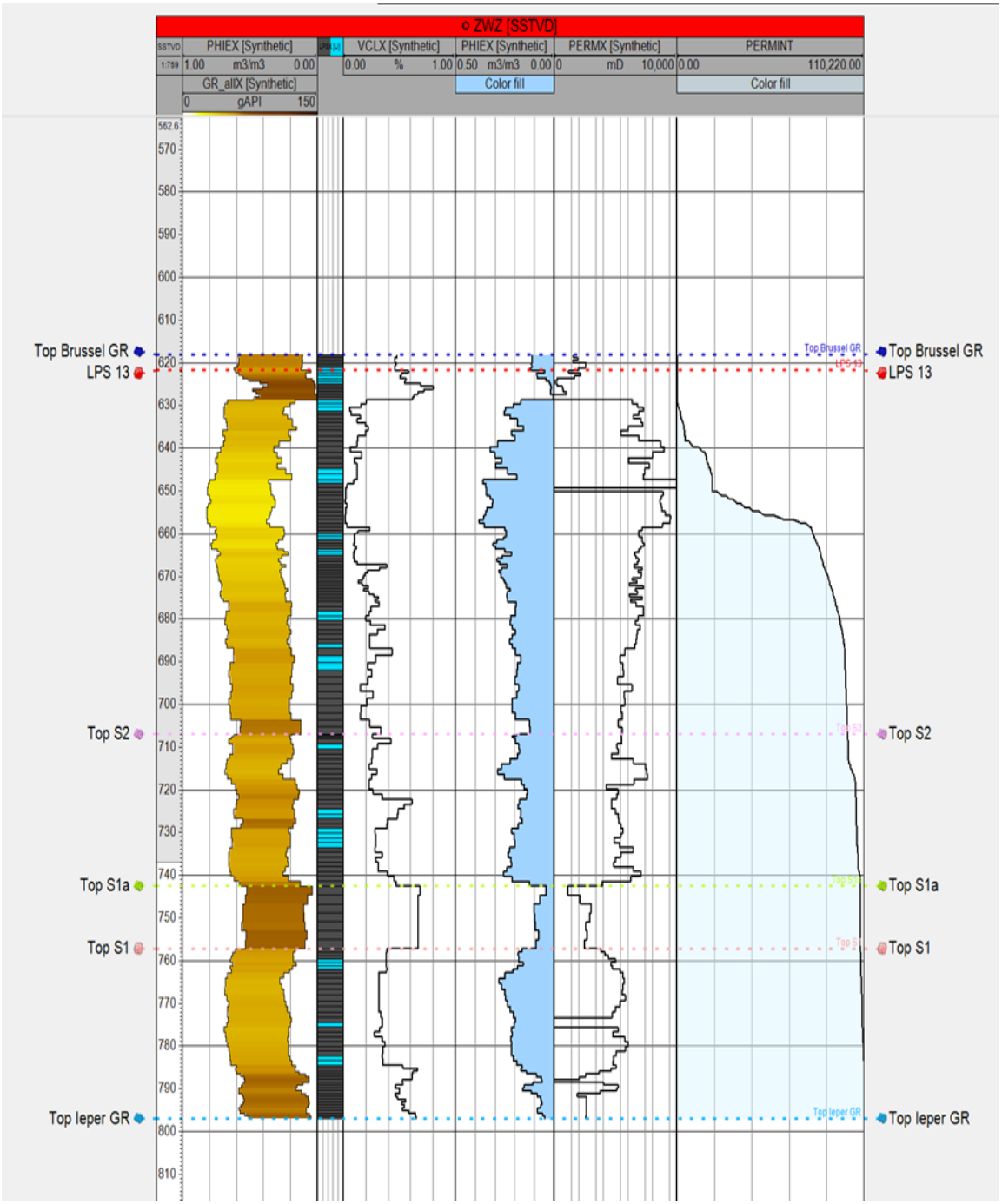

Figure 20: Intended future well placement derived from the WarmingUP characterisation of the Brussels Sand near Zuid-Zwijndrecht. The right-side shows the ratio of the total flow which can be extracted, highlighting 744m-bgl to be the maximum depth which should be drilled

6.2. Subsurface Constraints and Assumptions

Mass balance

All produced water is reinjected to ensure the mass balance. An equal mass flowrate therefore neglects any treatment of slurry, particles and scale. However, the main cause for accumulation of minerals on filters (scale) is from the degassing of CO_2 as production waters rise and depressurise [110]. However, the geothermal (greenhouse) project manager states a gas/water volumetric ratio of 0.06, which is low enough to warrant a closed system without a degasser. This also induces less corrosion and precipitation in the injection well [111]. Thus, a mass balance can be assumed amongst the doublet flow, as well as no degasser costs and emissions. The mass flowrate should be used at the HP component, as the lower temperature and higher density of reinjected water lowers the volumetric flowrate.

Thermal Balance

To avoid premature thermal breakthrough (interference), 1000m is assumed an acceptable doublet spacing between the production and injection well [49]. A different study conducted within the Brussels Sand indicated negligible regional groundwater flow [112]. An aquifer in The Netherlands showed that regional groundwater flow of less than 50 m/year provided an absolute energy balance ratio less than 4% [105]. Thus, low thermal interference (mixing) is expected in the Brussels sand between warm and cold plumes. This justifies the assumption that no changes to the production temperature is assumed throughout the 30-year duration. Also, during the early stages of production, heat loss is expected in the production well, as the colder ambient rock gradually warms up over time. This response time is not accounted.

Pressure constraint

Pressure constraints ensure no fractures occur and are case-dependent following specific SoDM (State Supervision of Mines) guidelines. Injection wells transport dense fluids, thus, have a higher maximum force than the production well [70]. Recently, fractures in injection well in Twente ceased operation due to safety concerns [113]. Thus, designing doublet operations within pressure constraints is essential for economic and environmental security. The principle vertical and horizontal stress depends on the formation and depth [114]. No analysis has been conducted at this preliminary stage; thus, generalisations are required.

The DoubletCalc1D (DC1D) pressure balance requires a user-defined constant pump pressure difference (Δp) between the two wells. The maximum Δp between the production and injection well constrains the maximum flowrate for safety [7]. A recommended Δp of 24 bar is used as injection pressures should avoid 15-16 bar [115]. An initial DC1D simulation shows around 10 bar at the producer and 13.5 bar at the injector. Thus, the injector pressure satisfies the recommended constraint. See section 6.5.3 for more about DC1D assumptions.

The hydraulic pump power is almost exclusively from the production well. DC1D does not model a separate injection pump, only the Δp of the loop. Although an injection pump may increase efficiency, it is not a requirement [67]. Thus, the pump power is assumed from a single ESP (electrical submersible pump) production pump, the required pump for the depths of the Brussels Sand. Lifetimes are long and service facilities are available worldwide. Up to 250m3/hr can be supplied within a 9.625" casing, which is the recommended minimum dimension for a geothermal well [116][117].

Injection temperature constraint

The maximum force occurs in the injection well during the maximum LTG-HP output, namely, during the lowest injection temperature and maximum flowrate. One reason for using DC1D is that geotechnical data can be translated to a maximum flowrate based on a specified pressure and injection temperature constraint. However, this provides insights only for the maximum output condition, which for a residential heat demand, does not occur often if auxiliary systems are used. Thus, the temporal extent is required to deduce the likelihood of fracturing. As the heat demand determines the injection constraint, the interchangeable use of DoubletCalc and CHESS is first required to understand the time duration to which the maximum force occurs.

A relatively low minimum injection temperature constraint of 5°C was first used in the CHESS simulation. As shown in appendix B1, the injection bar pressure is just below the recommended pressure constraint of 15-16. As shown in Fig. 21, a DHN system with a tank buffer and natural gas peak boiler, injection temperatures between 5°C and 6°C occur for only 39 hours in a year. Although, 8°C is often used as a safe minimum to avoid pipe fractures, the low frequency of such injection temperatures provides reasonable assumption of safety. The dynamic viscosity of the brine cP, namely, the product of force and time over area, only increases from ~1.4 cP to 1.5 cP when 8°C is reduced to 5°C. [115]. However, a more detailed geotechnical (stress) model is required before applying such system constraints after the initial design phase.

Injection (°C)	Hours
5-6	39
7-9	1962
10-12	722
13-15	720
16-18	681
19-21	1011
22-24	1051
25-27	2492
28-30	78
31-33	4

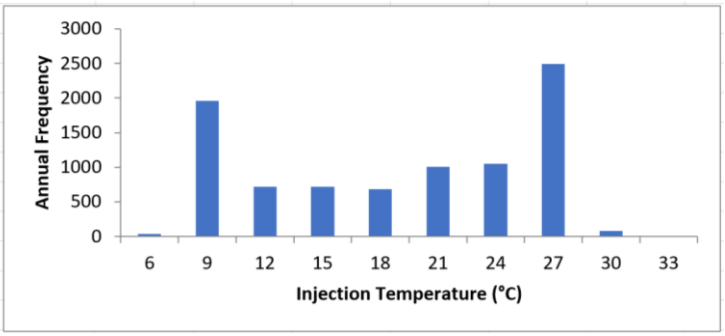

Figure 21: The annual injection temperature frequency distribution for the DHN system in Zwijndrecht

Operational constraint

A planned downtime for the LTG-HP maintenance of 5% each year (438 hours) is a typical assumption [118]. This may cover casing, tubes and filter inspection and cleaning to maintain flowrates [119]. Due to the low gas ratio mentioned previously in this section, the extent of mineral precipitation, namely, carbonates, can be assumed to be quite low. However, the low injection temperature does increase this risk [70]. Thus, 5% is a conservative estimate for a planned downtime during the lowest heat demand in summer. As later shown in the heat demand profile methodology (Section 6.6), no space heating demand is recorded during the 21st May and the 17th July. Thus, the LTG-HP downtime is extended to 650 hours. During this time, all demand is supplied by auxiliary technologies, namely, centralised natural gas boiler and thermal buffers.

The operational mode used in CHESS maximises flowrate and so is the last variable to reduce when demand lowers. Initial CHESS simulations of the network show that LTG extraction can fall as low as 0.2-0.3 MW. This operation is cost-ineffective when the ESP is operating at ~0.15MW rated power for the maximum flowrate, as extended use is likely to reduce the ESP lifetime and increase the re-investment costs during operation. Cleaning the doublet may require reversed doublet circulation [119], thus some ESP power may still be required. Negative thermal consequences are not quantified; however, 3.5 kg/s is applied post-process during the LTG-HP downtime. No thermal production supplies the DHN during this downtime, however, a low flowrate is maintained for both reverse cleaning, and to avoid cooling from a stagnant production well. The ESP power interpolation method highlighted later in Section 6.81 provides a negative value for such a low flowrate. It is unknown if the negative value is due to natural artesian flow, thus 10 kWh is used during these 650 hours.

6.3 Geothermal Output

The geothermal power equation is shown in Eq. 1 [67]. The only fixed parameters are a C_p of 3998 J/(kg·K) and ρ_w of 1021 kg/m^3. This represents values which are roughly 5% lower and 2% higher respectively than pure water, as the geothermal brine contains salt. This estimate is derived by solving for C_p and ρ_w from the DC1D output, for a salt content of 38g/kg (38000ppm), which is a representative estimate [120]. Although ΔT_i fluctuates, only the injection temperature deviates based on the demand profile. For a predetermined aquifer depth, the production temperature begins at a fixed value. The average geothermal gradient for exploration depths in The Netherlands is 31.3°C/km, which increases from an average shallow subsurface temperature of 10.1°C [57].

Equation 1:

$$e_{prod,i} = q_i \rho_w C_p \Delta T_i$$

$e_{prod,i}$	Geothermal energy production [W]
q_i	Geothermal water production flowrate [m^3/s]
ρ_w	Water density [kg/m^3]
C_p	Specific heat capacity of water [J/kg.K]
ΔT_i	Temperature difference between injector and producer at timestep i [K]

To increase LTG output, flowrate must be increased within the limits of the pressure constraint. Transmissivity is a defining variable for flowrate, namely, the groundwater flowrate under a hydraulic gradient through a unit width of aquifer thickness [121]. Thus, measures that extend the well exposure to larger areas of permeability are investigated. Increasing flowrate from mechanical or thermal stimulation is often quantified by a dimensionless negative 'skin factor', namely a zone of increased transmissivity. The skin factor characterises the well condition and degree of connectivity between the reservoir and well [122]. A positive skin represents when a well is damaged, such as from a mineral blockage.

Thus, treatments to increase flowrate are required through interventions which reduce skin. This can be as minor as the acidification of carbonates, or as extreme as hydraulic fracturing near the wellbore area [123][124]. High pressure surges which fracture the formation around the filter can cost €400-600k per well [119]. It may be necessary to rejuvenate extremely deteriorated flowrates to maintain the economic viability. However, this is not explored as a drill phase option, but rather, unforeseen costs (Section 7) provide sufficient leeway for such rejuvenation measures. Thus, a constant maximum flowrate over the system lifetime is assumed. To quantify flowrate depletion and rejuvenation over the system lifetime requires a formation-specific geotechnical analysis. However, the extent and vitality of a hydraulically induced negative skin factor is currently unavailable for the Brussels Sand.

An additional booster pump can increase pressure in the injection well and thus the flowrate [119]. It is not known whether LTG requires more force than gravity to overcome formation resistance for reinjection. Also, as the minimum injection temperature occurs during the maximum flowrate (CHESS), a further increase in the injection well pressure from a booster pump could cause unwanted pipe fractures. The Δp (24 bar) constraint cannot be extended, particularly as 5°C is assumed, which induces a maximum force very close to this pressure constraint. Also, DC1D cannot model a booster pump separately, thus, hydraulic fracturing and booster pumps are not explored. Deviated or directional drilling is the preferred mode.

6.4. Geothermal Directional Drilling

A method to quantify an increase in flowrate without precise geotechnical assessment is directional drilling. Deviated wellbores relative to the vertical can increase flowrate due to a heightened connectivity between the filter and the reservoir. Namely, more water can enter the well per second and per bar of drawdown. DoubletCalc can quantify the flowrate addition from deviations and is hereafter discussed. Fig. 22 shows the productivity (negative skin) improvements as the well orientation deviates from the vertical. Deviations less than 45° have an insignificant productivity increase, whilst past 45°, large increases occur [67].

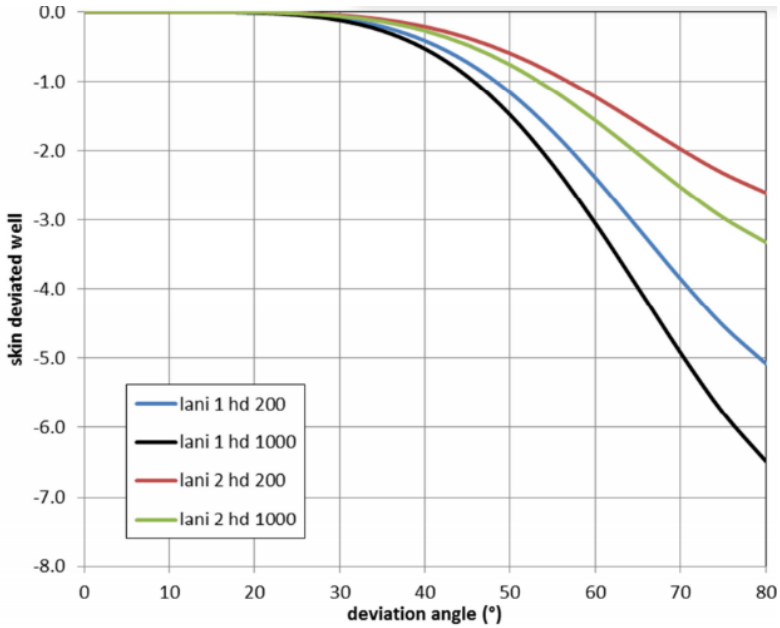

Figure 22: Skin due to penetration angle as a function of angle

A user-defined deviation in DoubletCalc will modify the vertical well simulation by quantifying the negative skin S_θ, as shown in Eq. 2. The model accuracy is corroborated by the validation methodology which considers four analytic methods [125]. The calculation of the negative skin factor applies for user-defined deviation angles up to 85°. Note that, r_w differs with depth and h and θ is measured perpendicular to the aquifer strata.

Equation 2:

$$S_\theta = -2.48 \frac{(sin\theta)^{5.87} \cdot {h_d}^{0.152}}{{I_{ani}}^{0.964}} \; for \; I_{ani} \geq 1$$

S_θ	Skin as a result of obliquely drilling the reservoir (dimensionless)
θ	Well deviation from the vertical (°)
h	Aquifer (sub)layer thickness (m)
r_w	Wellbore outer diameter (m)
h_d	Dimensionless aquifer (sub)layer thickness = $\frac{h}{r_w}$
k_h	Horizontal permeability (m^2)
k_v	Vertical permeability (m^2)
I_{ani}	Anisotropy index $\sqrt{\frac{k_h}{k_v}}$

Deviated drilling is beneficial for drill locations in urban environments which are spatially constrained. This can technically, such as a required voltage connection, or legislatively, such as a drill permit granted in a specific area. Hence why the industrial area of Zuid Zwijndrecht is the most feasible location. If large beds of low permeability are directly underneath the fixed location, a vertical trajectory cannot avoid unfavorable subsurface conditions. Thus, directional drilling offers flexibility through a radial dimension. This facilitates the avoidance of potential geological barriers and the realisation of penetrated zones of high permeability.

Relative to vertical drilling, horizontal directional drilling particularly benefits thin bedded aquifers, as the filter is exposed to larger regions of permeability [126]. A near horizontal well in Zevenbergen (85°), was drilled in the Brussels Sand 25km away from Zwijndrecht. However, the designed flowrates ($285m^3$/hour) could not be achieved, as sand clogged the filter and low vertical permeability impeded the flow. Replicating the intended horizontal design is seemingly harder than vertical drilling, thus a balance is required between additional flowrate and increased technical risk [127].

As the upper 100m of the Brussels Sand contains most of the net reservoir, the exploration thickness is not thin, compared to thicknesses of other geothermal aquifers (Vlieland and Delft Sandstone [128]). Thus, horizontal drilling is not a constraint, but a preferred measure to increase flowrate. Low permeable calcite streaks in transitionary layers are also present in Zwijndrecht, which result in intermittent lateral areas of high and low vertical permeability. Thus, as deviations increase towards horizontal, vertical permeability becomes a greater influence to the overall contribution of transmissivity. Thus, flowrate sensitivity increases as more risk is attributed to the prospect of the intended design not being replicated.

Although horizontal drilling can provide a significant increase in flowrate, this comes with a higher risk of low flowrates from sand blockage or if the intended vertical permeability is not achieved. Therefore, to reduce technical risk, a 75° deviation is preferred. From equation 2, this provides a -1.81 skin factor, which increases flowrate ≈20% relative to a vertical well (see Appendix B2). The deviation can be applied gradually as the pipe segments descend to 733m-744m TVD (true vertical depth). This is shown in Fig. X, along with the boundaries between the LTG, HP and DHN. The dogleg is the additional deviation per distance. It is assumed to begin at 50m, at which depth, 3° is added every 30m before reaching the 75° at the aquifer top. The production pump should be placed 200m-bgl [115]

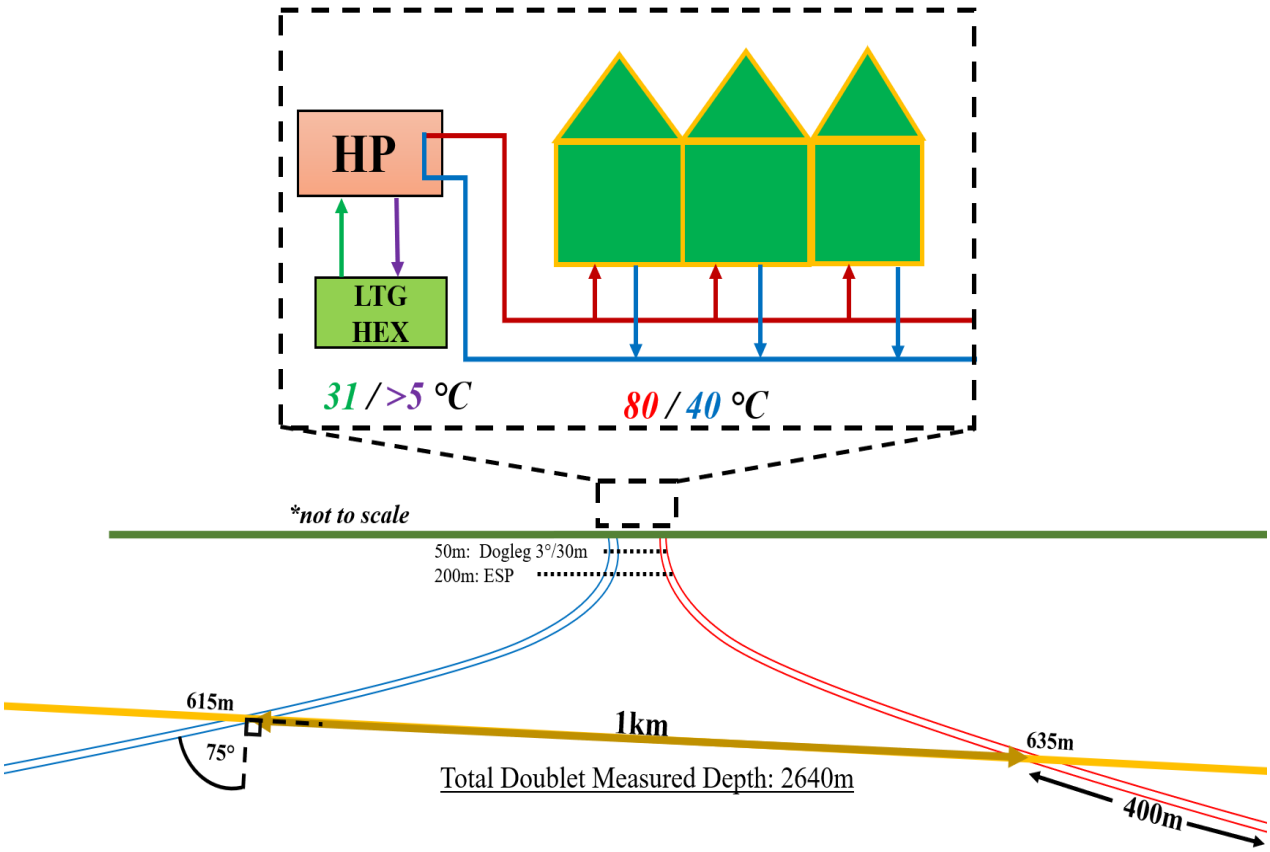

Figure 23: Schematic of the deviated drilling in Zwijndrecht and connection to the DHN system via an heat exchanger (HEX)

6.5 Geothermal Flowrate (DoubletCalc1D)

DC1D provides an indication of geothermal doublet power when specifying key technical parameters of reservoirs, casing schemes and pump properties. However, only the flowrate is relevant for an LTG-HP system, as the injection temperature is defined by the demand (via the HP). In section 6.1 and 6.2 the following was described: The aquifer transmissivity, the top and bottom aquifer depth at the producer and injector, the net aquifer, the deviation angle, the salinity, the pressure and temperature constraints, ESP depth, and the distance between the wells. The ESP pump-only efficiency is typically 70% [117]. The minimum injection temperature constraint has been defined, but not the profile over a year. Furthermore, the pipe dimensions are still to be defined. These are highlighted in this chapter. An overview of all DC1D technical parameters is highlighted in Fig. 26.

6.5.1 Injection Temperature

Although the geothermal power output is not directly used in CHESS, the injection temperature still influences the flowrate and ESP power in DC1D. As a single user-defined injection temperature input must be provided, the minimum injection temperature which occurs for 39 hours a year is not recommended. Density is a function of pressure, temperature and salinity. Viscosity and heat capacity are a function of temperature and salinity [67]. Although density increases with pressure (Boyle's Law) and decreases with temperature (Charles's Law) this mostly applies to ideal gases, as liquid water is barely compressible [129]. However, cold, dense and thus pressurised injection waters, will cause an increase in viscosity and thus ESP power requirements. This induces a considerably higher pressure drop effect in the injection well compared to the production well [67], as seen in Appendix B.

As the combined ΔP at the producer and injector is limited to 24 bar, flowrates will reduce when this limit is reached. The maximum flowrate reduces by $1/6^{th}$ if injection temperatures decrease from 15°C to 5°C. Therefore, as low temperatures increase viscosity [67], using a representative injection temperature to calculate flowrate is particularly important, especially for residential applications which derive large fluctuations in demand. The average injection temperature of 15°C shown in the frequency distribution (Fig. 21), is a representative basis to form the maximum flowrate constraint in CHESS. Namely, the fluid dynamic conditions are also an average.

6.5.2 Permeability

The transmissivity uncertainty range for the Brussels Sand in Zwijndrecht has already been described in Section 6.1. This serves as the foundation for modelling the influence of flowrate uncertainty which derives from the Dm geotechnical uncertainty (sub-question 4), namely, P90 (30 Dm) and P50 (35 Dm). Note that, the P10 (40 Dm) estimate is omitted as P90 economic certainty is often required for commercial investment [49], whilst the subsidy application requires P50 geotechnical certainty [130]. The transmissivity has already been defined, however, the permeability which comprises transmissivity is an input in DC1D, and must be tailored to replicate the results from the WarmingUP characterisation model. Small regions of high and low vertical permeability (LPS) detected in 3D cannot be represented in DC1D. As deviated wells derive most of the flow from vertical permeability, the anisotropic permeability ratio (kh/kv) is adjusted from 30 to 10 to recreate the 3D model [115].

6.5.3 Doublet Dimensions

Before simulating in DC1D, the pipe dimension is first rationalised. Increasing pipe diameter will increase flowrate up to a limit governed by the aquifer and well pressures. An increase in pipe diameter will eventually provide infinitesimal increases in flowrate. This limit is deduced by analysing flowrates from 5 outer diameters in DC1D, as seen in the standardised drilling dimensions in Fig. 24 [131]. First, modification is required. The inner drill casing is the outer diameter of the doublet; thus, pipe thickness is required for the inner diameter in DC1D. This is 0.5″ below 14″ and 0.75″ above [132]. Furthermore, a threaded connector is needed, namely some additional clearance space is required. This is 0.375″ for drills between 4 to 8.5″, and 0.5″ when above 8.5″ [133]. The cement thickness depends entirely on the formation stresses and is typically 0.5-1″ [133]. Cement is applied last as the required difference after quantifying the other component dimensions. The specific pipe sections are shown in Table 4.

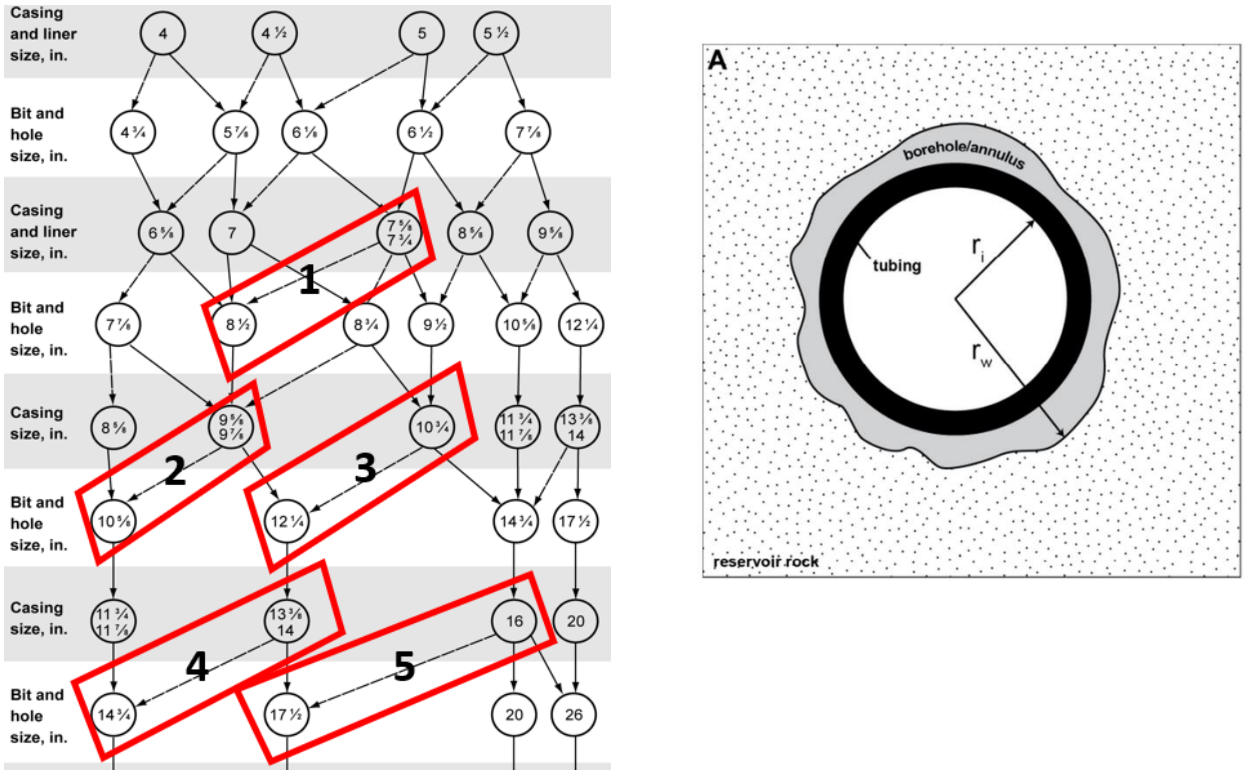

Figure 24: Standardised well dimensions [131] with a cross section of a doublet pipe [67]

Table 4: Estimated drill dimensions which result in the inner and outer pipe diameter for used in DC1D

Drill Dimensions (inches)	**1**	**2**	**3**	**4**	**5**
Hole and Drill	8.50	10.625	12.25	14.750	17.5
Clearance	0.375	0.5	0.5	0.500	0.5
Cement (flexible)	0.5	0.5	1.0	0.875	1.0
Drill Casing/Outer Pipe	7.625	9.625	10.75	13.375	16.0
Pipe thickness	0.5	0.5	0.5	0.5	0.75
Inner Pipe	7.125	9.125	10.25	12.875	15.25

As no specific cost documentation is available, the area per flowrate relationships is assumed to be a reliable indication. Fig. 25 and Table 5 shows the simulated relative flowrates per area amongst the well dimensions in Table 4. An additional smaller diameter was added to extend the trend. As shown, areas larger areas than 10.625″ have a steeper gradient increase, namely, less flowrate is achieved for the additional square inch of area. Therefore, an outer diameter of 10.625″ is a reasonable balance between additional flowrate and excessive doublet costs. The DC1D inputs and outputs are shown in Fig. 26. Note that, the transmissivity range detected by the 3D model has been recreated. The maximum mass flowrate for the P50 and P90 scenario is 36.2 kg/s and 30.92 kg/s respectively when an injection temperature of 15°C is used. The geothermal power should be neglected, as this is a CHESS output due to injection temperature also being an output.

Table 5: Numerical results area (inch) per flowrate (kg/s) simulated in DC1D

	Flowrate per Surface Area of Deviated Well (P50. injection 8C)					
Outer Diameter (inch)	**6.625**	**8.5**	**10.625**	**12.25**	**14.75**	**17.5**
Surface Area (inch²)	34.47	56.74	88.66	117.86	170.87	240.53
Inch² per Kg/s	1.10	1.66	2.44	3.18	4.52	6.25

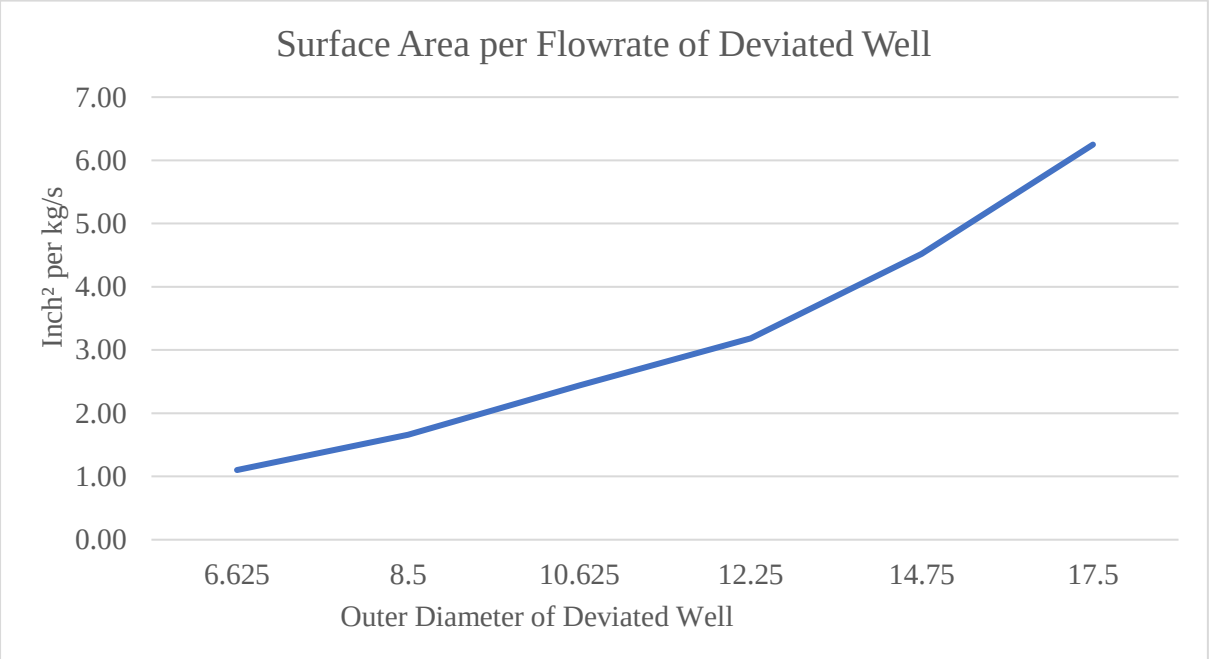

Figure 25: Graphed results from table 5 showing the surface area (inch) per flowrate (kg/s) simulated in DC1D, justifying 10.625″ to be an area-efficient pipe dimension for DC1D

Geotechnics (Input)

Property	min	median	max
aquifer permeability (mD)	500.0	700.0	800.0
aquifer net to gross (-)	0.5	0.55	0.6
aquifer gross thickness (m)	80.0	95.0	105.0
aquifer top at producer (m TVD)	572.0	635.0	699.0
aquifer top at injector (m TVD)	554.0	615.0	677.0
aquifer water salinity (ppm)	35000.0	38000.0	45000.0

Property	value
number of simulation runs (-)	1000.0
aquifer kh/kv ratio (-)	10.0
surface temperature (°C)	10.0
geothermal gradient (°C/m)	0.032
mid aquifer temperature producer (°C)]	0.0
inital aquifer pressure at producer (bar)]	0.0
[initial aquifer pressure at injector (bar)]	0.0
exit temperature heat exchanger (°C)	15.0
distance wells at aquifer level (m)	1000.0
pump system efficiency (-)	0.7
production pump depth (m)	200.0
pump pressure difference (bar)	24.0
outer diameter producer (inch)	10.63
skin producer (-)	0.0
skin due to penetration angle p (-)	-1.81
pipe segment sections p (m AH)	150.0,300.0,1320.0
pipe segment depth p (m TVD)	150.0,300.0,744.0
pipe inner diameter p (inch)	9.13,9.13,9.13
pipe roughness p (milli-inch)	2.0,2.0,2.0
outer diameter injector (inch)	10.63
skin injector (-)	0.0
skin due to penetration angle i (-)	-1.81
pipe segment sections i (m AH)	150.0,300.0,1300.0
pipe segment depth i (m TVD)	150.0,300.0,733.0

Geotechnics (Output)

Monte Carlo cases (stochastic inputs)	P90	P50	P10
aquifer kH net (Dm)	30.14	35.55	40.36
mass flow (kg/s)	30.92	36.2	40.8
pump volume flow (m³/h)	109.0	127.6	143.7
required pump power (kW)	103.8	121.5	136.9
geothermal power (MW)	2.01	2.37	2.74
COP (kW/kW)	18.3	19.6	20.9

aquifer pressure at producer (bar)	71.9	75.19	79.2
aquifer pressure at injector (bar)	70.9	73.89	77.76
pressure difference at producer (bar)	10.07	10.2	10.34
pressure difference at injector (bar)	13.3	13.44	13.58
aquifer temperature at producer * (°C)	30.7	31.84	32.96
temperature at heat exchanger (°C)	30.45	31.52	32.59

base case (median value inputs)	value
aquifer kH net (Dm)	36.58
mass flow (kg/s)	37.22
pump volume flow (m³/h)	131.2
required pump power (kW)	125.0
geothermal power (MW)	2.46
COP (kW/kW)	19.6

aquifer pressure at producer (bar)	75.18
aquifer pressure at injector (bar)	73.83
pressure difference at producer (bar)	10.18
pressure difference at injector (bar)	13.42
aquifer temperature at producer * (°C)	31.84
temperature at heat exchanger (°C)	31.54
pressure at heat exchanger (bar)	13.85

* @ mid aquifer depth

Figure 26: Overview of geotechnical inputs and outputs in DC1D for the Zwijndrecht case

6.6 Residential Heat Demand Profile

An annual hourly timeseries profile of the DNN load intended for 3300 representative home equivalents in Alkmaar is used. To transfer this to Zwijndrecht a 25% distribution loss is assumed between the measured DHN load (start of the network) and the end-user. From 3300 homes, the profile of one representative home is derived from an annual demand of 29.7 GJ/year. However, the primary backbone load recording in Alkmaar requires adjustment as local heat generation for DHW is absent. Thus, DHW is added to the profile by using a 79% space heating and 21% DHW demand ratio, which is typical ratio for a 32.5 GJ/year Dutch home [134]. The calculation of DHW is highlighted in Eq. 3, which is then added onto the space heating (SH) load recording to derive the total annual demand shown in table 6. The final heat demand profile for 2000 homes is shown in Appendix C.

Equation 3:

$$\mathrm{DHW_i} = \mathrm{SH_i} \cdot \left(\frac{1}{0.79}\right) - 1$$

Table 6: Annual space heating and DHW demand per connection and for 2000 homes in Zwijndrecht

SPACE HEATING + DHW		UNIT
Per connection	37,7	GJ/year
	10,5	MWh/year
Total (2000 homes)	75452	GJ/year
	20959	MWh/year

Two demand clusters of 800 (A) and 1200 (B) are used. When a single demand profile is aggregated, a simultaneity factor is often applied. This is due to peak demands not occurring simultaneously, meaning topological capacities of the pipes and HPs can be reduced [63]. No simultaneity factor is applied however, as the load recording represents many dynamic profiles within a DHN. It is important to note that the load was interpreted from a 65% higher demand (implying more residential end-users). This may suggest the relative regularity of simultaneously occurring peak demands is less in Alkmaar compared to Zwijndrecht. Namely, averaging the larger recorded load in Alkmaar may imply undersized peaks in Zwijndrecht. However, Fig. 27 shows the simultaneity factor relationship for space heating and DHW is similar after 200 homes [63]. Thus, the conversion from an Alkmaar demand of 3200 homes is a reliable representative of the associated peak demand for the 2000 homes.

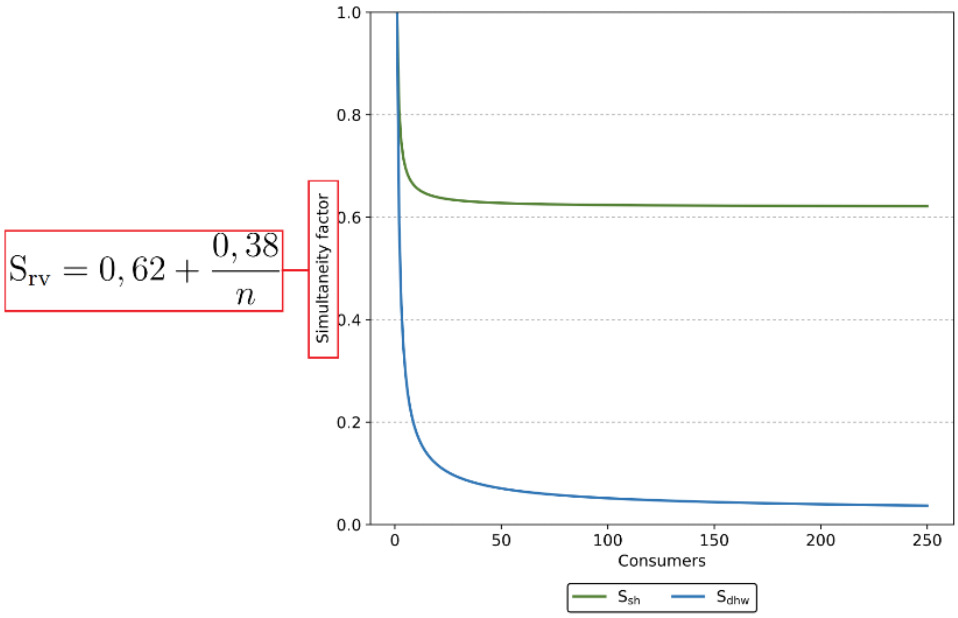

Figure 27: Annotated simultaneity factor relationships for space heating and domestic hot water preparation based on increased consumer distribution/dispersion [63]

6.7 CHESS

Conventional DHN design methodology typically leads to oversized network capacities and thus unrepresentative technoeconomic estimations. Typically, the forecast, plan, design and operation phases are executed sequentially, namely, from big picture to more specific operational details. This often results in sub-optimal design; particularly as oversized capacities aggregate onto other technologies [81]. As mentioned in section 6.0, CHESS is used to facilitate the mass and energy balance and preliminary sizing of the system for a specific time-defined simulation. Flowrate, temperature, and capacity constraints can be user-defined to coordinate operation under component activation priorities which can be tailored to stakeholder preferences. This derives operational and capacity data for the given simulation. This then guides estimates for investment and environmental performance.

Energy System Description Language (ESDL) serves as the initial base software for the system design via a map-based graphical user interface (GUI). This is where production, consumption, storage, transport and conversion capabilities can be techno-economically defined amongst various geo-orientated assets [135]. Tracing the network in ESDL facilitates a more realistic routing of the pipes than CHESS. Fig. 28 shows the ESDL trace which is then transferred to CHESS. Note that, the 2000 individual heat demand nodes from the primary distribution grid to a secondary distribution network is not possible at these resolutions. Thus, the secondary network thermal losses are accounted for in section 6.83.

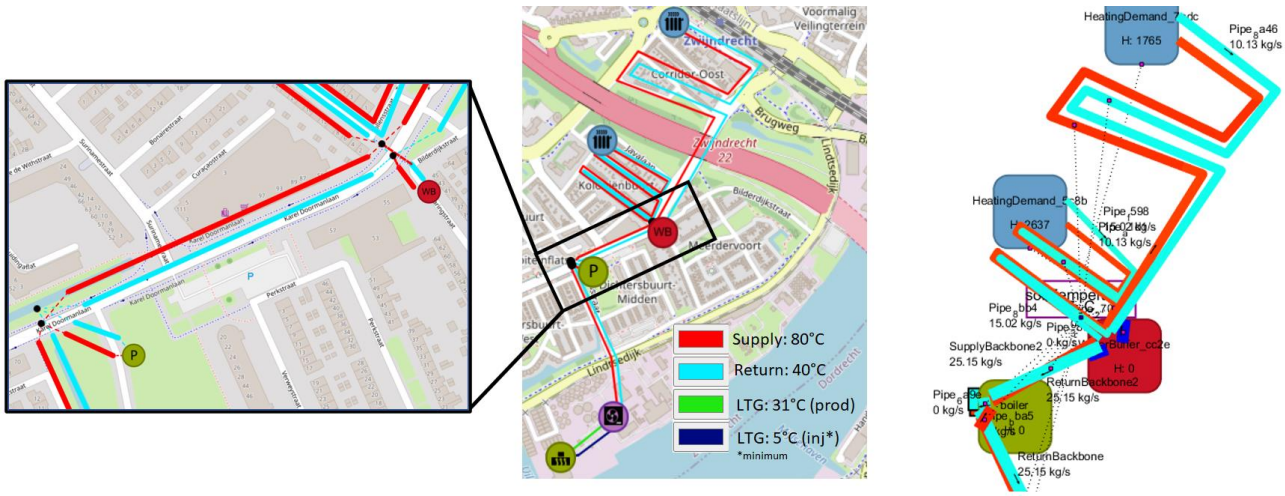

Figure 27: The ESDL map editor design of the system boundary. The geothermal production entering the 4-port HP is at the bottom (green-purple), the natural gas boiler is the green (P), the tank thermal energy storage (TTES) is the water buffer in red (WB) and the demand clusters are in blue

6.7.1 Constraints

Temperature

The intended (HVC) temperature regime for the primary backbone in Zwijndrecht is 85/45°C. However, during summer, only DHW is required, thus supply can reduce to 60°C [118]. This is the minimum temperature to prevent legionella bacteria [77]. However, CHESS can only model one temperature regime per simulation for each pipe. Thus, an 80/40 regime is more representative for the entire year. As mentioned in Section 3, 80/40 is characteristic of North-western European DHNs. If the desired supply and return temperatures are not met, the extent of imbalance is indicated by the variance in achieved temperatures in CHESS.

The ambient temperature profiles are required to model thermal losses. As DHN pipes are usually 80cm underground, soil temperature profiles must be used [81]. Table 7 shows the monthly soil temperature values provided by CHESS. For each timestep CHESS interpolates new values which approach the next monthly average. This method would be unsuitable for air temperature profiles, which require a larger time resolution to account for fluctuations. Fig. 28 shows soil temperature recordings 1m-bgl in The Netherlands [136], indicating very similar monthly recordings to the CHESS default values. As little monthly variance is seen, the interpolation method in CHESS between the average soil temperatures is deemed reliable.

Table 7: Monthly soil temperature (CHESS default values)

Date	°C
1-jan-19	5.3
1-feb-19	4.3
1-Mar-19	4.4
1-apr-19	6.5
1-May19	10
1-jun-19	13.5
1-jul-19	15.9
1-aug-19	17.1
1-sep-19	16.2
1-Oct-19	13.6
1-nov-19	10.3
1-dec-19	7.3

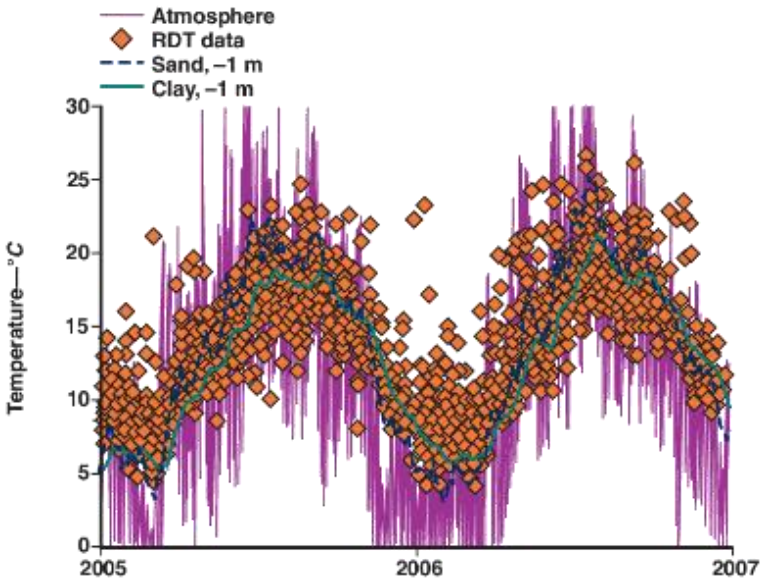

Figure 28: Soil temperature profiles 1m-bgl in The Netherlands [136]

LTG Flowrate

Operational mode 40 in CHESS operates the solver such that demand requested from the HP regulates flow as equal at both sides of the HP, i.e. the primary (geothermal) and secondary (DHN backbone). A preliminary simulation shows the secondary DHN flowrate is often lower than the maximum LTG flowrate. Thus, mode 40 results in low LTG flowrates and thus low COPs. Therefore, operational mode 50 is used, which calculates flowrate under an internal geothermal pump constraint for a given ΔT and geothermal power. This results in the maximum flowrate being achieved over 90% of the time, thus higher COPs are derived. The activation priority is user-defined to be the highest (1), as LTG-HP is the baseload supply.

DHN Capacity

No internal pipe DHN flowrate constraint is used in CHESS. This is possible through valves; however, pipe sizes are left flexible, and the appropriate size is tailored post-process to the simulated maximum velocity. This is noted as DN, followed by the nominal inner diameter of the pipe in millimetres. The primary distribution (backbone) has the largest DN and links the LTG source to the secondary distribution network. The primary distribution network has a total length of 1170m and the secondary network a total length of 5200m. If the DHN is well maintained, a lifetime of 50 years is possible [137]. Eq. 4 indicates how the minimum pipe diameter can be derived from the maximum volumetric flowrate (Q_w) and velocity (v_{max}) [138] which are CHESS solutions. Note that, an initial DN input is required for pressure and thermal losses calculations which reduce as DN increases due to less surface area exposure.

Equation 4:
$$d_{min} = \sqrt{\frac{Q_w}{v_{max}} \cdot \frac{4}{\pi}}$$

Table 8 is an example (P90) of the DHN pipe sizing. The appropriate DN is implemented post-process for the primary distribution network. The derived maximum flowrate and velocities of the distribution pipes for a one-year simulation in CHESS are shown. In this example, the pipes are almost always slightly oversized. Thus, the pipe size must be increased and constrained to the next standardised dimension, shown in green. The standardised pipe sizes and thermal conductivities of the pipe segments are shown in appendix D.1 [139]. It is common practice to oversize pipe diameters for the purposes of future expansions [61]. However, this generates unrepresentative economics for an initial assessment. This is expanded further in section 7.

Table 8: S= Supply, R= Return and A and B are the demand clusters. Two backbones are required due to auxiliary production (gas boiler) and storage (tank) as shown in Fig. 27

P90 / DHN Primary-Backbone / Buffer-2000m³ / Boiler-Priority-3					
CHESS PIPE NAME AND DESCRIPTION		m3/hr	vmax	DN (CHESS)	**DN**
SupplyBackbone	Backbone_S	122.9	1,01	0,208	250
ReturnBackbone	Backbone_R	122.9	0,99	0,209	250
SupplyBackbone2	Backbone2_S	182,37	1,50	0,207	250
ReturnBackbone2	Backbone2_R	182,37	1,47	0,209	250
Pipe_8bb4	DemandA_S	111,06	3,52	0,106	100
Pipe_f598	DemandA_R	111,06	3,45	0,107	100
Pipe_bba5	Boiler_R	75,97	0,61	0,209	200
Pipe_6a9e	Boiler_S	75,97	0,63	0,207	200
Pipe_a1d1	DemandB_S	72,61	1,03	0,158	150
Pipe_8a46	DemandB_R	72,61	1,01	0,160	150

6.7.2 GWHP

An all-electric GWHP is considered due to the predicted increase of renewable electricity generation in The Netherlands [98]. The preferred refrigerant is ammonia, due to a high COP of 6 for an evaporation and condensation temperature of 30 °C and 70 °C respectively. The same conditions provide a COP of 4.5 for refrigerant R134A [52]. Also, ammonia HPs use a reciprocating compressor, whereas R134a uses a screw compressor. The flowrate through a screw is generally much higher than a reciprocating compressor. So, whilst R134A can better meet the higher flow rate demands, a decrease in system efficiency occurs [140].

A vapor compression HP uses a reversed Rankine cycle [141]. However, the HP used in this study has different temperature glides of the external flows traversing the heat exchangers. Thus, the Carnot cycle does not represent the most efficient cycle. A Lorenz cycle with adapted temperature glides in both heat exchangers, minimises the temperature difference and thus entropy creation during the heat transfer [141]. Thus, the Lorenz cycle is used in CHESS. Note that, the HP is simplified to one unit, whilst multiple HPs are apparent in a cascading chain. Fig. 28 shows a comparison between the Lorenz and Carnot cycle [141]. Eq. 5 highlights the underlying COP function in CHESS. Eq. 6-11 shows the functions associated with a Lorenz cycle with multiple temperatures [142]. Table 9 highlight the specific thermal balance parameters for an ideal Lorenz LTG-HP in Zwijndrecht.

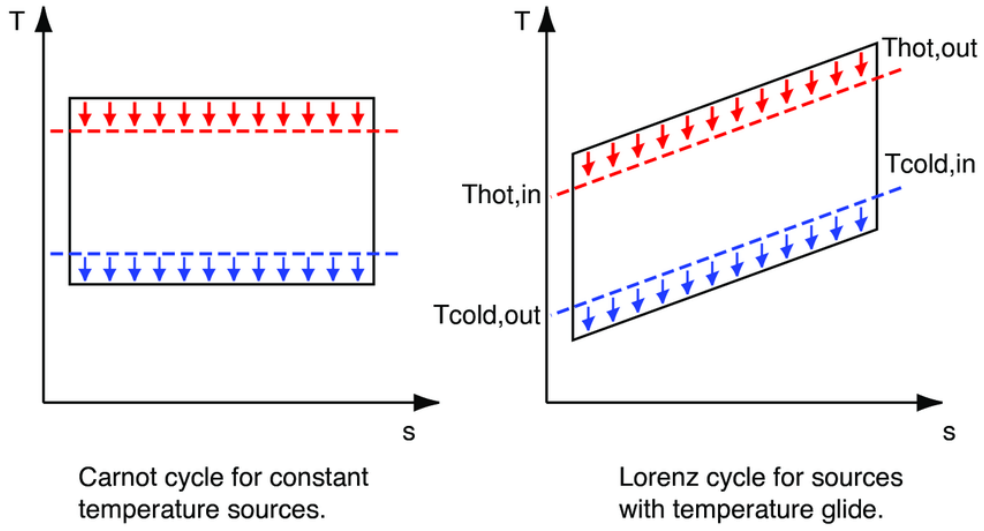

Figure 28: Comparison of Carnot and Lorenz cycles, respective to their adapted application cases. T = temperature and s = entropy [141]

Equation 5: $$COP_{HP} = \frac{Desired\ output\ (heat)}{Total\ input\ (work)} = \frac{\dot{Q}_H}{Q_{elec}} \approx \frac{\dot{Q}_L}{Q_{elec}} + 1$$

Equation 6: $$COP_{Lor} = \frac{T_{lm,H}}{T_{lm,H} - T_{lm,L}}$$

Equation 7: $$\dot{Q}_L = Cp_L\ \dot{m}_L(T_{L,i} - T_{L,o})$$

Equation 8: $$\dot{Q}_H = Cp_H\ \dot{m}_H(T_{H,o} - T_{H,i})$$

Equation 9: $$Q_{elec} = \dot{Q}_H - \dot{Q}_L$$

Equation 10: $$T_{lm,L} = \frac{T_{L,o} - T_{L,i}}{ln(T_{L,o}) - \ln(T_{L,i})}$$

Equation 11: $$T_{lm,H} = \frac{T_{H,o} - T_{H,i}}{ln(T_{H,o}) - \ln(T_{H,i})}$$

Table 9: The thermal balance parameters for an ideal Lorenz LTG-HP in CHESS

$\dot{Q}_L$	LTG power	CHESS solution (W)
Q_H	LTG-HP output	CHESS solution (W)
Q_{elec}	Total HP electricity	CHESS solution (W)
Cp_L	Specific heat capacity of LTG	3998 J/kg.k
Cp_H	Specific heat capacity of DHN	4181 J/kg.k
$\dot{m}_L$	LTG mass flowrate	CHESS solution (kg/s)
$\dot{m}_H$	DHN (backbone) mass flowrate	CHESS solution (kg/s)
$T_{L,i}$	LTG production	31°C
$T_{L,o}$	LTG Injection	CHESS solution (> 5°C)
$T_{H,o}$	DHN supply	CHESS solution 80°C for perfect balance
$T_{H,i}$	DHN return	CHESS solution 40°C for perfect balance

As the 4-port HP utilises secondary return flows ($T_{H,i}$) and LTG supply flows ($T_{L,i}$), the Lorenz efficiency is used. The Lorenz COP is denoted in Eq. 6, which represents the operation of an ideal HP utilising two varying temperature streams (glides), with constant heat capacities [142]. As mentioned in section 6.3, the specific heat capacities are not constant throughout and thus, 5% less power must be assumed to $\dot{Q}_L$. CHESS must solve for equation $\dot{Q}_L$, Q_H and COP_{Lor} and once the balance is satisifed, the HP electricity is then derived based on Eq. 9. Thus, Q_{elec} is a thermal balance solution.

The supply ($T_{H,o}$) of 80C and return ($T_{H,i}$) of 40C are desired objectives which are only met during a perfect thermal balance. The injection temperature ($T_{L,o}$) is determined by the value required to satisfy the thermal balance at a given timestep under the minimum temperature constraint of 5°C. Thus, $T_{L,o}$ fluctuates with heat demand whilst $T_{L,i}$ of 31°C is constant. As demand fluctuates throughout the year, minor imbalance from inertia occurs as the system calibrates. Thus, perfect thermal balances to the decimal are rarely met, whilst the largest imbalance is during large demand spikes, which have insufficient time allotted to achieve steady state. Especially if large pipe lengths separate demand from producers and buffers.

The maximum power constraint input for $\dot{Q}_L$ in CHESS for P50 and P90 scenarios is simply that which is derived from a $T_{L,o}$ of 5C and the maximum $\dot{m}_L$ which is derived from DC1D. This maximum condition is rarely reproduced in CHESS. The DC1D thermal balance only considers the primary (LTG) side, whilst the thermal balance in CHESS considers the primary and the secondary (DHN) side. Hence why two heat exchanger solutions must be solved within the thermal balance. Note that, for the purposes of CHESS modelling, the ammonia refrigerant acts as both heat exchangers. However, to prevent corrosion and fouling, an intermediate plate heat exchanger is often used [143]. This was also depicted in Fig. 23, as the bridge between the LTG and HP systems.

The thermal balance equations represent the condition of the ideal Lorenz cycle. Thus, a HP system efficiency must be defined, which is evidently a sensitive parameter considering the 30-year lifetime. The system efficiency depends on the refrigerant selected, if economisers (cascading) and internal control is used, and the size and design of the condenser compressor and evaporator [144]. This is often a compromise between efficiency benefits for the cost. Irreversibility reduction such as that from mechanical (compression), or thermal (refrigerant and the primary and secondary fluid) should warrant the investment. However, an exergo-economic analysis requires second law entropy rate [145][146], which is not available.
The heat pump system efficiency typically ranges between 50% and 70% for industrial heat pumps [52]. CHESS has a single system efficiency input, thus this must represent the system throughout the whole year. However, significant fluctuations are expected, as high thermo-mechanical losses are expected when the HP approaches max capacity.

To guide the determination of the system efficiency, some representative annual exegetic analyses are considered. An industrial pump upgrading 70°C waste heat to 120°C 10 MW (16 ton/hr) had a 50% efficiency [147]. An average Lorenz efficiency of 50% was observed for multiple Danish large HPs in DHNs. Project researchers set smaller heat HPs as 40% to reflect the poorer performance at small scale [148]. The average Lorenz efficiency for a 5MW shallow GWHP which upgraded to a minimum and maximum of 70°C and 85°C respectively (45°C return), had a Lorenz efficiency of 0.54 [148]. This GWHP is the closest documented representation to the system studied in Zwijndrecht. As the GWHP capacity and return temperature is slightly lower in Zwijndrecht, a conservative efficiency of 0.50 is used. Finally, large HPs for DHNs often have lifetimes of 15 years [149].

6.7.3 Natural Gas Boiler

A boiler must be considered due to unplanned and planned LTG-HP downtime. To eliminate the risk of unserved demand, sufficient boiler capacity is allocated to planned downtime and the day of the highest hourly peak demand. LTG investment price per installed MW is noted as 20x higher than a centralised gas boiler [150], whilst wholesale natural gas fuel is roughly half of the Dutch wholesale electricity price in 2030 [58][151]. Thus, having only the LTG-HP capacity would be cost-ineffective. Fig. 29 shows the frequency distribution (demand duration curve) for the two heat demand clusters. Above the annotated boundary, a natural gas boiler and/or a large enough storage is required. Industrial natural gas boilers with 98% load factors have a lifetime of 20-40 years. As the load factor is substantially less when used for a peak demand, 30 years is reasonable. As 48% of industrial boilers in the EU have an efficiency of 90% and higher, and another 39% has efficiencies between 85% and 90% [152], 90% is assumed. The lowest activation priority (3) is assigned to the natural gas boiler in CHESS.

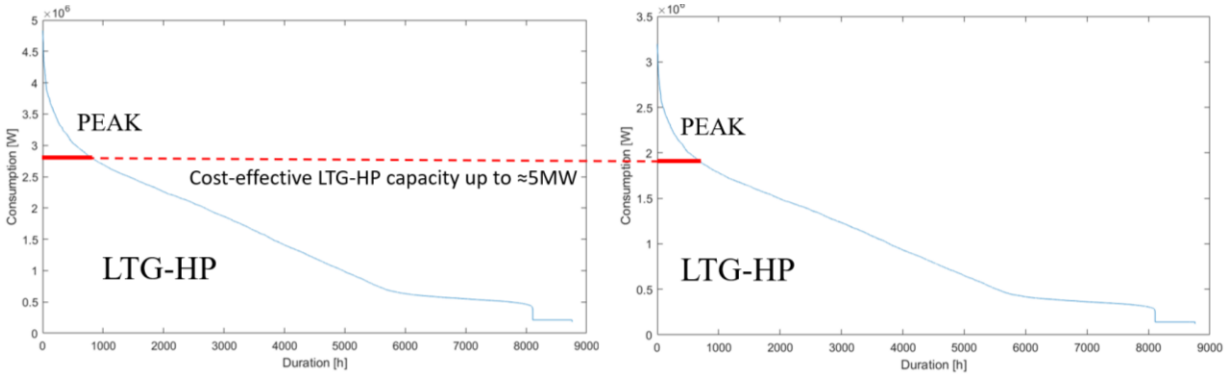

Figure 29: Annotated demand duration curve from a P50 CHESS simulation amongst demand cluster A (right) and B (left) showing the baseload-peak demand boundary

6.7.4 Tank Thermal Energy Storage

Depending on the generation type, the baseload usually covers between 50% and 90% of the total annual heat demand. Storage can reduce peak heat load and thus increases the baseload share [153]. Therefore, thermal storage facilitates higher LTG-HP output as activation can occur during low demand, to be used for high demands which surpass the LTG-HP capacity which is otherwise served by a boiler. A tank thermal energy storage is considered (TTES). Larger tanks have a higher efficiency from a higher volume/surface ratio. A state-of-the-art example is an Ecovat, which is an underground TTES made of concrete. High efficiencies of 85-95% at 90°C are noted. However, the smallest market option is 20,000m^3 (about 30 metres high and wide). This is unlikely to be placed above-ground in the Netherlands [154] and such a large underground storage is unlikely in Zwijndrecht [118].

An above ground TTES is to be used as a day-weekly buffer, with 2000m^3 recommended as the minimum for high thermal efficiency [155], and below 2000m^3 specific investment costs are high [156]. If unplanned LTG-HP downtime occurs during the peak demand day (156 MWh) January 18th, a 5MW boiler combined with a 2000m3 TTES can serve the worst-case scenario. For planned summer downtime, more than enough boiler capacity and space is available to serve demand. Note that, this situation is a test scenario. An activation priority of 2 is used in CHESS and only the LTG-HP is allowed to charge the TTES.

The TTES is assigned the middle activation priority (2). CHESS does not currently account for thermal storage losses and is post-processed into the results (section 6.8.3). The thermal losses are transferred to the 3rd priority natural gas boiler as additional TTES volume will result in value not synchronised to factory standard volume dimensions. An oversized TTES has higher losses and is cost-ineffective. Storage efficiencies are a function of ambient and stored temperature differences, insulation, the amount of full storage cycles, and volume [156]. Thus, generalising TTES thermal losses is difficult from contextualised literature.

TTES efficiency ranges between 50-90% [157][158]. The 80°C TTES in Zwijndrecht is unlikely to reach the high efficiency of the 90°C Ecovat, as volumes are smaller and ambient (air) temperatures are lower on average. Fig. 30 shows thermal losses as function of storage volume, and of temperature [159]. Both sources indicate characteristic TTES efficiencies between 50-75% for 1000m^3 and 5000m^3. Note that, thermal losses in these case studies are governed by many variables. For a 2000m^3 TTES, with a lot of cycles due to the day-weekly regime, a conservative efficiency of 60% is used and lifetime of 30 years is reasonable [154].

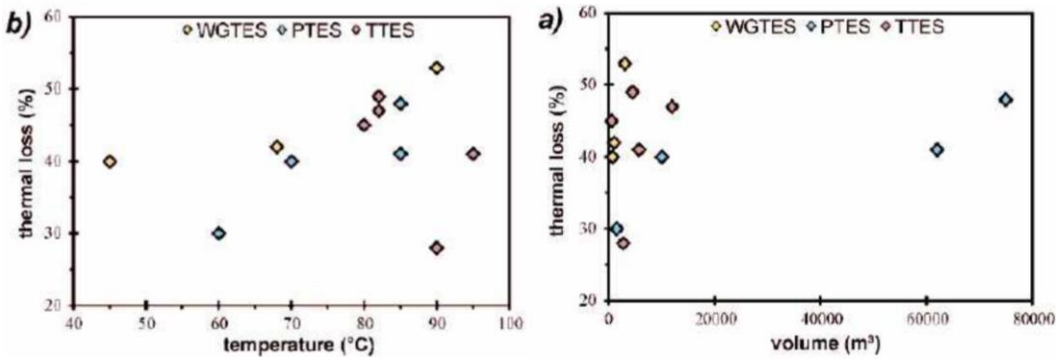

Figure 30: Thermal losses as a function of temperature and volume amongst various sensible thermal storages

6.8 Post-Processing

As CHESS is still in development, this chapter outlines the required adjustments to improve the technical model accuracy. These adjustments are made post-process, in the exported excel results. Additions and modification to the model concern ESP power requirements, geothermal power and thermal losses of the secondary distribution grid and the TTES.

6.8.1 ESP Power

The ESP from DC1D only applies to the maximum flowrate. Thus, ESP power requirements are required below the maximum flowrate by interpolating pressure and flowrate relationships. Eq.12 defines the ESP power requirements from doublet pump pressure difference (ΔP), LTG flowrate (q_i) and ESP efficiency (70%). Fig. 31 is an exported fingerprint plot and shows the relationship between ΔP and ESP pump power for the median P50 LTG case. To derive ESP power requirements below the maximum flowrate, Fig. 32, provides the quadratic function to interpolate ESP power as a function of q_i. The exponential work relates to resistance at higher pressures (see Fig. 10). As the quadratic interpolation function used to derive $e_{pump,i}$ from q_i uses a minimum limit of 10 bar (ΔP), a negative e_{pump} is noted below 42 m^3/hr. This occurrence is rare as the maximum flowrate occurs 90% of the time. For negative values that occur during the 650 hours of downtime, the ESP power is 10 kWh (see section 6.2).

Equation 12:

$$e_{pump,i} = \frac{q_i \Delta P_i}{\eta_{pump}}$$

$e_{pump,i}$	Required ESP electricity at timestep i [W]
ΔP_i	Pressure difference between injector and producer at timestep i [Pa]
η_{pump}	Pump efficiency [-] 0.7

Equation 13: $$e_{pump,i} = 352.38 \cdot \sqrt{30575003 - 160000 \cdot q_i}$$

Eq. 13 represents the ESP power interpolation formula derived from the DC1D fingerprint plot. Typical ESP system efficiencies (η) are pump (70%), motor (90%), cable (97%) transformer (99%) and converter (94%). This results in an overall efficiency of 55% [117]. Only the pump is calculated within DC1D, thus Eq. 14 accounts for the additional losses.

Equation 14: $$e_{total,i} = 1.243 \cdot e_{pump,i}$$

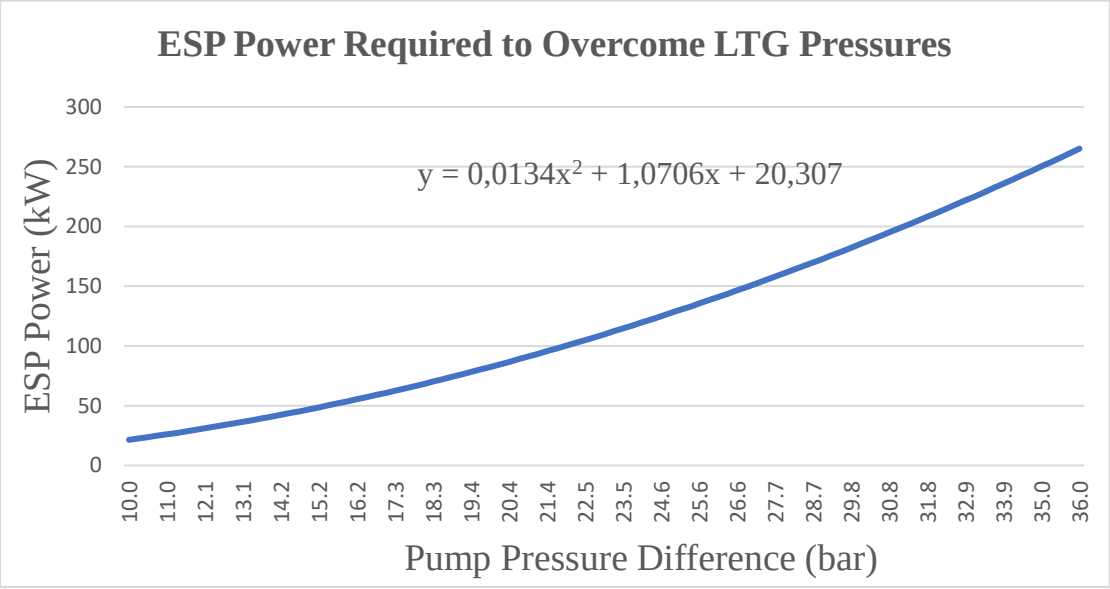

Figure 31: Exported data from a P50 DC1D fingerprint plot showing the required ESP power for a specific ΔP

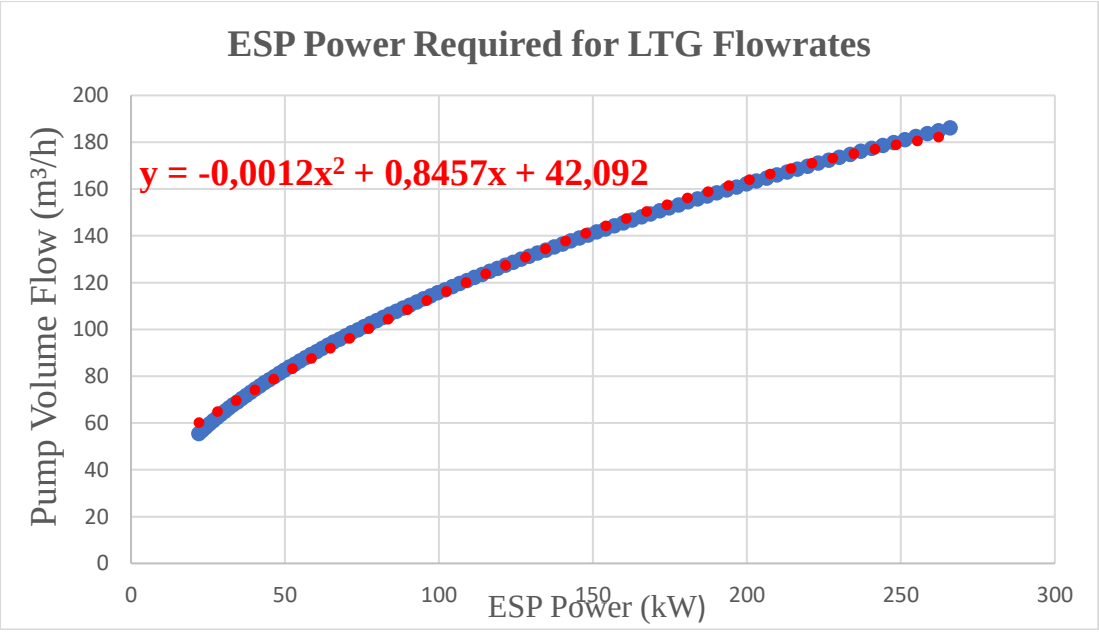

Figure 32: The quadratic function which is used to interpolate ESP power as a function of flowrate

Baker Hughes estimates a lifetime of around 5 years for a new ESP and this depends on the geological conditions, with corrosion being a typical large cause of failure [117]. There is generally a positive correlation between temperature and CO_2 and the corrosion rate for the range of temperatures applicable to Dutch doublets [160]. Therefore, LTG applications can be expected to have a longer lifetime than the average (deeper) doublet the 5-year estimate is based on. Furthermore, the average ESP lifetime is expected to increase into the future [117]. Thus, a lifetime of 6 years is assumed, with two purchases in year 0 as a back-up is required.

6.8.2 Geothermal Power

The CHESS fluid properties are universal to the LTG flowrate (one fluid property is defined in the .xml file). CHESS converts m^3/hr to kg/s with 1000 kg/m^3. However, geothermal fluids contain salts and only a volumetric LTG maximum flowrate can be set in CHESS. Thus, the volumetric flowrate requires an additional 2% to account for the geothermal brine having a density of 1021 kg/m^3. DC1D provides very detailed considerations to temperature, salinity, and pressure [67]. When solving for Cp_L, from $\dot{Q}_L$, 3998 J/kg.k is derived. CHESS does not distinguish between geothermal (Cp_L) and DHN (Cp_H) heat capacities. To resolve this overestimation, 5% less $\dot{Q}$, is translated via the COP at each timestep and the output difference is compensated by increasing the capacity and output of the gas boiler.

6.8.3 Thermal Losses

In CHESS, individual building demands are aggregated in clusters, as connecting 2000 secondary network branches to the primary backbone is impractical. Thus, secondary network losses must be accounted for. Primary network losses are recorded as around 5% of the total production. CHESS solves this from the ambient air temperature profile (Fig. 28) and the pipe length, diameter, and thermal conductivity. Despite the low primary distribution losses, the secondary distribution network losses are high due to the increased surface area exposure. Total network losses for high temperature networks account for 10-30% [161].

A business case for a DHN in Amersfoort and Brassem both used a total thermal distribution loss of 15% for a 70/40 temperature regime [162]. Thus, an 80/40 temperature regime is likely to have total losses of 20%. The annual average primary backbone thermal losses are ≈5%, thus an additional 15% of total production is post-processed into the exported CHESS results. As the max LTG-HP capacity is often reached, 15% of demand is added to the natural gas boiler. This results in additional fuel annually and a higher capacity cost for the boiler.

CHESS simulates the TTES as an ideal buffer without thermal loss. Storage efficiency is often expressed by degree of utilisation for the proportion of stored and withdrawn energy. Thus, internal and external energy losses must be accounted [157]. External losses are accounted by the primary DHN pipes, thus internal losses are required. The TTES is used as a day-weekly buffer, however, the rule-based control in CHESS maintains maximum capacity during the summer, thus simulating a seasonal storage. A model predictive controller would ensure a fully discharged buffer during summer, to reduce large thermal losses. Thus, thermal losses per hour are best quantified from discharged energy not stored. Eq.15 is used to calculate thermal losses from energy discharged (η_{total} is 60%). This energy deficit is transferred to additional natural gas boiler capacity and annual output.

Equation 15: $$Thermal\ Loss\ (MWh) = \frac{Discharge\ (MWh)}{\eta_{total}} - Discharge\ (MWh)$$

As the annual simulation is applied to a 30-year economic lifetime, the volumetric difference between the first and last hour is negated. This is expressed in the adapted Eq. 16 [163]. Note that, the TTES volume begins at half capacity to facilitate steady state as the simulation starts at high winter demand. The energy which is embedded within the initial starting capacity from year is also negated by 1/30th of 1000m^3, as per the economic lifetime.

Equation 16:

$$Q_{TTES} = \frac{\left(\Delta V + \frac{0.5V_{max}}{t}\right) \cdot \rho \cdot c_p \, (T_{max} - T_{min})}{3.6 \cdot 10^9}$$

Q_{TTES}	Thermal correction for TTES (MWh/year)
ΔV	Tank volume difference from start and end of year (m^3)
t	30 (years)
ρ	998 (kg/m^3)
c_p	4181.3 (J/kg K)
T_{max}	80 (°C)
T_{min}	40(°C)

6.9 Business as usual (HR-Boiler)

The collective system is compared to the technical and economic performance of a business as usual (BAU) scenario. It is a legal requirement in The Netherlands to not charge more than 'otherwise' for heat, which is 95% from natural gas, mainly individual boilers [12]. Heat prices are regulated by the ACM each year in accordance with this principle for the average Dutch home [96]. The HR-Boiler is used as the baseline. HR-boilers extract almost all the heat from natural gas combustion and extra heat from flue gases. This results in a high efficiency for space heating (104%), whilst DHW is less (72%) [164]. Using the ratio of space heating (79%) and DHW (21%) from Section 6.6, the relative efficiency is 97.3%. Note that, this ultimately depends on the usage characteristics. The average lifetime used is 15 years [164]. The natural gas the emission factor is 203.04 kgCO_2-eq/MWh and is mostly consistent but is slightly refined each year [165]. Table 10 shows all the macro-technical variables from section 6. No change in efficiency is assumed throughout the lifetime as the individual systems are mature, such that additional gain towards the maximum theoretical efficiency is likely to be infinitesimal.

In 2030, the equivalent carbon emission per kWh of central electricity production is predicted to be 0.09 kgCO_2-eq/kWh. This is an 81.3% reduction relative to 2019 (0.48 kgCO_2-eq/kWh) [58][59]. The 2030 emission factor is used from 2030-2060 and represents the consumer-side energy, meaning electric power transmission and distribution losses are already accounted. As predictions are rationalised from upcoming projects, a lack of 2050 project data means that the 2030 emission factor is the most accurate future estimate. Policy targets are not considered as large uncertainty exists for the predominant direction of electrification, storage, and hydrogen infrastructure [12]. The precise role and extent of these technologies determines the electricity emission factor. Uncertainty is large for fast ramping natural gas turbines, which are projected to account for 30% of the 2023 Dutch power mix, but between 5 and 27% in 2050 [166].

Table 10: Macro-technical variables used amongst the individual system components

MACRO-TECHNICAL VARIABLES		
Emission Factor ($kgCO_2/MWh$)		
Natural Gas	203	
Electricity (2030)	90	
Lifetime (Years)		**Efficiency (%)**
LTG	30	-
ESP	6	55
GWHP	15	50
TTES ($2000m^3$)	30	60
Central Boiler	30	90
Individual HR-Boiler	15	97
DHN	≈50	≈80

7.0 Economic Methodology

In this section, the methodology for determining the economic performance of DHN components and the individual natural gas boiler (BAU scenario) is derived. Technological investments use a current price estimate from either capacity functions, absolute values or from expert estimates. To estimate and assess the economic performance of the P50 and P90 scenarios, the annualised costs and NPV are used. To compare to the collective system to the BAU scenario, the levelized cost of heat (LCOH) is used over the equivalent system lifetime. A summary of all macro-economic variables highlighted in this section are first shown in Table 11. This provides context to the different system costs which are elaborated hereafter. If prices do not require technical results the total costs are simply presented.

Table 11: Marco-economic variables used amongst the individual system components

MACRO-ECONOMIC VARIABLES		
Financial		
Equity ratio	30	%
Debt ratio	70	%
Cost of Equity	15	%
Cost of Debt	2	%
Corporate Tax Rate	22	%
Economic Lifetime	30	Years
WACC (Collective System)	5.4	%
Capital Recovery Factor (Collective)	6.8	%
Discount Rate (Individual System)	3	%
Capital Recovery Factor (BAU)	5.1	%
LTG Insurance	7	% CAPEX
Unforeseen Costs	10	% CAPEX
Subsidy Duration (SDE++)	15	Years
Supplier Role	5	% Revenue

2021 HVC Energy Prices		
Small Consumer Heat	87	€/MWh
Connection and Delivery	513	€/Home/Year
2030 Projected Energy Prices		
Small Consumer Heat	116	€/MWh
Connection and Delivery	183	€/Home/Year
Large Consumer Gas	28	€/MWh
Large Consumer Electricity	57	€/MWh
Carbon Price	47	€/tonne

7.1 LTG

The doublet drilling costs require detailed investigation for accuracy. The horizontal drilling price in the U.S. are 1.5 to 2.5 times more than a vertical well [167]. Another study indicated 1.7 times higher exploration price for horizontal drilling per distance [168]. These prices are for deep wells, whilst relative drill price is less for shallower explorations [49]. Thus, a 1.5 times relative price factor is considered for a horizontal well, but as the deviation is 75° (83% from horizontal), the factor becomes 1.41 times higher per metre drilled than a vertical well.

This is then translated to the geothermal CAPEX equation shown in Eq. 17 [68], which excludes surface infrastructure and considers the cost of a vertical well. Due to the deviation, which is explored in Zwijndrecht, the depth (d) applied to the deviated well is the total measured depth (MD) of 2640m. When dividing the total by the MD, the drill price becomes €1686/m. When applying the 1.41 factor this now becomes €2377/m. The is corroborated by the relative deviated drill price for a 700m (TVD) deviated drill to be noted as being €2300/m at 700m and €2400 at 1000m. As the TVD in Zwijndrecht is 744m, a conservative price of €2350/m is used. The small variance between the two prices justifies a fixed value (no range) in the economic model. Thus, for a total MD of 2640m, the total drill cost is €6.2 million.

Equation 17:

$$CAPEX_{,drill}\ (€) = 375000 + 1150d + 0.3d^2$$

The CAPEX for the surface facilities also requires some attention as some technologies are not required depending on the depth and the aquifer conditions. A gas separation unit (degasser) is not required, as a negligible gas ratio was reported in the Brussels Sand in Zevenbergen (25km away) [111]. This unit typically costs €1m with annual maintenance of €150k/year [169]. Also, a blowout preventer is not required for LTG pressures, typically €0.2-0.3m [49]. A price and total cost breakdown are shown in Table 12, in which all prices are derived from [49] apart from the ESP and well abandonment cost. All components apart from the ESP last for at least 30 years [49][117]. The ESP has an average lifetime of 5 years (expected to increase in the future) [117]. A spare is required, thus two are purchased in year 0 and an additional ESP every 6 years. An ESP in the Paris Basin with rated power capacity of 250 kW_e cost €0.18m and an O&M (operation and maintenance) cost of €63.5k a year [117]. As seen in Section 8.1, the ESP capacity in Zwijndrecht is 120-160 kW for P90 and P50. Although this is roughly half the capacity of the Paris Basin ESP, it is unknown if this is the lowest capacity ESP on the market. Thus, the cost for a 250 kW_e capacity ESP is used.

The operating company must pay for the well abandonment cost and is responsible for any leakage and subsequent clean up. SoDM guidelines must be followed for plugging the well [170]. A deep onshore oil (near vertical) well was repurposed for geothermal production as oil exploration became economically unviable. The well was plugged from 4918m back to 4120m and based on three design plans, the cost ranged from €1.08-1.31 million [171]. As no other documentation exists, a cost of €1m is assumed in year 0 to be kept in a reserve fund. The O&M for LTG (not ESP), namely for staff, administration, monitoring, insurance, spare parts and waste disposal is 180k [49], resulting in a total fixed annual O&M of €0.234m

Unforeseen costs are said to range from 5-12% of total construction costs for a Dutch doublet of 2200-2300m TVD [91]. As the MD in the Brussels Sand is 2640m due to the deviation, an unforeseen cost of 10% of the total LTG CAPEX is assumed. This provides conservative leeway for additional unexpected variable O&M costs. Furthermore, an additional 7% of LTG CAPEX is added as an insurance cost, to decrease financial loss for investors if doublet performance is lower than P90. The insurance policy pay-out by the ministry of economic affairs is the fractional difference between the P90 and realised capacity, multiplied by 85% of the doublet CAPEX [172]. Thus 17% of the LTG CAPEX is added in total.

Table 12: LTG data for drilling and surface facilities (CAPEX + O&M)

LTG ECONOMIC	
Drill Price	€2350/m
Doublet (MD)	2640m
CAPEX (Million €)	
Drill Total	**6.2**
2x Liner Hanger	0.3
ESP	0.18
Heat Exchanger	0.241
Power Cabling/Converter	0.125
Land and Site Permit	0.2
Management/SDE/SoDM	0.2
Process Control	0.105
Blowout Preventer	0
Degasser	0
Drilling Labour and Energy	0.273
Other Operation Expenses	0.2
Flow Control/Clean out	0.475
Well Abandonment (reserves)	1
Surface Facilities + Other	**3.3**
Total Investment (+17%)	**11.15**
Fixed O&M / year	0.234

7.2 GWHP

The GWHP lifetime is noted as 15 years [149]. The investment per unit depends entirely on the type of HP, as shown by the price-capacity functions shown in figure 33. The total investment however is bound by different ratios of costs. The average ratios of a GWHP investment are shown in figure 34. The relevant costs concern the construction, consulting, and HP investment, which amounts to 58% of the total investment [64]. The source and electricity account for 42% of the total investment, which is determined in Table 12 and from the CHESS operational output estimates respectively. Thus, Eq.17 is the modified CAPEX function for the relevant costs of the GWHP [64]. The annual fixed O&M for an industrial ammonia HP is estimated to be 2% of the total CAPEX in 2030 [173]. All costs are thus a function of the capacity seen in Section 8.1.

Equation 17:

$$CAPEX\ (Million\ €) = 0.58\ \cdot (GWHP_{\ capacity} \cdot 0.6398 + 0.5043)$$

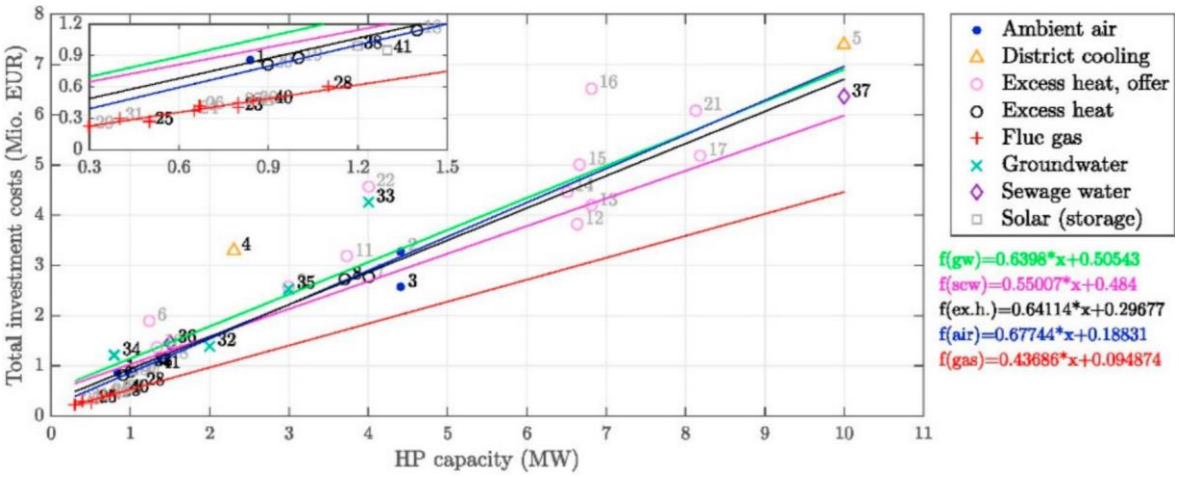

Figure 33: The total investment costs for HPs using different sources. The GWHP source is noted in green.

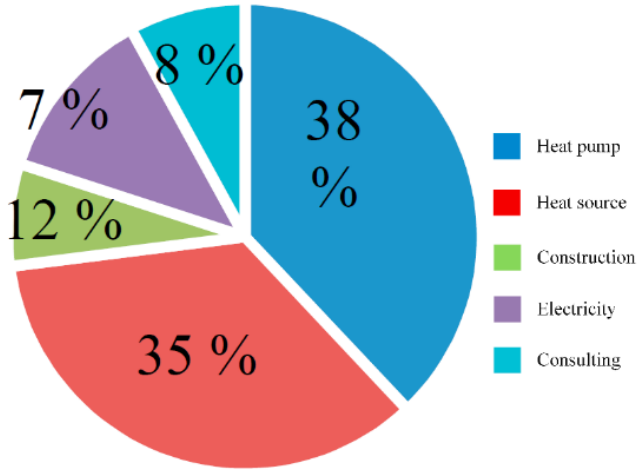

Figure 34: Breakdown of investment cost ratios for a GWHP

7.3 Auxiliary systems

A TTES lifetime of 30 years [154] and the price-capacity function from Fig. 35 generates a relative price for a 2000m^3 TTES to be €194/m3 [156] (CAPEX is €0.389m). The fixed O&M costs are calculated as 2% of the total investment costs per year, without the costs of the transmission pipeline (DHN) cost [156] This electricity cost for the DHN internal pump is determined via CHESS. Industrial natural gas boiler lifetimes range from 25-40 years. It is assumed 30 years is justifiable due to the low utilisation (peak supply), compared to large industrial boilers which operate at 98% full load [152]. For the required natural gas capacities in Zwijndrecht, a CAPEX of €17.6 kW$_{,th}$ and the fixed O&M is €1.82 kW$_{,th}$ is applied.

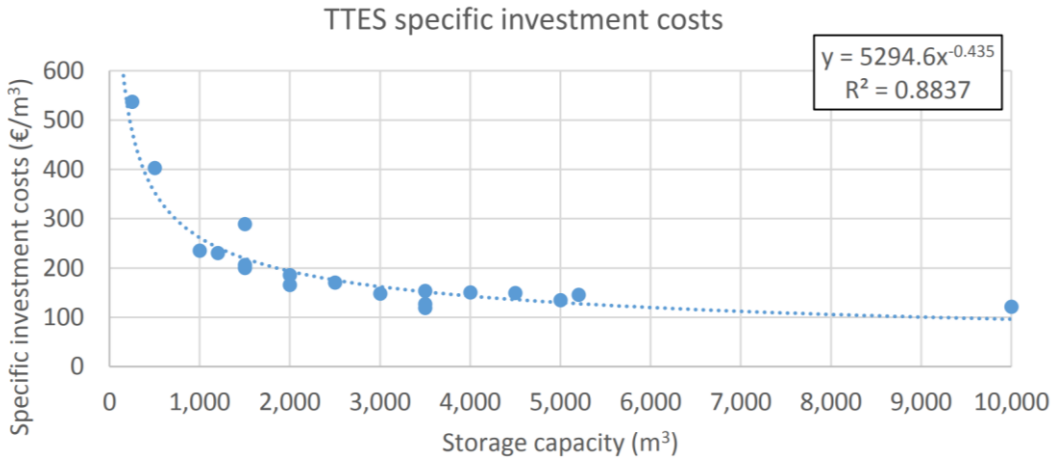

Figure 35: Relative investment cost (€/m^3) as a function of storage capacity (m^3)

7.4 Distribution Network

The costs for disconnecting the natural gas grid is the responsibility of the gas supplier [118]. As the economic assessment is from the perspective of the thermal producer, distribution system operator and energy supplier as one single entity, the replacement of end-user gas appliances are not considered. However, up to 2028, temporary natural gas boilers are used whilst the DHN is expanded, and technologies are implemented [118]. Thus, a temporary centralised natural gas boiler investment cost is a necessary requirement for the transition, as seen in Table 14. Note that, the natural gas fuel costs and benefits are not accounted for as the system lifetime begins in 2030. The role of energy supplier is assumed by negating 5% of revenues for administrative and financial overheads [118].

Pipes should be designed to be large enough for future expansions to connect new users [61]. However, this results in an additional cost with an unquantified benefit as well as reduced relative thermal loss (see pipe catalogue). For the purposes of a techno-economic analysis, pipes must be sized to fit the intended design without assumed expansion. As HVC have accounted for other production systems for 3200 homes, DHN data is modified to derive the required system boundary. The delivery sets and the primary and secondary distribution traces for phases which are not considered, were removed. Table 14 shows the DHN costs per connection is €7209. This includes a horizontal drill (asphalt road) and an unforeseen cost of 10%. No surface pipes are required for the doublet distance, as the deviation provides this.

The primary backbone of DN250 was tested in CHESS to determine if a lower diameter can apply to 2000 homes. As previously shown in Table 8, all simulated maximum velocities which derive the DHN pipe sizes for 2000 homes are oversized. Namely, a requirement of 208mm results in the pipe to be constrained to the next factory standard of DN250. Pipe sizes were noted to be the most sensitive parameter to total DHN costs in Switzerland [81]. The system should be designed such that the DHN flow of the primary backbone ($\dot{m}_H$ from the HP) is lowered to facilitate DN200. As Table 13 shows, measures which can reduce the maximum velocity such that an inner diameter of 208mm reduces to DN200 (€1300/m) from DN250 will reduce the price by €400/m. Provided the measures to reduce flow provide a net benefit, considerable savings can be derived for large pipe lengths, such as the 1170m length for the primary distribution in Zwijndrecht.

DN	€/m
20	600
25	625
32	650
40	700
50	780
65	850
80	900
100	950
125	1050
150	1100
200	1300
250	1700
300	1800
350	2500
400	3000
450	3500

Table 13: Default CHESS parameters for the primary and secondary distribution network

DHN INVESTMENT COSTS (Million €)	
Backbone & Primary Pipeline	1,750
Control stations	0,549
Secondary Network	7,418
Delivery Sets + Connection line	2,816
Auxiliary Heat Plant (temporary)	0,216
Project Management Connections	0,358
Unforeseen/Price Indexation	1.311
Total investment (2000 homes)	**14,417**
Average cost per connection (k€)	**7209**

Table 14: DHN investment costs including temporary heat plant

Thus, a reduction to DN200 desirable, such as through a valve which regulates the maximum flowrate in one area and compensates for the area in another. This was conducted via an excel solver. However, as the restricted flow in one pipe increases the flow in another, without an optimisation tool that can consider all pipes, the ideal DN solution was too time-consuming for a trial-and-error methodology. See Appendix D.2 for an example in which 3.5 kg/s flow reduction is required to reduce the pipe diameter. Note that, this example used only a buffer, thus the primary backbone diameter connected to LTG is larger than the collective system with a buffer and a boiler. Therefore, for the purposes of this study, the 200m primary backbone is counted as DN250, whilst the remaining 970m is DN200. This prevents unnecessary costs, which, otherwise could be reduced by optimisation tools such as WANDA, which optimise flow capacity [174].

7.5 BAU (HR-boiler)

The HR-boiler for the reference scenario has a technological lifetime of 15 years and a CAPEX of €2250 for a replacement boiler [164]. The annual fixed O&M and connection fee is €100 and €182.5 respectively. The CAPEX and fixed O&M highlighted in sections 7.2 to 7.5 is summarised in Table 14.

Table 14: Price-capacity functions and fixed O&M for the production, storage and the DHN

TTES + BOILER				
CAPEX			**Fixed O&M**	
GWHP	Function		2%	CAPEX
TTES	194	€/m^3	2%	CAPEX
Central Boiler	17.6	€/kW_{th}	1.82%	CAPEX
Individual HR-Boiler	2250	€/Unit	100	€/Year
DHN	7209	€/Home	3%	CAPEX

The estimated LCOH for the HR-boiler must be higher than the P50 and P90 scenarios for the collective system to be economically viable. This is due to new consumers regulations for small consumers by The Netherlands Authority for Consumers and Markets (ACM), who determine on behalf of the government, the maximum heat tariff. The ACM regulates heat prices annually by capping the price to that which an average household would pay to heat their property with natural gas [96]. Thus, comparing the LCOH of the BAU scenario is first required to determine if a potentially positive NPV can even apply.

7.6 Economic Uncertainty

Key uncertainty parameters to apply are rationalised from a sensitivity analysis conducted on a deep direct use geothermal techno-economic model in The Netherlands. The study found the most sensitive variables to NPV in decreasing order were heat price, heat demand, subsidy amount, operational cost, well capacity and drilling cost [91]. Thus, uncertainty in the heat demand is omitted as future insulation upgrades are unknown and context dependent. The drilling costs were previously estimated in Section 7.1 to not have much variance from the available literature. The relative price of drilling could be analysed; however, such price changes predominantly follow a volatile hydrocarbon industry and natural gas price [175], which is also unpredictable.

Well capacity from flowrate uncertainty is thus used for geotechnical uncertainty scenarios. This is denoted as the P50 and P90 transmissivity which determines the flowrates highlighted in Fig. 26 by the reservoir characterisation from WarmingUP. The CHESS solver determines technical topology differences (fuel and capacity), which has overall impacts to the economic and environmental (CO_2-eq) system performance. In 2021, HVC charged 5% less for district heating (€87/MWh), 16.4% less connection/supply fee (€400/year), the ACM constraint for the meter costs (€27/year) and 31.5% less for the delivery set (€86) [176]. Thus, a 2021 HVC price is one constituent of the low revenue scenario. This assumes a 2021 heat benefit, whilst considering a higher 2030 fuel price. Namely, a large consumer gas price (€28/MWh), large consumer electricity price (€57/MWh) and the carbon price (€47/tonne) [58].

For the high revenue scenario, the same €513 total connection fee is assumed but a heat price assumes the 2030 small consumer natural gas price of €113.3/MWh [58] divided by the 97.3% HR-boiler efficiency (Section 6.9), thus €116/MWh. This 2030 fuel price from PBL is the most reliable prediction as technological investment development trends are considered [58]. Thus, the revenue uncertainty has a justifiable and robust range. Note that the 2030 carbon price of €75/tonne is only used for the BAU and centralised natural gas boilers in the collective system as the 2030 electricity price has a carbon price embedded [58].

Subject to technical performance, the collective system can apply for the SDE++ operational subsidy for renewable technologies. The amount of subsidy depends on the technology and extent of CO_2 reduction. LTG-HPs fall under the category of 'Low-CO_2 heat' [130]. The requirements are a minimum depth of 500m (within the North Sea Group formation), in which heat upgraded via a HP must have an SPF higher than 3, and a rated thermal output of at least 500 kWth. If LTG-HP is applied to the built environment, a maximum of 3500 full load hours are eligible for the subsidy. The DoubletCalc thermal output must be rationalised with at least a P50 certainty [130]. Note that, P90 is often a financial requirement [49], thus this is of more relevance when attempting to attract commercial and/or consumer investment.

The application phases are defined by subsidy intensity limits, namely, the maximum euros allocated per tonne of CO_2 avoided. The phases are chronological such that cost-effective emission reductions have priority. Thus, applying for a lower (relative) subsidy will increase the probability of success [58]. Conversely, a higher subsidy in later rounds will have a lower ranking. Therefore, in this instance, the probability of receiving a share of the €5 billion decreases. A limit of one technology per site applies [58]. The maximum subsidy available for phases 1, 3 and 4 are used as revenue uncertainty parameters.

The base amount is the maximum amount of the subsidy for each of the phases and is ranked by the subsidy intensity shown in Eq. 18. The parameters are fixed by the Dutch government. The emission trading scheme (ETS) is not embedded in the preliminary correction amount as this is calculated separately. Note that, the correction amount will change throughout the subsidy duration and is partly determined by an unpredictable market value [58]. Thus, no correction is made as market remuneration occurs after the fact. As the subsidy depends on the full load hours and rated power, a breakdown with benefits is shown later in Table 19.

Equation 18:

$$Subsidy\ Intensity\ \left(\frac{€}{\mathrm{kg}CO_2}\right) = \frac{\left[Phase\ Base\ Amount\ \left(\frac{€}{kWh}\right)\right] - \left[Longterm\ price\ \left(\frac{€}{kWh}\right)\right]}{Emission\ Factor\ \left(\frac{\mathrm{kg}CO_2}{kWh}\right)}$$

Another revenue consideration is the initial price paid by small customers for their heating which is not currently regulated by the ACM. This is a one-off connection and project fee known as the BAK ('Bijdrage Aansluitkosten') which is typically paid by the housing project developer and is partially passed onto the customer [177]. HVC estimate €2500 could be passed onto the user [118], thus the gross DHN cost of €7211 per home becomes €4711 per home. This is very close to €4500 net connection used by the CE Delft business case [49]. However, this is quantified as a flexible benefit due to the use of the LCOH. The BAK is first ignored amongst the fuel price and subsidy scenario. Then €2500 from year 0 is added to determine the viability of the HVC estimate. The three revenue scenarios are shown below and are embedded within P50 and P90 geotechnical uncertainty. When considering situations with and without a €2500 BAK, 12 techno-economic uncertainty scenarios are derived.

- **LOW:** 2021 HVC PRICE + SUBSIDY ALLOCATION 1
- **MEDIUM:** 2030 HEAT PRICE + SUBSIDY ALLOCATION 3
- **HIGH:** 2030 HEAT PRICE + SUBSIDY ALLOCATION 4

7.4 Financial Methodology

To determine the present value of future benefits and costs, they must be discounted via a discount rate which considers opportunity costs. This must be done for every future cash flow to determine the net present value (NPV) [178]. However, for this analysis, the weighted average cost of capital (WACC) is used as the discount rate for the collective system, shown in Eq. 19. This ensures the NPV includes the cost of equity and debt for every future cash flow as well as depreciation. Thus, using WACC as the discount rate accounts for financial flows [179][180] Note that, a consumer discount rate of 3% is used for residential systems, which only incur opportunity costs and inflation, not the risk associated with the large collective system [181]

Equation 19:

$$WACC = Equity\ Ratio \cdot Cost\ of\ Equity + Debt\ Ratio \cdot Cost\ of\ Debt \cdot (1 - tax)$$

The WACC depends on the financial structure of the venture, such as extent of equity and location (differing risk amongst countries). Geothermal projects typically have debt-equity ratios between 60-80% [68][182], therefore 70% is used. However, geothermal can include green financing, thus the cost of debt is 2% (otherwise 3%) [183]. Interest payments are tax-deductible, such that the cost of debt is multiplied by (1 – tax rate). The corporate tax rate in The Netherlands from 2022 onwards is 21.70% for profits exceeding €200k [184]. Deducting the corporate tax rate means the true cost of debt essentially becomes 1.57%. Geothermal projects have high associated risk before production occurs and high economic volatility (beta factor) from the residential application. Thus, a high recommended return on equity of 14.5% to attract commercial investment is required [185]. The WACC thus becomes 5.45%.

This is then applied to the NPV shown in Eq. 20 [186], to derive the present value at each year (i) over the 30-year economic lifetime. If the total discounted benefits (B) are more than discounted costs (C), then the project is profitable. To derive an understanding of the annualised lifetime costs, the NPV is multiplied by the capital recovery factor (α) shown in Eq. 21 [186]. This is a function of the discount rate (r) and project lifetime (n). As the discount rate differs amongst collective (5.45%) and BAU (3%) scenarios, the capital recovery factors are 6.8% and 5.1% respectively. Note that, the NPV is only applied to collective system as only this contains the benefits. The BAU scenario is only used as an initial cost-based indicator.

Equation 20:

$$NPV = \sum_{i=0}^{n} \frac{B_i - C_i}{(1+r)^i}$$

Equation 21:

$$\alpha = \frac{r}{1-(1+r)^{-n}}$$

The LCOH provides a transferable metric to compare against similar projects or technologies and thus, guide investment decisions. As only the costs are considered for producing a unit of thermal production, it is the preferred metric to compare against the BAU scenario, which does not have associated revenue. The LCOH equation is denoted in equation 21 [186]. For the collective system, all capital costs occur in year 0 apart from an ESP purchase every 6 years (with two in year 0) and a second GWHP investment at year 15. For the BAU scenario, the lifetime needs to be the same despite the HR-boiler having a lifetime of 15 years. Thus, two system lifetime cycles are used for relative comparison. As boilers currently exist in homes, the lifetime is assumed to be half complete, thus the HR-boiler CAPEX occurs in year 8 and 23. The fixed O&M has already been defined and the variable O&M namely, the energy costs are defined in Section 8.1.

The denominator of the LCOH represents the energy produced, which must be discounted. FO&M and VO&M are fixed and variable operation and maintenance costs respectively. The collective system and the BAU scenario have different production system efficiencies. The collective system has already incorporated the production efficiency via CHESS. However, the demand must be increased for the BAU scenario by dividing by the 97.3% system efficiency. An important consideration for the LCOH is the unaccounted thermal losses from the DHN. Although CHESS simulates the additional energy produced from thermal losses when solving the thermal balance, no negative costs in the form of lost revenue is accounted when using the LCOH, which is a production-orientated cost metric. Only the NPV will account for the thermal loss which does not reach the end-user via a loss in revenue. Thus, the LCOH compares different technologies whilst the NPV serves as a business-orientated economic performance indicator.

Equation 22:

$$LCOH = \frac{\sum_{t=1}^{n} \frac{CAPEX_t + FO\&M_t + VO\&M_t + CO_{2_t}}{(1+r)^t}}{\sum_{t=1}^{n} \frac{MWh_t}{(1+r)^t}}$$

8.0 Results

The annual technical data from the BAU scenario and the collective system simulated in CHESS under P50 and P90 flowrates is shown in Table 15 and 16 respectively. Table 17 shows the individual nature gas boiler (BAU) scenario and how the collective system reduces $CO2_{-eq}$ emissions by 67.7% and 72.9% for P90 and P50 scenarios respectively. Table 18 shows the estimated levelized cost of heat (LCOH) reductions are 5.48% to 6.6% respectively for P90 and P50 scenarios. The load factor is relatively low, as this metric considers a low injection temperature which results in a high capacity. Although this high capacity is rarely reached, it does provide additional revenue for the SDE++ subsidy, as the annual awarded sum is based on the capacity and full load hours of the system, as shown in Table 19.

Although both scenarios produce the 3500 full load hours required for the SDE++, the P90 flowrate has an LTG-HP efficiency of 2.93. As the COP > 3 constraint noted by the SDE++ guide [130] does not elaborate if the ESP power constitutes work, consideration is required. The combined LTG-HP may require additional adjustments to increase the SPF for the P90 scenario. This can be from the HP side, such as increasing the system efficiency with additional investment to reduce irreversibility. Or this can be from the ESP side, such as reducing flowrate during low demand as the operational mode used in CHESS maximises flow. If measures are required for the SDE++ subsidy application, either or both can be assumed sufficient to increase the SPF to above 3 for the P90 scenario. However, technical data from P50 can be submitted in the SDE++ application [130]. Thus, it can be reasonably assumed that both scenarios can apply for the SDE++ criteria for the revenue analysis.

Table 15: Annual technical results for the P50

ANNUAL TECHNICAL DATA: P50 (LTG) + 2000m^3 Buffer					
LTG				**ESP**	
Output (MWh/a)	Capacity (MW)	Load Factor (%)	Average ΔT (°C)	Total (MWh/a)	Capacity (MW)
16842	3,86	54%	14,42	1270	0,16
GWHP			**SPF (-)**		
Output (MWh/a)	Capacity (MW)	Electricity (MWh/a)	LTG	GWHP	LTG-HP
21561	5,07	4719,28	13,26	4,57	3,60
TTES (MWh/a)		**BOILER**		**DHN (MWh/a)**	
Annual Discharge	Thermal Losses	Total (MWh/a)	Capacity (MW)	Internal Pump	Thermal Losses
870	348,01	2845	6,22	46,15	3393
TOTAL SYSTEM (MWh/a)			**$CO2_{-eq}$ EMISSIONS**		
Electricty	Natural Gas	Imbalance	Electricty (tCO_2/a)	Natural Gas (tCO_2/a)	**BAU Reduction (%)**
6036	3161	6,31	543	642	**72,91**

Table 16: Annual technical results for the P90

ANNUAL TECHNICAL DATA: P90 (LTG) + 2000m^3 Buffer					
LTG				**ESP**	
Output (MWh/a)	Capacity (MW)	Load Factor (%)	Average ΔT (°C)	Total (MWh/a)	Capacity (MW)
13359	2,95	55,9%	14,81	996	0,12
GWHP			**SPF (-)**		
Output (MWh/a)	Capacity (MW)	Electricity (MWh/a)	LTG	GWHP	LTG-HP
18766	4,32	5407	13,42	3,47	2,93
TTES (MWh/a)		**BOILER**		**DHN (MWh/a)**	
Annual Discharge	Thermal Losses	Total (MWh/a)	Capacity (MW)	Internal Pump	Thermal Losses
1009	404	3698	6,99	46	4192
TOTAL SYSTEM (MWh/a)			**$CO2_{-eq}$ EMISSIONS**		
Electricty	Natural Gas	Imbalance	Electricty (tCO2/a)	Natural Gas (tCO2/a)	**BAU Reduction (%)**
6448	4109	24	580	834	**67,66**

Table 17: Techno-economic performance of BAU scenario

BAU (NATURAL GAS BOILER)	(Million €/year)	Home (K€/year)
Boiler Investment (year 8 and 23)	4.5	2250
Annual Gas Grid Connection Fee	0.365	182.5
Annual Natural Gas Cost (with CO_2)	2.44	1221
Annual O&M	0.20	100
Annualised Cost	**3.30**	**1649**
LCOH €/MWh		**153.3**
CO_2 tonnes/year (BAU System)		**4375**

Table 18: Collective system costs, with numbered brackets indicating the required (re)investment years

COLLECTIVE SYSTEM COSTS		P90	P50
System Investment costs (Million €/year)			
CAPEX	Net DHN	14.4	14,4
	LTG	10.1	10,1
	ESP (0;0;6;12;18;24;30)	0.180	0,180
	GWHP (0;15)	1.90	2,17
	TTES	0.39	0,39
	Natural Gas Boiler	0.12	0,11
Annual System Costs (Million €/year)			
Fuel	Natural Gas	0.15	0,12
	Electricity	0.37	0,34
	Carbon	0.07	0.06
FO&M	DHN	0.43	0.43
	LTG	0.17	0.17
	ESP	0.06	0.06
	GWHP	0.04	0.04
	TTES	0.01	0.01
	Natural Gas Boiler	0.01	0.01
Annualized Costs		**3.25**	**3.21**
Annualized Cost (€/building)		**1625**	**1606**
LCOH (€/MWh)		**144.7**	**142.9**
REDUCTION FROM BAU (NATURAL GAS BOILER)			
LCOH		**5.48%**	**6.63%**
Annualized Costs		**1.45%**	**2.65%**

Table 19: Subsidy allocation parameters from the SDE++ [130] calculated from Eq. 18 based on the LTG-HP capacities simulated from Section 8.1, showing the annual subsidy allocations for P50 and P90 scenarios

	Phase/Base amount (€/kWh)		
Application Phase	*1*	*3*	*4*
Subsidy intensity limit (€/tCO_2)	65	180	300
Maximum Base Amount per phase	0,0438	0,0629	0,081
Subsidy intensity (€/tCO_2)	65,06	180,12	289,16
Subsidy (€/MWh)	15,80	34,90	53,00
Annual P90 Subsidy (Million €)	**0,239**	**0,528**	**0,802**
Annual P50 Subsidy (Million €)	**0,280**	**0,619**	**0,941**

Fig. 36-39 shows the progression of NPV amongst the 30-year lifetime amongst low, medium and high revenue scenarios for P90 and P50 flowrates, with and without a €2500 connection fee (BAK), in year 0. The NPV ranges from €-4.7m to €11.7m and all scenarios with subsidies and a €2500 connection fee have a positive NPV irrespective of heat price. If low flowrates are produced and no subsidies are awarded, the required connection fee to break even is €3522 and €1622 for 2021 and 2030 heat prices respectively. This worst-case scenario was deduced by a simple excel solver, by setting the target as NPV = 0.

P50: NO BAK	**LOW**	**MEDIUM**	**HIGH**
PAYBACK PERIOD	**>30**	**18**	**13**
NPV (Million €)	**-3.7**	**3.53**	**6.77**

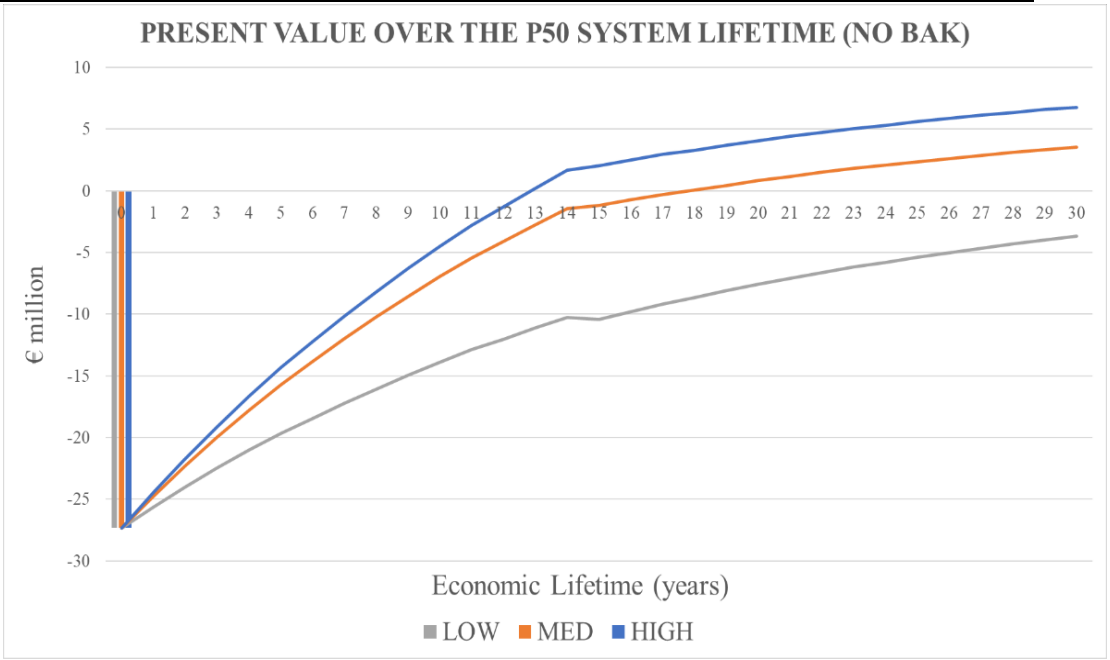

Figure 36: NPV progression for P50 (no BAK)

P50: WITH BAK	LOW	MEDIUM	HIGH
PAYBACK PERIOD	26	11	10
NPV (Million €)	1.3	8.53	11.77

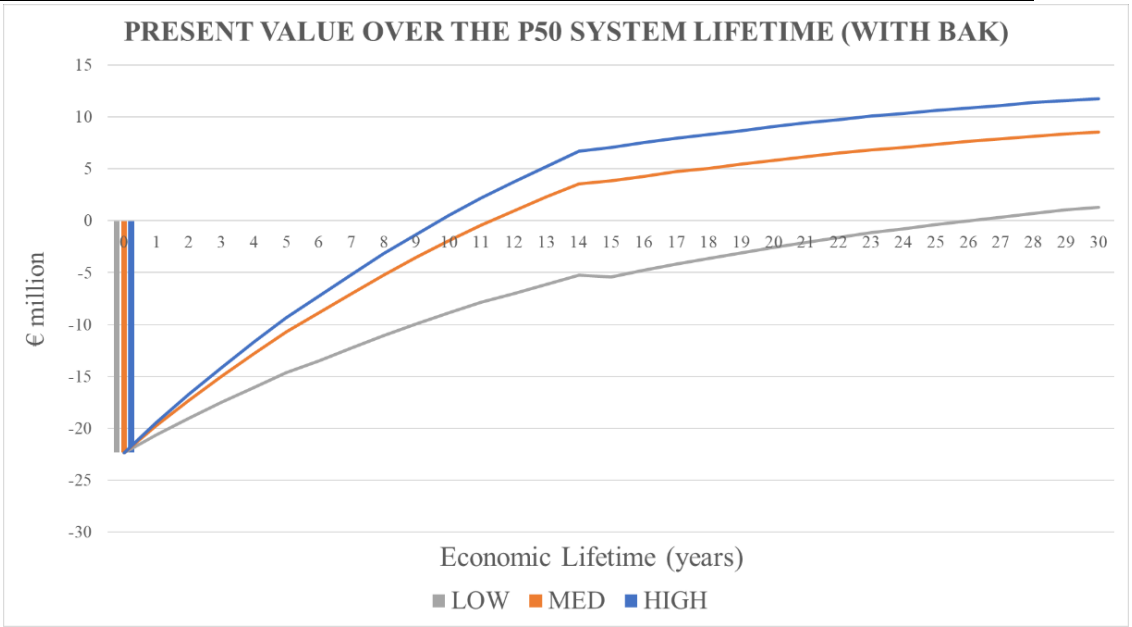

Figure 37: NPV progression for P50 (with BAK)

P90: NO BAK	LOW	MEDIUM	HIGH
PAYBACK PERIOD	>30	21	14
NPV (Million €)	-4.7	2.07	4.83

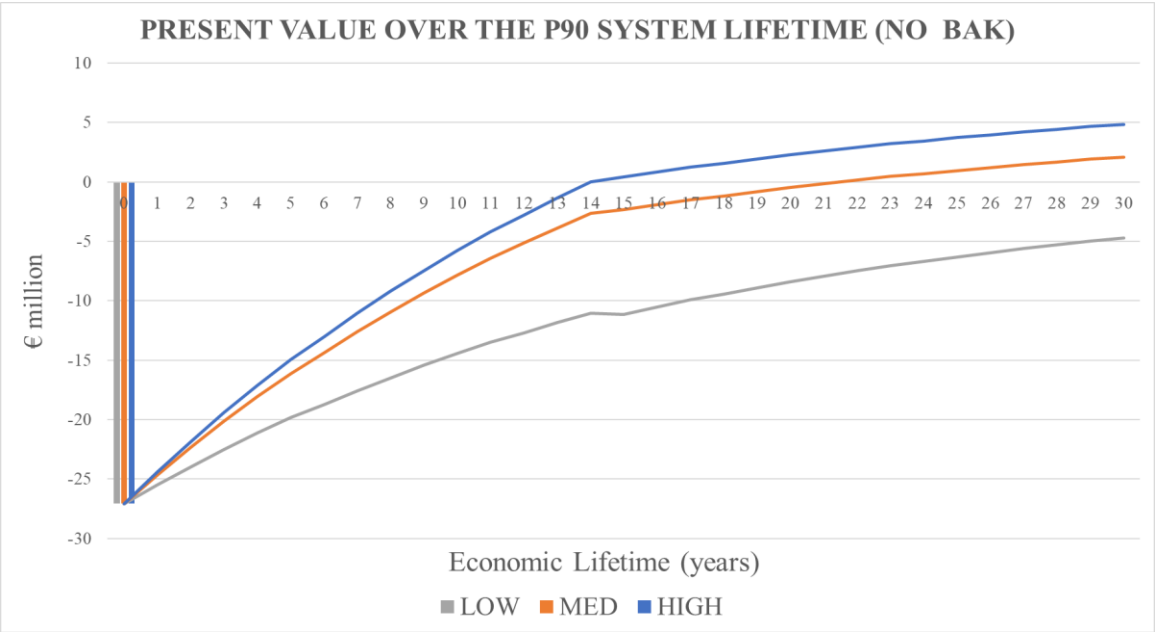

Figure 38: NPV progression for P90 (no BAK)

P90: WITH BAK	LOW	MEDIUM	HIGH
PAYBACK PERIOD	29	13	11
NPV (Million €)	0.3	7.07	9.83

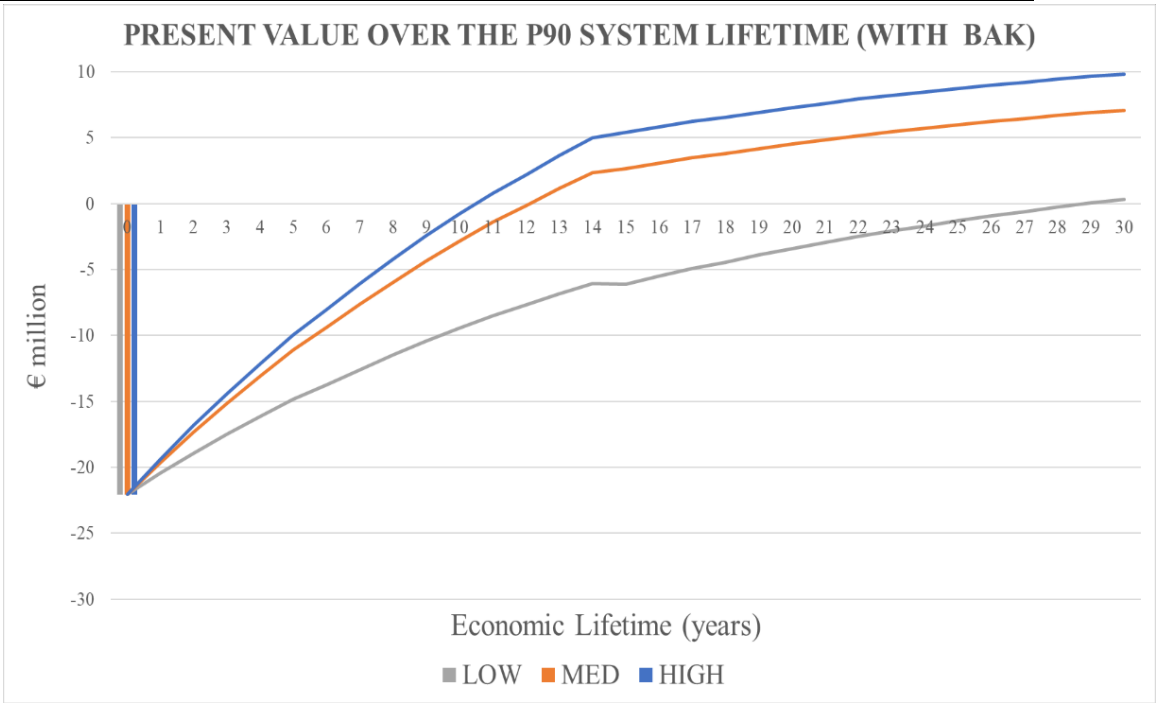

Figure 39: NPV progression for P90 (with BAK)

8.2. Case Study Comparison

The CE Delft [49] study estimated an emission reduction for 2030 to be 61-63% less than a gas boiler for a 70C supply and an SPF for the combined LTG-HP system which does not reach higher than 3.2. In Zwijndrecht, an 80°C supply showed an emission reduction of 67-73% and an SPF of 2.93-3.6. This may seem unexpected as the model in Zwijndrecht has a better technical performance for a higher supply temperature. However, CE Delft uses a fixed 8°C injection temperature. For a residential heat demand, a consistent 8°C is very unlikely, unless an extremely large storage capacity was present to maintain a constant thermal production throughout the year. However, no large thermal storage was noted in the study.

When a dynamic heat demand profile is used, low demand recorded during summer derives a high COP. This is due to less electrical work from the HP compressor compared to the ESP which derives the ambient source at a high LTG-only COP. Thus, the magnitude of LTG output is higher in the CE Delft [49] study, but the relative efficiency is lower. This is also shown by the lower emission savings of the P90 scenario in Zwijndrecht, due to the higher HP electricity use. In short, a static heat demand profile for a residential application without seasonal storage, does not represent the typical system condition. Especially when 300m^3/hr is assumed, which is over double the P50 flowrate. In Zwijndrecht, the dynamic heat demand shows that an injection temperature which is lower than 9°C, occurs for only 2001 hours in a year (Fig. 21).

Another factor for the higher SPF simulated in CHESS is the more efficient Lorenz cycle efficiency and the different aquifer pressures which determine the ESP power required to overcome formation resistance. These variable interactions are not easy to interpret amongst different demand characteristics. Especially as a 50% system efficiency Lorenz cycle was used in Zwijndrecht compared to a 70% (less efficient) Carnot cycle, which was used by CE Delft [49]. When comparing the economic viability, the CE Delft study [49] required a one-off connection fee (BAK) of €2,000-4,000 per dwelling was required, as well as the SDE+. However, in Zwijndrecht, all 2030 heat price scenarios have a positive NPV. Furthermore, the worst-case scenario (P90 and no subsidy) requires a €3552 and €1623 connection fee for the 2021 and 2030 heat price respectively. Therefore, a better economic indication is apparent in Zwijndrecht.

Compared to the small German DHN [80] mentioned in section 2.4, which supplied 127 homes with a GSHP (60°C DHW and 40°C space heating), the collective system for 2000 homes had nearly the exact same results. The German DHN was shown to reduce CO_2 emissions by 64% and annualised costs by 5%, relative to an individual natural gas reference boiler scenario [80]. Note that, different costs and electricity grid emissions apply in Germany in 2016 compared to The Netherlands in 2030. Thus, this indicates that the larger GWHP system for 2000 homes in 2030, can derive a similar techno-economic performance as an efficient GSHP which supplied high efficiency German homes in 2016. As the carbon price was considered, it shows this is ineffective as the centralised natural gas boiler still provides cost-effective peak demands regardless of this cost.

However, the minor extent to which the P90 and P50 scenarios differ economically may seem surprising from the individual LTG perspective. However, CHESS allocates the cheap natural gas boiler capacity and fuel to the P90 scenario to replace this deficit. Furthermore, the price capacity function for the GWHP causes the investment costs to increase. So, whilst less electricity is required for the P50 LTG-HP, the overall capacity increases from a higher LTG capacity. Therefore, when the DHN system is considered, the economic risk of P90 flowrates is very low, as the solver compensates by activating more boiler capacity and thus emissions rise from more natural gas use. Thus, when multiple sources of cheaper but higher emission production are used within the DHN, this can lower economic risk, but the system becomes less sustainable.

9.0 Discussion

Despite the collective system appearing to have better economic performance than the BAU, the metric of LCOH requires some consideration. As LCOH is production-based, only the production system efficiency is accounted, not the DHN distribution losses. Thus, the collective system with distribution losses amongst the DHN will appear to have a better economic performance than suggested. In other words, thermal losses are not contextualised to end-user revenue in which more heat is produced to maintain the thermal balance (energy received) which has a positive implication to the LCOH. So, whilst the production efficiency is accounted for by modifying the demand, the thermal losses of distribution are not accounted for in the LCOH. Only the NPV accounts for the reduction in revenue from the DHN thermal losses.

As expected, the higher P50 flowrate has a lower LCOH than P90, as additional operational energy is generated from very little additional ESP cost. Namely, the increased transmissivity of 5 Dm (which facilitates a 20% higher flowrate), provides a marginal thermal benefit of the magnitude of the SPF of the LTG system (~13). When compared to the P90 scenario, a P50 flowrate requires 283 MWh more electricity annually for the ESP to generate an additional 3866 MW,th. This explains why the P50 scenario was modelled as having a 5.25% more CO_2 emission reduction than the P90 scenario.

Whilst the system is technically profitable over the 30-year economic lifetime, it is not a very commercial attractive venture relative to other investments. The payback period investor requirements can be as low as 7 years for a GSHP system [95]. However, it should be noted that the estimates used were on the conservative side to try to mitigate investor insecurity. Namely, the 7% insurance cost, which determines an unquantifiable benefit in the event of a lower than P10 capacity. Furthermore, the well abandonment cost was assumed, even though the LTG lifetime is economic rather than technical and thus, this is not necessarily required in year 30, but a €1 million fund was reserved, nonetheless.

Limitations and recommended further technical research for stakeholders is now discussed. Uncertainty from LTG output is primarily considered as a function of the transmissivity of the aquifer. However, different variables can reduce LTG flowrate, such as temperature and pressure, which DC1D considers. Viscosity and friction resistance in the injector can be twice as much as in the producer [70][192]. However, these functions are not embedded in CHESS. Hence why the maximum flowrate was derived from a 15°C average temperature in DC1D, for the CHESS flowrate constraint. The precise thermal influences on flowrate are required.

A plate heat exchanger was not modelled in CHESS, as the 4-port HP refrigerant essentially assumes a perfect transfer. However, the material, depth, configuration, size, flowrate, sand scaling all influences the heat transfer efficient [187]-[190], and thus requires substantiation. Scaling, such as from calcite, silica and barite reduce the surface area exposure and thus, also require additional mitigation costs [70][191].

The change in ΔT between cold and warm aquifer thermal plumes is required throughout the thermal lifetime. This thermal interference is not assumed in the technical model, however, after several years, the production temperature may reduce. Therefore, researching the 1000m doublet distance and the extent and temperature reduction is required. Also, the optimal distance for a specific increase in the vitality is recommended. This may can done on the software DoubletCalc2D.

Injection-related fracturing occurs when injection pressure exceeds the minimal principal stress in a rock formation [70]. Fracturing can be desirable, i.e., localised hydraulic simulation to increase productivity (reduce skin factor) at the filter, or unwanted physical well damage. A colder and denser injection temperature may cause early-stage well damage if sufficient monitoring is not applied. Thus, reductions in injection temperature should consider injectivity index safety limits to prevent well damage, such as that observed in Twente recently [113].

CHESS recommendations are now provided. A main need is to add thermal storage losses as a function of size, shape, material, capacity, and cycles. Also, different desired temperature regimes per simulation run, to allow for a lower temperature requirement in summer when no space heating demand is required 9only DHW ≈60°C). As HVC recommended the supply-return regime to be 85/45 (°C), thus an 80/40 regime was used to account for the lower temperature in summer and represent the average building condition (see Table 2). Also, having time-defined activation priorities amongst the topology is required. Currently, the activation priority is fixed for the entire simulation and leads to the following problems:

- Seasonal technologies such as aquathermy, require different flows depending on the season. For example, the surface water can either supply the HP directly, such as in autumn, or charge the aquifer in summer. Currently, different simulations for the seasons are required if flows are to be matched to surface water temperatures.
- Planned downtime maintenance for the LTG-HP cannot be simulated as occurring at a precise time, such as during a period low summer demand. Implementing this would reduce the post-processing of LTG-HP output.
- The activation priority 2 for the day-week buffer always acted as seasonal storage during summer as the LTG-HP would charge when demand is low, which resulted in post-processing (Eq. 16). A deactivation period during summer would prevent this.

The flowrate constraint for LTG uses the same fluid properties as the DHN. Thus, a mass flowrate and Cp input for the geothermal fluid would prevent post-processing for the brine:

- Universal Cp in CHESS = 4181 J/kg°C for DHN, but LTG is ≈4000 (3.8% salt).
- Connect DoubletCalc functions to injection temperature to calibrate flowrate.
- Add a quadratic function to the LTG flowrate for an ESP module which simulates the production pump electricity.

The geothermal heat pump is placed in an industrial area in which a variety of waste heat could be utilised. This may provide cost-effective heat pump and/or peak boiler capacity reduction. Unless processes are carbon intensive coal-driven, utilising industrial processes should expect a net reduction relative to a gas boiler. However, this ultimately depends on somewhat subjective definitions of emission intensity which differ internationally. Waste heat must have sufficient temperature, capacity, ramp time and strategic and synchronised schedule durations.

By using more reliable heat demand data which is geographically connected to specific cluster locations will facilitate the assignment of different temperature regimes. By doing so, return temperatures for inefficient homes can become the supply temperatures for efficient homes. Thus, rather than designing a branched 'tree' network, further research should focus on a cascading ring system, potentially with localised booster HPs, not a natural gas boiler. This may improve the techno-economic performance. The tool WANDA within the Design Toolkit beta release in 2022 is recommended to be used for such a design. This facilitates optimal pipe route decisions as well as volume capacity, a limitation of the CHESS design.

10.0 Conclusion

This study derived a robust techno-economic model of an LTG-HP system within a medium-high temperature DHN in The Netherlands. The intention as to examine the poor economic which may dissuade investors from conducting a more detailed feasibility into LTG-HP systems. The Zwijndrecht case is interesting as the intended supply is high, meaning theoretical efficiency is low. This is partially why no documented examples of a DHN exists which supplies residents from a LTG-HP upgrading the source by more than 50°C. Therefore, it becomes highly relevant when commercial interest arises to examine an LTG (31 °C) system which supplies inefficient residential homes.

The aim was to resolve the limitations of the only known business case of an LTG-HP within a residential DHN. Namely, the use of generalised static inputs which provide transferability, but not a robust techno-economic performance indication or justifiable uncertainty range. The specific geotechnical and revenue uncertainty considered, flowrates, heat price and subsidy allocation. A robust contextual techno-economic indication was developed to provide scientific and stakeholder insights into the viability of such systems. The WarmingUP project characterised the Brussels Sand aquifer, which serves as the geotechnical basis to derive the range of maximum flowrates from DoubletCalc1D. The P50 (36.2 kg/s) and P90 (30.9 kg/s) flowrates were embedded within the thermal balance (solver) CHESS.

The LTG-HP systems studied provides a more positive indication than the ThermoGIS indication and CE Delft [49] study which formed the basis of comparison. The system is profitable for all 2030 energy price scenarios irrespective of subsidies. However, when compared to other ventures, it is less commercially attractive without subsidies. Recommendations are provided in the context of improving the techno-economic model accuracy. Also, suggested improvements to the CHESS tool are provided in the context of thermal production integration.

11.0 References

[1] *A European Green Deal*. European Commission - European Commission. (2021, September 10). Retrieved September 24, 2021, from https://ec.europa.eu/info/strategy/priorities-2019-2024/european-green-deal_en.

[2] Letcher, T. M. (2014). *Future energy: Improved, sustainable and clean options for our planet*. Elsevier Science & Technology.

[3] Matek, B., & Gawell, K. (2015). The benefits of baseload renewables: A misunderstood energy technology. *The Electricity Journal*, *28*(2), 101–112. https://doi.org/10.1016/j.tej.2015.02.001

[4] Huttrer, G. W. H. W., Geothermal Power Generation in the World 2015-2020 Update Report (2020). Reykjavik.

[5] Kaczmarczyk, M., Tomaszewska, B., & Operacz, A. (2020). Sustainable utilization of Low Enthalpy geothermal resources to electricity generation through a Cascade System. *Energies*, *13*(10), 2495. https://doi.org/10.3390/en13102495

[6] Moeck, I. S. (2014). Catalog of geothermal play types based on geologic controls. *Renewable and Sustainable Energy Reviews*, *37*, 867–882. https://doi.org/10.1016/j.rser.2014.05.032

[7] J.D. van Wees, Kronimus, A., van Putten, M., Pluymaekers, M. P. D., Mijnlieff, H., van Hooff, P., Obdam, A., & Kramers, L. (2012). Geothermal aquifer performance assessment for direct heat Production – methodology and application to ROTLIEGEND AQUIFERS. *Netherlands Journal of Geosciences - Geologie En Mijnbouw*, *91*(4), 651–665. https://doi.org/10.1017/s0016774600000433

[8] Ministerie van Algemene Zaken. (2020, July 13). *Government stimulates geothermal heat*. Renewable energy | Government.nl. Retrieved September 24, 2021, from https://www.government.nl/topics/renewable-energy/government-stimulates-geothermal-heat.

[9] GeoEnergy, T. (2020, March 17). *Last year, geothermal energy use in increased by 51% in the Netherlands*. Think GeoEnergy - Geothermal Energy News. Retrieved September 24, 2021, from https://www.thinkgeoenergy.com/last-year-geothermal-energy-use-in-increased-by-51-in-the-netherlands/

[10] European Geothermal Congress 2019, Provoos, M., Albeda, L., Godschalk, B., Van der Werff, B., & Schoof, F., Geothermal Energy Use, Country Update for The Netherlands (2019). Den Haag; EGEC.

[11] GeoEnergy, T. (2021, April 1). *Netherlands reports 10% annual growth of Geothermal Use 2020*. Think GeoEnergy - Geothermal Energy News. Retrieved September 23, 2021, from https://www.thinkgeoenergy.com/netherlands-reports-10-annual-growth-of-geothermal-use-2020/.

[12] Beckman, K., & van den Beukel, J. (2019). *The great Dutch gas transition*. oxfordenergy. Retrieved September 23, 2021, from https://www.oxfordenergy.org/wpcms/wp-content/uploads/2019/07/The-great-Dutch-gas-transition-54.pdf.

[13] Schoof, F., & van der Hout, M. (2018). (publication). *Master Plan Geothermal Energy in the Netherlands*. EBN, DAGO, Stichting Platform Geothermie, Stichting Warmtenetwerk.

[14] Niessink, R., & Rosler, H. (2015). (rep.). *Development of Heat Distribution Networks in the Netherlands*. ECN.

[15] Schepers , B., & van Valkengoed, M. (2009). (rep.). *Overzicht van grootschalige en kleinschalige warmtenetten in Nederland* . Delft: CE.

[16] *Warmingup*. WarmingUp. (n.d.). Retrieved September 24, 2021, from https://www.warmingup.info/.

[17] *Current world population*. Worldometer. (n.d.). Retrieved September 24, 2021, from https://www.worldometers.info/world-population/.

[18] Lampropoulos, I., Alskaif, T., Schram, W., Bontekoe, E., Coccato, S., & van Sark, W. (2020). Review of energy in the built environment. *Smart Cities*, *3*(2), 248–288. https://doi.org/10.3390/smartcities3020015

[19] Report "buildings and climate change: Status, challenges and opportunities". (2007). *Management of Environmental Quality: An International Journal*, *18*(5). https://doi.org/10.1108/meq.2007.08318eae.007

[20] International Energy Agency (IEA) f. (2017). (rep.). *Towards a zero-emission, efficient, and resilient buildings and construction sector*.

[21] Frankfurt School-UNEP Centre. (2019). (rep.). *GLOBAL TRENDS IN RENEWABLE ENERGY INVESTMENT 2019*.

[22] BECQUÉ, R. E. N. I. L. D. E. (n.d.). *ACCELERATING BUILDING EFFICIENCY*. Accelerating Building Efficiency. Retrieved September 24, 2021, from https://publications.wri.org/buildingefficiency/.

[23] Choiniere, C. J., & Horowitz, J. K. (2001). A production function approach to the gdp-temperature relationship. *SSRN Electronic Journal*. https://doi.org/10.2139/ssrn.267352

[24] Destek, M. A. (2016). Renewable energy consumption and economic growth in newly industrialized countries: Evidence from asymmetric causality test. *Renewable Energy*, *95*, 478–484. https://doi.org/10.1016/j.renene.2016.04.049

[25] IEA. (2021). (rep.). *Greenhouse Gas Emissions from Energy: Overview*.

[26] IEA. (2015). (rep.). *Energy Technology Perspectives 2015*.

[27] IEA. (2013). (rep.). *Transition to sustainable buildings.*

[28] Chen, J. (2020). *Evaluating the economic feasibility of the Passive House in China* (thesis).

[29] Certified buildings map. (n.d.). Retrieved September 24, 2021, from https://database.passivehouse.com/en/buildings/map/.

[30] IPCC. (2014). *CHAPTER 9: Buildings* (pp. 681-682). Retrieved from https://www.ipcc.ch/site/assets/uploads/2018/02/ipcc_wg3_ar5_chapter9.pdf

[31] La Fleur, L., Rohdin, P., & Moshfegh, B. (2019). Investigating cost-optimal energy renovation of a multifamily building in Sweden. *Energy and Buildings*, *203*, 109438. https://doi.org/10.1016/j.enbuild.2019.109438

[32] Tokarik, M. S., & Richman, R. C. (2016). Life cycle cost optimization of passive energy efficiency improvements in a Toronto house. *Energy and Buildings*, *118*, 160–169. https://doi.org/10.1016/j.enbuild.2016.02.015

[33] Dan, D., Tanasa, C., Stoian, V., Brata, S., Stoian, D., Nagy Gyorgy, T., & Florut, S. C. (2016). Passive house DESIGN—AN efficient solution for residential buildings in Romania. *Energy for Sustainable Development*, *32*, 99–109. https://doi.org/10.1016/j.esd.2016.03.007

[34] Sorrell, S. (2015). Reducing energy demand: A review of issues, challenges and approaches. *Renewable and Sustainable Energy Reviews*, *47*, 74–82. https://doi.org/10.1016/j.rser.2015.03.002

[35] Ástmarsson. B.. Jensen. P.. & Maslesa. E. (2013). Sustainable renovation of residential buildings and the landlord/tenant dilemma. *Energy Policy*. *63*. 355-362. https://doi.org/10.1016/j.enpol.2013.08.046

[36] Filippidou, F., Nieboer, N., & Visscher, H. (2017). Are we moving fast enough? The energy renovation rate of the Dutch non-profit housing using the national energy LABELLING DATABASE. *Energy Policy*, *109*, 488–498. https://doi.org/10.1016/j.enpol.2017.07.025

[37] TKI Urban. (2019). *Warmte-Infrastructuur Nederland met verlaagde Systeem Temperatuur* Topsector Energie. Retrieved from https://projecten.topsectorenergie.nl/storage/app/uploads/public/5e9/4a7/3ef/5e94a73ef0fab488622523.pdf

[38] PBL. (2012). *Heating the built environment more sustainably by 2050*. PBL. Retrieved from https://ec.europa.eu/energy/sites/ener/files/documents/ReportART14NL_2_EN.pdf

[39] Calero, M., Cordella, M., Garbarino, E., Mathieux, F., & Wolf, O., MEErP preparatory study On taps and Showers: Final report (2014).

[40] Bertelsen, N., & Vad Mathiesen, B. (2020). EU-28 residential heat supply and consumption: Historical development and status. *Energies*, *13*(8), 1894. https://doi.org/10.3390/en13081894

[41] Balode, L., Dolge, K., & Blumberga, D. (2021). The contradictions between district and individual heating towards Green deal targets. *Sustainability*, *13*(6), 3370. https://doi.org/10.3390/su13063370

[42] Anenberg, S. C., Achakulwisut, P., Brauer, M., Moran, D., Apte, J. S., & Henze, D. K. (2019). Particulate matter-attributable mortality and relationships with carbon dioxide in 250 urban areas worldwide. *Scientific Reports*, *9*(1). https://doi.org/10.1038/s41598-019-48057-9

[43] IRENA (2021), Renewable Power Generation Costs in 2020, International Renewable Energy Agency, Abu Dhabi.

[44] Marina, A., Spoelstra, S., Zondag, H. A., & Wemmers, A. K. (2021). An estimation of the European industrial heat pump market potential. *Renewable and Sustainable Energy Reviews*, *139*, 110545. https://doi.org/10.1016/j.rser.2020.110545

[45] Volkova, A., Pieper, H., Koduvere, H., Lepiskar, K., & Siirde, A. (2021). Heat pump potential in the Baltic States. https://doi.org/10.6027/ner2021-02

[46] Lampropoulos, I., Alskaif, T., Schram, W., Bontekoe, E., Coccato, S., & van Sark, W. (2020). Review of Energy in the Built Environment. Smart Cities, 3(2), 248-288. https://doi.org/10.3390/smartcities3020015

[47] IRENA (2019), Innovation landscape brief: Flexibility in conventional power plants, International Renewable Energy Agency, Abu Dhabi.

[48] Maddah, S., Goodarzi, M., & Safaei, M. (2020). Comparative study of the performance of air and geothermal sources of heat pumps cycle operating with various refrigerants and vapor injection. Alexandria Engineering Journal, 59(6), 4037-4047. https://doi.org/10.1016/j.aej.2020.07.009

[49] CE Delft. (2019). Beyond Gas. Retrieved from https://www.ce.nl/publicaties/download/2764

[50] CE Delft. (2018). Vereffenen kosten warmtetransitie. Retrieved from https://www.ce.nl/publicaties/download/2515

[51] CE Delft. (2019). Energiestrategie Haarlem. Retrieved from https://www.ce.nl/publicaties/download/2686

[52] De Kleijn Energy Consulting. (n.d.). *COP warmtepomp*. Industrialheatpumps.nl. Retrieved September 20, 2021, from https://industrialheatpumps.nl/nederlands/werkingsprincipes/cop_warmtepomp/

[52] Spitler, J.D. (2005) Ground Source Heat Pump System Research – Past, Present and Future (Editorial). International Journal of HVAC&R Research. 11(2):165-167

[53] Casasso, A., & Sethi, R. (2019). Groundwater-related issues of ground source heat pump (GSHP) systems: Assessment, good practices and proposals from the European experience. *Water*, *11*(8), 1573. https://doi.org/10.3390/w11081573

[54] Niemelä, T., Kosonen, R., & Jokisalo, J. (2017). Energy performance and environmental impact analysis of cost-optimal renovation solutions of large panel apartment buildings in Finland. *Sustainable Cities and Society*, *32*, 9–30. https://doi.org/10.1016/j.scs.2017.02.017

[55] Niemelä, T., Kosonen, R., & Jokisalo, J. (2017). Cost-effectiveness of energy performance renovation measures in Finnish brick apartment buildings. *Energy and Buildings*, *137*, 60–75. https://doi.org/10.1016/j.enbuild.2016.12.031

[56] Walker, S., Katic, K., Maassen, W., & Zeiler, W. (2019). Multi-criteria feasibility assessment of cost-optimized alternatives to comply with heating demand of existing office buildings – A case study. *Energy*, *187*, 115968. https://doi.org/10.1016/j.energy.2019.115968

[57] Bonté, D., van Wees, J.-D., & Verweij, J. M. (2012). Subsurface temperature of the onshore netherlands: New temperature dataset and modelling. *Netherlands Journal of Geosciences - Geologie En Mijnbouw*, *91*(4), 491–515. https://doi.org/10.1017/s0016774600000354

[58] PBL, TNO, CBS and RIVM. (2020). *Klimaat- en Energieverkenning 2019* . Retrieved from https://www.pbl.nl/sites/default/files/downloads/pbl-2019-klimaat-en-energieverkenning-2019-3508.pdf.

[59] European Environment Agency. (2021). *Greenhouse gas emission intensity of electricity generation* Retrieved September 20, 2021, from https://www.eea.europa.eu/data-and-maps/daviz/co2-emission-intensity-8#tab-googlechartid_googlechartid_googlechartid_googlechartid_chart_11111.

[60] Sanner, B. (2018). *Report on different kind of barriers for shallow geothermal in deep renovation*. GEO4CIVHIC Consortium. Retrieved from https://ec.europa.eu/research/participants/documents/downloadPublic?documentIds=080166e5bffb5b54&appId=PPGMS

[61] Warmtenetwerk Vlaanderen, COBEN, & Oost-Vlaanderen Energielandschap. (2020). *guideline district heating for local authorities.* North Sea Region.

[62] Gjengedal, S., Stenvik, L. A., Storli, P.-T. S., Ramstad, R. K., Hilmo, B. O., & Frengstad, B. S. (2019). Design of groundwater heat pump systems. principles, tools, and strategies for controlling gas and precipitation problems. *Energies*, *12*(19), 3657. https://doi.org/10.3390/en12193657

[63] Green Energy Association. (2018). The competitiveness of district heating compared to individual heating: When is district heating the cheapest source of heating?. Green Energy Association. Retrieved from https://www.euroheat.org/wp-content/uploads/2018/05/03052018-Thecompetitiveness-of-district-heating-compared-to-individual-heatingv2.pdf

[64] Pieper, H., Ommen, T., Buhler, F., Paaske, B. L., Elmegaard, B., & Markussen, W. B. (2018). Allocation of investment costs for large-scale heat pumps supplying district heating. *Energy Procedia*, *147*, 358–367. https://doi.org/10.1016/j.egypro.2018.07.104

[65] Installatietechniek, K. V. (2015). ISSO-publicatie 82.1 Energieprestatie woningen.

[66] European Commission: Joint Research Centre - Institute for Energy and Transport. (2012). Background Report on EU-27 District Heating and Cooling Potentials, Barriers, Best Practice and Measures of Promotion. Luxembourg: European Commission. Retrieved from http://www.diva-portal.org/smash/get/diva2:994924/FULLTEXT01.pdf

[67] Mijnlieff, H. F., Obdam, A. N. M., van Wees, J. D. A. M., Pluymaekers, M. P. D., & Veldkamp, J. G. (2014). (rep.). *DoubletCalc 1.4 manual* . TNO. Retrieved from https://www.nlog.nl/sites/default/files/6ab98fc3-1ca1-4bbe-b0a2-c5a9658a3597_doubletcalc%20v143%20manual.pdf.

[68] European Geothermal Congress, Vrijlandt, M. A. W., Struijk, E. L. M., Brunner, L. G, Veldkamp, J. G., Witmans, N., Maljers, D., & van Wees, J. D., *ThermoGIS update: a renewed view on geothermal potential in the Netherlands* 11-14 June 20196–6 (2019). Den Haag; TNO.

[69] *Reactie op Raadsonderzoek Geothermie groningen noordwest*. WarmteStad. (2018, July 6). Retrieved October 15, 2021, from https://warmtestad.nl/nieuws/reactie-op-raadsonderzoek-geothermie-groningen-noordwest

[70] Veldkamp, J. G., Loeve, D., Peters, E., Nair, R., Pizzocolo, F., & Wilschut, F. (2016). (rep.). *Thermal fracturing due to low injection temperatures in geothermal doublets*. Utrecht: TNO

[71] Buijze, L., van Bijsterveldt, L., Cremer, H., Paap, B., Veldkamp, H., Wassing, B. B. T., van Wees, J.-D., van Yperen, G. C. N., ter Heege, J. H., & Jaarsma, B. (2019). Review of induced seismicity in geothermal systems worldwide and implications for geothermal systems in the Netherlands. *Netherlands Journal of Geosciences*, *98*. https://doi.org/10.1017/njg.2019.6

[72] CONCERTO (n.d.). *5. Shallow Geothermal Systems*. Geothermal Communities. Retrieved September 22, 2021, from https://geothermalcommunities.eu/assets/elearning/6.22.Shallow%20Geothermal%20SYstems.pdf.

[73] Khosravy, M. (2021). Recent Progress in District Heating with Emphasis on Low-Temperature Systems. *Geothermal Energy*. Retrieved from https://www.intechopen.com/online-first/74667

[74] Santos, C. A., Díez Borge David, & Rosales-Asensio, E. (2017). *District heating and cooling networks in the European Union*. Springer.

[75] Lund, H., Werner, S., Wiltshire, R., Svendsen, S., Thorsen, J. E., Hvelplund, F., & Mathiesen, B. V. (2014). 4th generation district heating (4GDH). *Energy*, *68*, 1–11. https://doi.org/10.1016/j.energy.2014.02.089

[76] Schmidt, D. (2018). Low Temperature District heating for Future Energy Systems. *Energy Procedia*, *149*, 595–604. https://doi.org/10.1016/j.egypro.2018.08.224

[77] Hansen, C. H., Gudmundsson, O., & Detlefsen, N. (2019). Cost efficiency of district heating for low energy buildings of the future. *Energy*, *177*, 77–86. https://doi.org/10.1016/j.energy.2019.04.046

[78] Grzegórska, A., Rybarczyk, P., Lukoševičius, V., Sobczak, J., & Rogala, A. (2021). Smart Asset Management for district heating systems in the Baltic Sea Region. *Energies*, *14*(2), 314. https://doi.org/10.3390/en14020314

[79] Jangsten, M. (2016). *Survey of Radiator Temperatures in Buildings Supplied by District Heating* (thesis). Retrieved from https://celsiuscity.eu/wp-content/uploads/2020/01/194-Jangsten-thesis.pdf

[80] Heiselberg, P. K. (2016). CLIMA 2016 - proceedings of the 12th REHVA World Congress: volume 10. Aalborg: Aalborg University, Department of Civil Engineering.

[81] Working Committee QM District Heating. (2018). Handbook on Planning of District Heating Networks. *Verenum*. Retrieved September 22, 2021, from http://www.verenum.ch/Dokumente/Handbook-DH_V1.0.pdf.

[82] Erbs Poulsen, S., Bjørn, H., Mathiesen, A., Henrik Nielsen, L., Vangkilde-Pedersen , T., Ditlefsen, C., & Røgen, B. (2019). European Geothermal Congress 2019. In *Geothermal Energy Use, Country Update for Denmark*. Den Haag; GEUS. Retrieved from https://europeangeothermalcongress.eu/wp-content/uploads/2019/07/CUR-09-Denmark.pdf

[83] *Albertslund, Denmark* . Celsiuscity. (2019, November). Retrieved September 22, 2021, from http://celsiuscity.eu/wp-content/uploads/2019/11/Albertslund.pdf

[84] *GEOTHERMAL DISTRICT HEATING IN THISTED - DENMARK*. Heat Pumping Technologies . (2018). Retrieved September 22, 2021, from https://heatpumpingtechnologies.org/annex47/wp-content/uploads/sites/54/2018/12/annex-47sub-projetcsthistedgeothermal.pdf

[85] Boissavy, C., Henry, L., Genter, A., Pomart, A., Rocher, P., & Schmidlé-Bloch, V. (2019). European Geothermal Congress 2019. In *Geothermal Energy Use, Country Update for France* . Den Haag. Retrieved from http://europeangeothermalcongress.eu/wp-content/uploads/2019/07/CUR-11-France.pdf

[86] Lavagna, M., Baldassarri, C., Campioli, A., Giorgi, S., Dalla Valle, A., Castellani, V., & Sala, S. (2018). Benchmarks for environmental impact of housing in Europe: Definition of archetypes and LCA of the Residential Building Stock. *Building and Environment*, *145*, 260–275. https://doi.org/10.1016/j.buildenv.2018.09.008

[87] Smith, D. P. (2019). Fitting geothermal energy into the Energy Transition. *Netherlands Journal of Geosciences*, *98*. https://doi.org/10.1017/njg.2019.5

[88] Blokker, E. J. M., & Pieterse-Quirijns, E. J. (2013). Modeling temperature in the drinking water distribution system. *Journal - American Water Works Association*, *105*(1). https://doi.org/10.5942/jawwa.2013.105.0011

[89] Koo, C., Hong, T., Lee, M., & Seon Park, H. (2014). Development of a new energy efficiency rating system for existing residential buildings. *Energy Policy*, *68*, 218–231. https://doi.org/10.1016/j.enpol.2013.12.068

[90] Allaerts, K., De Oliveira, F., Hollmuller, P., Guglielmetti, L., Quiquerez, L., Maragna, C., Rey, C., Gauthier, G., Kleinlugtenbelt, R., Octaviano, R., & Clarijs, M. (2021). (publication). *UTES and its integration in the heating system - Defining optimal design and operational strategies for the demonstration cases*. GEOTHERMICA. Retrieved from https://www.heatstore.eu/documents/HEATSTORE_WP3_D3.3_Final_v2021.06.23.pdf

[91] van Dongen, B. (2019, January 17). *The economic potential of deep, direct use geothermal systems in the Netherlands* (thesis). Retrieved from https://repository.tudelft.nl/islandora/object/uuid%3A4b1f0f67-f990-4e7e-a4be-104bdf07ebdc

[92] TNO (2010). *Map Viewer*. Thermogis. Retrieved September 23, 2021, from https://www.thermogis.nl/en/map-viewer

[93] Barcelona, H., Senger, M., & Yagupsky, D. (2021). Resource assessment of the copahue geothermal field. *Geothermics*, *90*, 101987. https://doi.org/10.1016/j.geothermics.2020.101987

[94] Smit, R. C. A., Salimi, H., & Wolf, K. H. A. A. (2014). Optimization of geothermal-well-doublet placement. *Proceedings 76th EAGE Conference and Exhibition 2014*. https://doi.org/10.3997/2214-4609.20140830

[95] Nakagawa, M. P. D., Fujiono, H. P. D., McCartney, J. S., & Reed, A. J. D. (2011). Geothermal Academy: Focus Center for data collection, analysis, and dissemination. https://doi.org/10.2172/1045164

[96] ACM. (2015, February 5). *ACM favours study into the Dutch heat act*. ACM.nl. Retrieved September 23, 2021, from https://www.acm.nl/en/publications/publication/13818/ACM-favors-study-into-the-Dutch-Heat-Act

[97] United Nations Environment Programme (2020). *2020 Global Status Report for Buildings and Construction: Towards a Zero-emission, Efficient and Resilient Buildings and Construction Sector*. Nairobi

[98] PBL (2020). (rep.). *Netherlands Climate and Energy Outlook 2020*. Retrieved from https://www.pbl.nl/sites/default/files/downloads/pbl-2020-netherlands-climate-and-energy-outlook-2020-summary-4299.pdf

[99] Statistics Netherlands. (2019, March 12). *Natural gas trade deficit for the first time in 2018*. Statistics Netherlands. Retrieved September 23, 2021, from https://www.cbs.nl/en-gb/news/2019/11/natural-gas-trade-deficit-for-the-first-time-in-2018

[100] Gasunie (2017). *Gasunie in beweging: jaarverslag 2017.*

[101] *Times are changing for district heating*. Warmopweg.nl. (2018, January 9). Retrieved September 23, 2021, from https://warmopweg.nl/times-are-changing-for-district-heating/

[102] *Reactie op Raadsonderzoek Geothermie groningen noordwest*. WarmteStad. (2018, July 6). Retrieved October 15, 2021, from https://warmtestad.nl/nieuws/reactie-op-raadsonderzoek-geothermie-groningen-noordwest

[103] Parallel. (2020). Netherlands building ages. Retrieved September 23, 2021, from https://parallel.co.uk/netherlands/#14.31/51.81009/4.63785/0/40

[104] *Nationale EnergieAtlas*. Kaarten | Nationale Energie Atlas. (2021, February). Retrieved September 23, 2021, from https://www.nationaleenergieatlas.nl/kaarten.

[105] Sommer, W., Valstar, J., van Gaans, P., Grotenhuis, T., & Rijnaarts, H. (2015). The impact of aquifer heterogeneity on the performance of Aquifer Thermal Energy Storage. *Water Resources Research*, *49*(12), 8128–8138. https://doi.org/10.1002/2013wr013677

[106] Ganguly, S., Mohan Kumar, M. S., Date, A., & Akbarzadeh, A. (2017). Numerical investigation of temperature distribution and thermal performance while charging-discharging thermal energy in Aquifer. *Applied Thermal Engineering*, *115*, 756–773. https://doi.org/10.1016/j.applthermaleng.2017.01.009

[107] Chen, J., Wilson, C. R., Famiglietti, J. S., & Scanlon, B. R. (2018). Groundwater storage monitoring from space. *Comprehensive Remote Sensing*, 295–314. https://doi.org/10.1016/b978-0-12-409548-9.10361-6

[108] Asquith, G., Krygowski, D., Henderson, S., & Hurley, N. (2004). Gamma Ray Log. *Basic Well Log Analysis*. https://doi.org/10.1306/mth16823c3

[109] Mineralogical Society of America. (1996). *Reactive transport in porous media*.

[110] Hartog, N., & Antics, M. (2015). (rep.). *A Case Study for several Greenhouse Geothermal Systems in The Netherlands*. Retrieved from https://www.kasalsenergiebron.nl/content/research/14898_Injectiviteitsproblemen_bij_geothermische_bronnen_in_Nederland.pdf

[111] GeoEnergy, T. (2020, June 17). *Shallow(ER) geothermal resources successfully utilised for Dutch Greenhouse Operations*. Think GeoEnergy - Geothermal Energy News. Retrieved September 24, 2021, from https://www.thinkgeoenergy.com/shallower-geothermal-resources-successfully-utilised-for-dutch-greenhouse-operations/

[112] Drijver, B. (2011). In *High temperature aquifer thermal energy storage (HT-ATES) - water treatment in practice*. Utrecht; IF Technology . Retrieved from https://www.iftechnology.com/wp-content/uploads/2018/05/Drijver-et-al-2012-High-temperature-aquifer-thermal-energy-storage-HT-ATES-sustainable-and-multi-usable-1.pdf

[113] Ministerie van Economische Zaken en Klimaat. (2021, September 13). *Injectie van Productiewater door nam in Twente Onder Verscherpt Toezicht*. Nieuwsbericht | Staatstoezicht op de Mijnen. Retrieved September 24, 2021, from https://www.sodm.nl/actueel/nieuws/2021/06/28/injectie-van-productiewater-door-nam-in-twente-onder-verscherpt-toezicht

[114] Zoback, M. (2018). *Reservoir Geomechanics*. Cambridge: Cambridge University Press. https://doi.org/10.1017/CBO9780511586477

[115] TNO (2021). *Personal communication*

[116] Proceedings World Geothermal Congress 2005, Kaya, T., & Mertoglu, O., Engineering Aspects of Geothermal Production Well with Down Hole Pumps (2005). Retrieved from https://www.geothermal-energy.org/pdf/IGAstandard/WGC/2005/1029.pdf

[117] van ´t Spijker, H., & Ungemach, P. (2016). (rep.). *Definition of Electrosubmersible pump (ESP) design and selection workflow*. https://www.kasalsenergiebron.nl/content/user_upload/Definition_of_ESP_design-_final_version_20160629_-public_v2.pdf

[118] HVC (2021). *Personal communication*

[119] Schoof, F. (2014). (rep.). *Handboek Geothermie 2014*. Kas als Energiebron. Retrieved from https://www.kasalsenergiebron.nl/content/user_upload/Handboek_Geothermie_DEEL_1_-_2014.pdf

[120] Batzle, M., & Wang, Z. (1992). *Seismic properties of pore fluids*. Geophysics, Vol. 57, 1396-1408. Retrieved from http://riogrande.nmt.edu/outside/courses/hyd571/supplemental/batzle_wang_geophysics_1992.pdf

[121] Ferris, J. G., Stallman R. W., Knowles, D. B., & Brown, R. H. (1962). *Theory of aquifer tests*. USGS. Retrieved from https://pubs.usgs.gov/wsp/wsp1536-E/pdf/wsp_1536-E_a.pdf

[122] Pavel, P. & Novotný, R. (2005). EVALUATION OF STORATIVITY AND SKIN FACTOR FROM AQUIFER TEST. Scientia Agriculturae Bohemica. 36. 77-80.

[123] Nguyen, M. C., Dejam, M., Fazelalavi, M., Zhang, Y., Gay, G. W., Bowen, D. W., Spangler, L. H., Zaluski, W., & Stauffer, P. H. (2021). Skin factor and potential formation damage from chemical and mechanical processes in a naturally fractured carbonate aquifer with implications to CO2 Sequestration. *International Journal of Greenhouse Gas Control*, *108*, 103326. https://doi.org/10.1016/j.ijggc.2021.103326

[124] Waters, D., & Weijermars, R. (2021). Predicting the performance of undeveloped multi-fractured Marcellus Gas Wells using an analytical flow-cell model (FCM). *Energies*, *14*(6), 1734. https://doi.org/10.3390/en14061734

[125] Veldkamp, J. G., & Egberts, P. J. P. (2014). (rep.). *Modelling horizontal wells in DoubletCalc*. TNO. Retrieved from https://www.nlog.nl/sites/default/files/equivalent%20skin%20horizontal%20well.pdf

[126] Aziz, K. (2000). Productivity and injectivity of Horizontal Wells. https://doi.org/10.2172/751965

[127] Bakema, G., & Buik , N. (2019). (rep.). *Geothermie putten in ondiepe fijnzandige formaties*. IF Technology. Retrieved from https://www.kasalsenergiebron.nl/content/user_upload/Geothermie_Putten_in_ondiepe_fijnzandige_formaties_def_2.pdf

[128] Donselaar, M., Groenenberg, R. & Gilding, D. (2015). *Reservoir Geology and Geothermal Potential of the Delft Sandstone Member in the West Netherlands Basin.* Retrieved from https://www.researchgate.net/publication/311100231_Reservoir_Geology_and_Geothermal_Potential_of_the_Delft_Sandstone_Member_in_the_West_Netherlands_Basin

[129] Satter, A., & Iqbal, G. M. (2016). Reservoir fluid properties. *Reservoir Engineering*, 81–105. https://doi.org/10.1016/b978-0-12-800219-3.00004-8

[130] *SDE++ 2020 Stimulation of Sustainable Energy Production and Climate Transition*. RVO. (2020). Retrieved September 24, 2021, from https://english.rvo.nl/sites/default/files/2020/11/Brochure%20SDE%20plus%20plus%202020.pdf.

[131] Mitchell, R. F., Miska, S., & Aadnøy, B. S. (2011). *Fundamentals of drilling engineering*. Society of Petroleum Engineers

[132] Culver, G. (1998). (rep.). *Chapter 6 DRILLING AND WELL CONSTRUCTION*. Osti. Retrieved from https://www.osti.gov/etdeweb/servlets/purl/895127

[133] *API coupling and threads for casing & tubing (OCTG coupling)*. Octalsteel. (n.d.). Retrieved September 24, 2021, from https://www.octalsteel.com/api-coupling-and-threads

[134] Kruyt, B., & Buiting , T. (2010). (rep.). *Warmtetarieven voor huishoudens KOSTEN VOOR WARMTEWONINGEN IN VERGELIJKING MET GASWONINGEN EN EEN VOORUITBLIK OP DE MOGELIJKE GEVOLGEN VAN DE WARMTEWET*. BECO Groep. Retrieved from http://www.stadsverarming.nl/wp-content/uploads/2016/08/2010.06.07-BECO_Warmtetarieven_Warmtestad.pdf

[135] Matthijssen, E. (n.d.). *Welcome to the ESDL MAPEDITOR documentation*¶. ESDL MapEditor documentation. Retrieved September 24, 2021, from https://esdl-mapeditor-documentation.readthedocs.io/en/latest/

[136] Blokker, E. J. M., & Pieterse-Quirijns, E. J. (2013). Modeling temperature in the drinking water distribution system. *Journal - American Water Works Association*, *105*(1). https://doi.org/10.5942/jawwa.2013.105.0011

[137] Sandvall, A. F., Ahlgren, E. O., & Ekvall, T. (2017). Cost-efficiency of urban heating strategies – modelling scale effects of low-energy building heat supply. *Energy Strategy Reviews*, *18*, 212–223. https://doi.org/10.1016/j.esr.2017.10.003

[138] White, F. M. (2011). *Fluid mechanics*. McGraw-Hill. Retrieved from https://warwick.ac.uk/fac/sci/eng/staff/ymc/members/former/azimi/project/references/white_frank_m._-_fluid_mechanics_4th_ed_mcgraw_hill.pdf.

[139] *Product Catalogue District Energy* . LOGSTOR. (2020). Retrieved September 24, 2021, from https://www.logstor.com/.

[140] Nielsen, G. (2019, August). *Use of ammonia in comfort cooling and heat pump* . Retrieved September 24, 2021, from https://xrgy.no/wp-content/uploads/2019/08/Use-of-ammonia-in-comfort-cooling-and-heat-pump-applications.pdf.

[141] Zehnder, M. (2004). Efficient air-water heat pumps for high temperature lift residential heating, including oil migration aspects. https://doi.org/10.5075/epfl-thesis-2998

[142] Marina, A., Spoelstra, S., Zondag, H. A., & Wemmers, A. K. (2021). An estimation of the European industrial heat pump market potential. *Renewable and Sustainable Energy Reviews*, *139*, 110545. https://doi.org/10.1016/j.rser.2020.110545

[143] ASHRAE (2007). Geothermal energy. In ASHRAE (Ed.), *ASHRAE handbook: Heating, ventilating, and air-conditioning applications* (pp. 32.31-32.30). Atlanta, GA: American Society of Heating, Refrigerating and Air-Conditioning Engineers, Inc.

[144] Halozan, H. (2010) *Limits of Heat Pumps in LowEx Design*, Proceedings ECBCS Annex 49 Conference The Future for Sustainable Built Environments with High Performance Energy Systems, 19th - 21st October 2010, Munich, Germany

[145] Jensen, J. K. (2015). *Industrial heat pumps for high temperautre process applications: A numerical study of the ammonia-water hybrid absorption-compression heat pump*. DTU Mechanical Engineering. Retrieved from https://orbit.dtu.dk/en/publications/industrial-heat-pumps-for-high-temperature-process-applications-a.

[146] Ally, M. R., Munk, J. D., Baxter, V. D., & Gehl, A. C. (2015). Exergy analysis of a two-stage ground source heat pump with a vertical bore for residential space conditioning under simulated occupancy. *Applied Energy*, *155*, 502–514. https://doi.org/10.1016/j.apenergy.2015.06.004

[147] Spoelstra, S. (2014). *Industrial Heat Pumps*. *ECN*. Eindhoven.

[148] Pieper, H., Ommen, T., Kjær Jensen, J., Elmegaard, B., & Brix Markussen, W. (2020). Comparison of COP estimation methods for large-scale heat pumps used in energy planning. *Energy*, *205*, 117994. https://doi.org/10.1016/j.energy.2020.117994

[149] IF Technology, & AT Osborne. (2019). (rep.). *Haalbaarheidsstudie TEO in Kaag en Braassem*. Retrieved from https://atosborne.nl/wp-content/uploads/2020/04/Rapport-Haalbaarheidsstudie-TEO-Kaag-en-Braassem.pdf

[150] Gudmundsson, O., Thorsen, J. E., & Zhang, L. (2013). Cost analysis of district heating compared to its competing technologies. *Energy and Sustainability IV*. https://doi.org/10.2495/esus130091

[151] Schoots, K., & Hekkenberg, M. (2016). (rep.). *Nationale Energieverkenning 2016*. TNO . Retrieved from https://publications.ecn.nl/bs/2016/ECN-O--16-035

[152] Rutten, L. (2019, September 25). *Natural gas steam boiler industry - energy*. Retrieved September 24, 2021, from https://energy.nl/wp-content/uploads/2021/01/Technology-Factsheets-Natural-Gas-Boiler-Industry.pdf

[153] Dincer, I., & Rosen, M. A. (2015). Heat Storage Systems. *Exergy Analysis of Heating, Refrigerating and Air Conditioning*, 221–278. https://doi.org/10.1016/b978-0-12-417203-6.00006-5

[154] De Groot, S. R. M. (2020). (rep.). *Economic and thermal performance of Ecovat and comparable thermal energy storage technologies*. Ecovat. Retrieved from https://refman.energytransitionmodel.com/publications/2125

[155] de Guadalfajara, M, Lozano, M., & Serra, L. (2014). Analysis of Large Thermal Energy Storage for Solar District Heating. https://doi.org./10.13140/2.1.3857.6008

[156] PlanEnergi. (2017). (rep.). *D2.3 Large Storage Systems for DHC Networks*. PlanEnergi. Retrieved from https://planenergi.dk/wp-content/uploads/2018/04/WP2_D2.3_20180305_P02_Large-storage-systems-for-DHC-networks.pdf

[157] Bott, C., Dressel, I., & Bayer, P. (2019). State-of-technology review of water-based closed seasonal thermal energy storage systems. *Renewable and Sustainable Energy Reviews*, *113*, 109241. https://doi.org/10.1016/j.rser.2019.06.048

[158] Hauer, A. (2011.). *Storage Technology Issues and Opportunities* . IEA. Retrieved September 24, 2021, from https://iea.blob.core.windows.net/assets/imports/events/337/Hauer.pdf

[159] Heuvel, M. M. M. M. van den. (2020, October 7). *Peak buffering by the Ecovat Thermal Energy Storage System* (thesis). *Ecovat*. Retrieved from https://www.ecovat.eu/wp-content/uploads/2020/10/0950302-Peak-Buffering-by-the-Ecovat-Thermal-Energy-Storage-System-Master-Thesis-Marijn-van-den-Heuvel-gecomprimeerd.pdf

[160] Veldkamp, J. G., Goldberg, T. V., Bressers, P. M. M. C., & Wilschut, F. (2016). (rep.). *Corrosion in Dutch geothermal systems*. TNO. Retrieved from https://www.nlog.nl/sites/default/files/2016.03.15_tno%202015%20r10160_corrosion%20in%20dutch%20geothermal%20systems_public.pdf

[161] Segers , R., Niessink , R., van den Oever, R., & Menkveld, M. (2019). (rep.). *Warmtemonitor 2017*. TNO & CBS. Retrieved from https://www.cbs.nl/nl-nl/achtergrond/2019/23/warmtemonitor-2017

[162] Niewold, F., & Scholten, B. (2019). (rep.). *RAPPORT | BUSINESS CASE INTEGRALE AANPAK TEO EN KLIMAATADAPTATIE IN AMERSFOORT SCHOTHORST*. IF Technology . Retrieved from https://www.stowa.nl/sites/default/files/assets/PROJECTEN/Projecten%202016/project449.003%20thermische%20energie/Rapport%20-%20Business%20case%20integrale%20aanpak%20TEO%20en%20klimaatadaptatie%2C%20Amersfoort%20Schothorst%20-%20Definitief.pdf

[163] Li, T., Liu, Y., Wang, D., Shang, K., & Liu, J. (2015). Optimization analysis on storage tank volume in Solar Heating System. *Procedia Engineering*, *121*, 1356–1364. https://doi.org/10.1016/j.proeng.2015.09.019

[164] CE Delft. (2021, January 4). *Hr-combiketel* . Retrieved September 24, 2021, from https://ce.nl/wp-content/uploads/2021/04/01_Factsheet-HR-combiketel_DEF.pdf.

[165] Zijlema, P. J. (2018). (rep.). *The Netherlands: list of fuels and standard CO2 emission factors version of January 2018*. Netherlands Enterprise Agency. Retrieved from https://english.rvo.nl/sites/default/files/2017/04/The_Netherlands_list_of_fuels_version_January_2017_final.pdf

[166] Ministry of Economic Affairs of The Netherlands. (2016). (rep.). *Transition to sustainable energy*. Retrieved from https://www.government.nl/documents/reports/2016/04/28/energy-report-transition-tot-sustainable-energy

[167] Joshi, S. D. (2003). Cost/benefits of Horizontal Wells. *Society of Petroleum Engineers Inc*. https://doi.org/10.2118/83621-ms

[168] Dankwa, O. K., Opoku Appau, P., & Gomah Ahmed, S. N. (2018). Comparison of the economics and performance of horizontal and Vertical Wells. *International Journal of Petroleum and Petrochemical Engineering*, *4*(3). https://doi.org/10.20431/2454-7980.0403001

[169] Stichting Platform Geothermi. (2015). (rep.). *Notitie bijvangst koolwaterstoffen bij aardwarmte* . Retrieved from https://geothermie.nl/images/bestanden/notitie_bijvangst_def_EZ_19_10-2015.pdf

[170] Kas als Energiebron. (2016). (rep.). *GEOTHERMAL WELL INTEGRITY STUDY*. Retrieved from https://www.kasalsenergiebron.nl/content/user_upload/Geothermal_Wells_integrity_study_report_final.pdf

[171] Osundare, O., Falcone, G., & Ichim, A. (2018). (rep.). *Estimation of Plugging and Abandonment Costs Based on Different EU Regulations with Application to*

Geothermal Wells. Retrieved from https://pangea.stanford.edu/ERE/pdf/IGAstandard/SGW/2018/Osundare.pdf

[172] Ministry of Economic Affairs. (2017). (rep.). *Energy Agenda: Towards a low-carbon energy supply*. Retrieved from https://www.government.nl/documents/reports/2017/03/01/energy-agenda-towards-a-low-carbon-energy-supply

[173] Mathiesen, B., Blarke, M., Hansen, K., Connolly, D (2011). *The role of large-scale heat pumps for short term integration of renewable energy*. Retrieved from https://vbn.aau.dk/en/publications/the-role-of-largescale-heat-pumps-for-short-term-integration-of-r

[174] Akpan, P. U., Jones, S., Eke, M. N., & Yeung, H. (2015). Modelling and transient simulation of water flow in pipelines using Wanda Transient Software. *Ain Shams Engineering Journal*, *8*(3), 457–466. https://doi.org/10.1016/j.asej.2015.09.006

[175] Anderson, B., Tester, J., & Augustine, C. (2006). (rep.). *A COMPARISON OF GEOTHERMAL WITH OIL AND GAS WELL DRILLING COSTS* . Retrieved from https://citeseerx.ist.psu.edu/viewdoc/download?doi=10.1.1.554.6442&rep=rep1&type=pdf

[176] HVC. (2021). *Warmtetarieven 2021*. Retrieved September 24, 2021, from https://nieuws.hvcgroep.nl/sites/nieuws.hvcgroep.nl/files/2021-05/HVC%20JV2018-Clickable%20PDF%20DEF.pdf.

[177] Oxera. (2020). (rep.). *Alternatives to the gas reference price*

[178] Mital, A., Kilbom Åsa, & Kumar, S. (2000). *Ergonomics guidelines and problem solving*. Elsevier.

[179] Birge, J. R., & Linetsky, V. (2008). *Financial engineering* (Vol. 15). Elsevier. Retrieved from https://ur.zlibcdn2.com/book/571920/db96c4

[180] Trinomics. (2020). (rep.). *Final Report Cost of Energy (LCOE).* Retrieved from http://trinomics.eu/wp-content/uploads/2020/11/Final-Report-Cost-of-Energy-LCOE.pdf

[181] Wall, A., Dobson, P., & Thomas, H. (2017). (rep.). *Geothermal Costs of Capital: Relating Market Valuation to Project Risk and Technology*. Berkeley. Retrieved from https://publications.mygeoenergynow.org/grc/1033704.pdf

[182] Lensink , S. (2017). (rep.). *Correctiebedragen 2018*. ECN. Retrieved from http://docplayer.nl/106217995-Introductie-op-proces.html.

[183] RVO. (2019). (rep.). *Beleidsevaluatie Regeling groenprojecten 2010-2017: eindrapport* Retrieved from https://www.rijksoverheid.nl/documenten/rapporten/2020/04/22/beleidsevaluatie-regeling-groenprojecten-2010-2017

[184] ACM. (2019). (rep.). *WACC calculation for heat exchangers in The Netherlands*. Europe Economics. Retrieved from https://www.acm.nl/sites/default/files/documents/2019-12/wacc-calculation-for-heat-exchangers-in-the-netherlands.pdf

[185] Sander, L., & Cleijne , H. (2017). (rep.). *Financiering SDE+ 2018* (p. 2). Amsterdam: ECN.

[186] Blok, K., & Nieuwlaar, E. (2021). *Introduction to energy analysis*. Routledge.

[187] Wasch, L.; Shoeibi-Omrani, P.; Twerda, A. Integrated Scale Management for Geothermal. In Proceedings of the European Geothermal Congress 2019, Den Haag, The Netherlands, 11–14 June 2019; p6

[188] Zhu, J., & Zhang, W. (2004). Optimization design of plate heat exchangers (PHE) for Geothermal District Heating Systems. *Geothermics*, *33*(3), 337–347. https://doi.org/10.1016/j.geothermics.2003.08.013

[189] Bae, S., Nam, Y., Lee, K., & Choi, J. (2019). Analysis on thermal performance of ground heat exchanger according to design type based on thermal response test. *Energies*, *12*(4), 651. https://doi.org/10.3390/en12040651

[190] Eswiasi, A., & Mukhopadhyaya, P. (2020). Critical review on efficiency of ground heat exchangers in Heat Pump Systems. *Clean Technologies*, *2*(2), 204–224. https://doi.org/10.3390/cleantechnol2020014

[191] Izgec, O., Demiral, B., Bertin, H., & Akin, S. (2005). (rep.). *CALCITE PRECIPITATION IN LOW TEMPERATURE GEOTHERMAL SYSTEMS: AN EXPERIMENTAL APPROACH* . Stanford University . Retrieved from https://pangea.stanford.edu/ERE/pdf/IGAstandard/SGW/2005/izgec.pdf

[192] Degens, G., Zijp, M., de Boe, J., Obdam, A., & Jedari Eyvaz, F. (2012). (rep.). *BIA Geothermal – TNO Umbrella Report into the Causes and Solutions to Poor Well Performance in Dutch Geothermal Projects*. TNO. Retrieved from https://www.nlog.nl/sites/default/files/bia%20geothermal%20%E2%80%93%20tno%20umbrella%20report%20into%20the%20causes%20and%20solutions%20to%20poor%20well%20performance%20in%20dutch%20geothermal%20projects.pdf

12.0 Appendix

Appendix A: Porosity and permeability readings simulated from the 3D subsurface model conducted by the WarmingUP aquifer characterisation

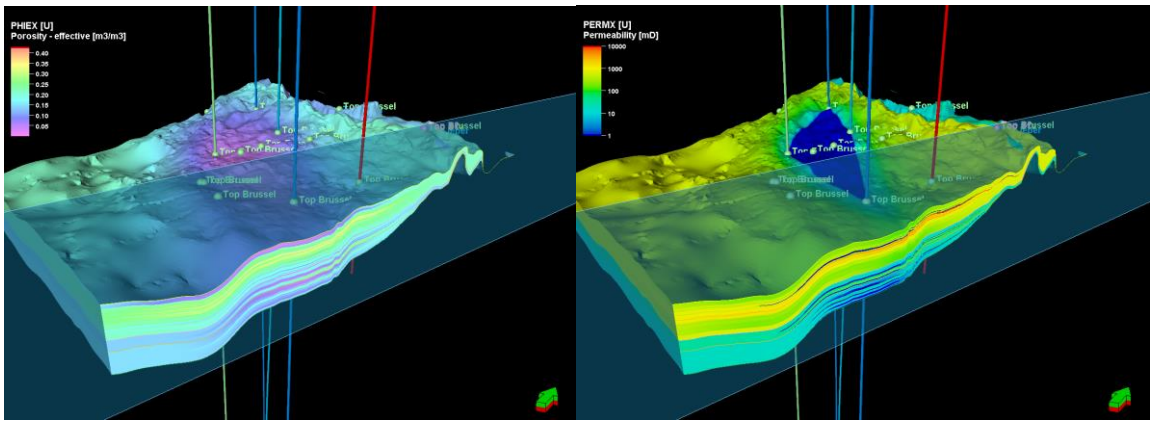

Appendix B1: DoubletCalc1D input-output interface showing the ΔP in the injection well for the P50 scenario to be less than 15 bar (14.79 bar), thus the injection temperature complies within the recommended safety constraint.

Geotechnics (Input)

Property	min	median	max
aquifer permeability (mD)	500.0	700.0	800.0
aquifer net to gross (-)	0.5	0.55	0.6
aquifer gross thickness (m)	80.0	95.0	105.0
aquifer top at producer (m TVD)	572.0	635.0	699.0
aquifer top at injector (m TVD)	554.0	615.0	677.0
aquifer water salinity (ppm)	35000.0	38000.0	45000.0

Property	value
number of simulation runs (-)	1000.0
aquifer kh/kv ratio (-)	10.0
surface temperature (°C)	10.0
geothermal gradient (°C/m)	0.032
mid aquifer temperature producer (°C)]	0.0
inital aquifer pressure at producer (bar)]	0.0
[initial aquifer pressure at injector (bar)]	0.0
exit temperature heat exchanger (°C)	5.0
distance wells at aquifer level (m)	1000.0
pump system efficiency (-)	0.7
production pump depth (m)	200.0
pump pressure difference (bar)	24.0
outer diameter producer (inch)	10.63
skin producer (-)	0.0
skin due to penetration angle p (-)	-1.81
pipe segment sections p (m AH)	150.0,300.0,1320.0
pipe segment depth p (m TVD)	150.0,300.0,744.0
pipe inner diameter p (inch)	9.13,9.13,9.13
pipe roughness p (milli-inch)	2.0,2.0,2.0
outer diameter injector (inch)	10.63
skin injector (-)	0.0
skin due to penetration angle i (-)	-1.81
pipe segment sections i (m AH)	150.0,300.0,1300.0
pipe segment depth i (m TVD)	150.0,300.0,733.0

Geotechnics (Output)

Monte Carlo cases (stochastic inputs)	P90	P50	P10
aquifer kH net (Dm)	29.97	35.63	40.31
mass flow (kg/s)	27.42	32.28	36.32
pump volume flow (m³/h)	96.7	113.7	127.9
required pump power (kW)	92.1	108.3	121.8
geothermal power (MW)	2.88	3.4	3.86
COP (kW/kW)	30.2	31.4	32.7
aquifer pressure at producer (bar)	71.91	75.2	79.15
aquifer pressure at injector (bar)	70.83	73.9	77.79
pressure difference at producer (bar)	8.96	9.08	9.21
pressure difference at injector (bar)	14.67	14.79	14.93
aquifer temperature at producer * (°C)	30.72	31.83	32.95
temperature at heat exchanger (°C)	30.45	31.48	32.57

base case (median value inputs)	value
aquifer kH net (Dm)	36.58
mass flow (kg/s)	33.13
pump volume flow (m³/h)	116.8
required pump power (kW)	111.2
geothermal power (MW)	3.5
COP (kW/kW)	31.5
aquifer pressure at producer (bar)	75.18
aquifer pressure at injector (bar)	73.83
pressure difference at producer (bar)	9.06
pressure difference at injector (bar)	14.79
aquifer temperature at producer * (°C)	31.84
temperature at heat exchanger (°C)	31.5
pressure at heat exchanger (bar)	15.03

* @ mid aquifer depth

Appendix B2: Flowrates for a vertical well (0 skin factor), showing a 20% difference between the deviated well (B1)

Geotechnics (Input)

Property	min	median	max
aquifer permeability (mD)	500.0	700.0	800.0
aquifer net to gross (-)	0.5	0.55	0.6
aquifer gross thickness (m)	80.0	95.0	105.0
aquifer top at producer (m TVD)	572.0	635.0	699.0
aquifer top at injector (m TVD)	554.0	615.0	677.0
aquifer water salinity (ppm)	35000.0	38000.0	45000.0

Property	value
number of simulation runs (-)	1000.0
aquifer kh/kv ratio (-)	10.0
surface temperature (°C)	10.0
geothermal gradient (°C/m)	0.032
: mid aquifer temperature producer (°C)]	0.0
inital aquifer pressure at producer (bar)]	0.0
[initial aquifer pressure at injector (bar)]	0.0
exit temperature heat exchanger (°C)	15.0
distance wells at aquifer level (m)	1000.0
pump system efficiency (-)	0.7
production pump depth (m)	200.0
pump pressure difference (bar)	24.0
outer diameter producer (inch)	10.63
skin producer (-)	0.0
skin due to penetration angle p (-)	0.0
pipe segment sections p (m AH)	150.0,300.0,1320.0
pipe segment depth p (m TVD)	150.0,300.0,744.0
pipe inner diameter p (inch)	9.13,9.13,9.13
pipe roughness p (milli-inch)	2.0,2.0,2.0
outer diameter injector (inch)	10.63
skin injector (-)	0.0
skin due to penetration angle i (-)	0.0
pipe segment sections i (m AH)	150.0,300.0,1300.0
pipe segment depth i (m TVD)	150.0,300.0,733.0

Geotechnics (Output)

Monte Carlo cases (stochastic inputs)	P90	P50	P10
aquifer kH net (Dm)	30.17	35.56	40.43
mass flow (kg/s)	24.96	29.2	33.01
pump volume flow (m³/h)	87.9	102.9	116.3
required pump power (kW)	83.7	98.0	110.8
geothermal power (MW)	1.59	1.91	2.22
COP (kW/kW)	18.3	19.5	20.8

aquifer pressure at producer (bar)	71.89	75.18	79.17
aquifer pressure at injector (bar)	70.91	73.88	77.77
pressure difference at producer (bar)	10.19	10.31	10.44
pressure difference at injector (bar)	13.44	13.56	13.69
aquifer temperature at producer * (°C)	30.72	31.83	32.99
temperature at heat exchanger (°C)	30.43	31.45	32.52

base case (median value inputs)	value
aquifer kH net (Dm)	36.58
mass flow (kg/s)	30.0
pump volume flow (m³/h)	105.8
required pump power (kW)	100.7
geothermal power (MW)	1.97
COP (kW/kW)	19.6

aquifer pressure at producer (bar)	75.18
aquifer pressure at injector (bar)	73.83
pressure difference at producer (bar)	10.3
pressure difference at injector (bar)	13.55
aquifer temperature at producer * (°C)	31.84
temperature at heat exchanger (°C)	31.47
pressure at heat exchanger (bar)	13.85

* @ mid aquifer depth

Appendix C: Space heating and DHW demand for 2000 representative homes in Zwijndrecht. The P50 LTG-HP output is also plotted to show the peak demand. Note that the thermal losses are not calculated, thus the peak demand is higher.

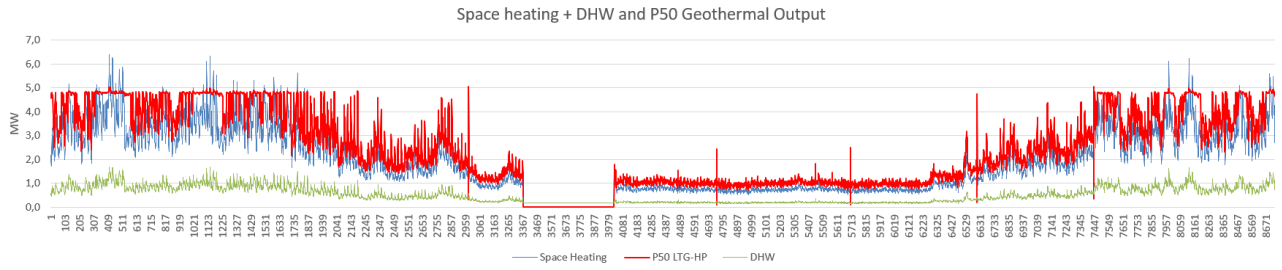

Appendix D1: Pipe catalogue characteristics which are used in CHESS

NEW PIPE CATALOGUE

Roughness = 0.1 mm

DN Size	ID (mm)	WT (mm)	PUR (mm)	HDPE (mm)	Loss (W/m²K)
20	21.7	2.6	28.55	3	2.0049
25	28.5	2.6	25.15	3	1.8669
32	37.2	2.6	30.8	3	1.4609
40	43.1	2.6	27.85	3	1.4522
50	54.5	2.9	29.35	3	1.2831
65	70.3	2.9	28.95	3	1.172
80	82.5	3.2	32.55	3	1.0292
100	107.1	3.6	39.65	3.2	0.82813
125	132.5	3.6	39.25	3.4	0.77572
150	160.3	4	37.25	3.6	0.75899

DN Size	ID (mm)	WT (mm)	PUR (mm)	HDPE (mm)	Loss (W/m²K)
200	210.1	4.5	43.85	4.1	0.62758
250	263	5	58.7	4.8	0.4819
300	312.7	5.6	57.85	5.2	0.46474
350	344.4	5.6	66.6	5.6	0.4101
400	393.8	6.3	71.1	5.7	0.37879
450	444.4	6.3	80.5	6	0.33609
500	495.4	6.3	94.4	6.6	0.2918
600	595.8	7.1	87.2	7.8	0.29533
700	695	8	85.8	8.7	0.28833
800	795.4	8.8	84.1	9.4	0.28362
900	894	10	82.8	10.2	0.27951
1000	994	11	81	11	0.27726
1100	1096	11	79.2	11.8	0.2752

Conductivities of steel pipe, insulation, plastic casing

K	W / m K
Steel pipe	52.15
PUR insulation	0.027
HDPE plastic	0.4

Appendix D2: Example of the described pipe optimisation methodology

The max $\dot{m}_H$ DHN flow to satisfy COP > 3

Max recorded flow in CHESS	ṁ_H (kg/s)	33,8649
	m3/s	0,0350
Peak velocity	m/s	0,6383
Original DN before solve	m	0,2642
DN 250 (solve if oversized)	**m**	**0,2500**
Max flow for DN250	**ṁ_H (kg/s)**	**30,33097383**
100€/m more for DN250 to DN300? Or reduce flow by 3.5kg/s? Cost-benefit analysis!		

$$d = \sqrt{\frac{4 \cdot Q}{(\pi \cdot v)}}$$